Upper Limb Modelling, Dynamic Analysis, And Force Distribution Using Fuzzy Logic

BY

Reza Fazel-Rezai

A Thesis

Submitted to the Faculty of Graduate Studies

in Partial Fulfilment of the Requirements

for the Degree of

DOCTOR OF PHILOSOPHY

Department of Electrical and Computer Engineering

University of Manitoba

Winnipeg, Manitoba, Canada

Thesis Advisor: E. Shwedyk, Ph.D., P.Eng.

(XV+135 = 150 pp.)

National Library
of Canada

Acquisitions and
Bibliographic Services

395 Wellington Street
Ottawa ON K1A 0N4
Canada

Bibliothèque nationale
du Canada

Acquisitions et
services bibliographiques

395, rue Wellington
Ottawa ON K1A 0N4
Canada

Your file Votre référence

Our file Notre référence

0-612-51635-0

Canada

THE UNIVERSITY OF MANITOBA

FACULTY OF GRADUATE STUDIES

*****

COPYRIGHT PERMISSION PAGE

Upper Limb Modelling, Dynamic Analysis, and Force Distribution Using Fuzzy Logic

BY

Reza Fazel-Rezai

A Thesis/Practicum submitted to the Faculty of Graduate Studies of The University of Manitoba in partial fulfillment of the requirements of the degree of Doctor of Philosophy

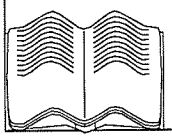

ABSTRACT

The upper limb plays a crucial role in manipulation, perception, prehension and exploration. It has extraordinary adaptability and is of vital importance in human activity. While there is an impressive understanding of upper limb anatomy, the present state of knowledge with respect to kinetic analysis of upper limb movement is not as well developed. Values from variables such as joint forces and moments, transferred and generated powers and energies give a quantitative evaluation of movement and can be used in various applications. To determine these quantitative values, a kinetic analysis is needed. In many situations, it is also desirable to know the internal joint forces and individual skeletal muscle forces because knowledge of the joint loading encountered by the human body could play a crucial role in determining the possible mechanism and in prevention of injury during occupational and sports activities.

This thesis addresses the problem of determining joint forces and moments, power and energy flows, individual muscle forces and internal joint forces for the upper limb. There are two major objectives. The first is to do a kinetic analysis of the upper limb based on three dimensional motion data. The second is to determine power flows and individual muscle forces based on the kinetic and kinematic variables. A link-segment model with ten degrees of freedom, along with the kinematic variables based on motion data, is used to develop the kinetic equations which govern the dynamic behaviour of a limb. To determine individual muscle forces that occur during upper limb motion, a new approach based on fuzzy logic is developed. The fuzzy model uses not only the forces and moments extracted from the kinetic equations, but also the kinematic variables of the motion.

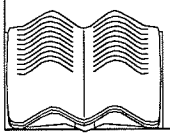

ACKNOWLEDGMENTS

I wish to thank Almighty God for being with me in all struggles I have endured during the course of my study. I would like to acknowledge Dr. E. Shwedyk, my advisor, for his guidance, constant encouragement and constructive criticism. Thanks are also extended to Dr. S. Onyshko, my co-advisor, for his advice on several topics throughout the completion of this thesis. I wish to thank Dr. J. Cooper for her generous counsel.

I wish to express my sincere appreciation to my family, my father and mother, for their patience and sacrifice during my educational life and to my wife, Sima, for her understanding, kindness, inspiration and unconditional support. This thesis is dedicated to her.

The financial support by the Ministry of Culture and Higher Education of Iran and University of Manitoba through the fellowship are appreciated.

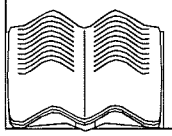

TABLE OF CONTENTS

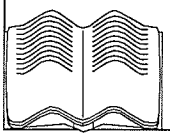

LIST OF FIGURES

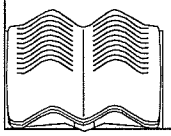

LIST OF TABLES

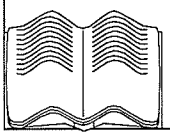

CHAPTER 1. INTRODUCTION

1.1. MOTIVATION

The upper limb plays a crucial role in manipulation, perception, prehension and exploration. It has extraordinary adaptability and is of vital importance in human activity. Observations, from macroscopic to microscopic, have provided anatomic details of the upper limb. While there is an impressive understanding of upper limb anatomy, the present state of knowledge with respect to kinetic analysis of upper limb movement is not as well developed.

For motion analysis of the upper limb, a macroscopic approach is more suitable. Models used for motion analysis are quite varied. Many upper limb models are designed in two dimensional space, typically to reduce the complexity of the analysis. In some cases the motion of the involved segments can be assumed to be planar because of constraints placed on the overall activity. In other instances, the investigator might only be interested in those aspects of the motion that occur in a particular plane; for example, the side view of a gymnast on a balance beam. Although motion analysis in two dimensional space has added considerably to the understanding of the basic functional behaviour of the upper limb, three dimensional modelling is more appropriate to generate realistic information about both normal and pathological upper limb movements and to do a dynamic analysis of such movements.

Dynamic analysis gives a quantitative evaluation of movement and can be used in various applications: orthopedics, rehabilitation, ergonomics and sports. For example, orthopedic surgeons have to be able to assess the patients' problems, put them in the proper perspective, select

the best individual treatment and carry it out. Quantitative values from variables such as joint forces and moments, transferred and generated powers and energies could help the surgeon, not only to make a better decision in the choice of treatment, but also to evaluate the outcome of the surgery. To determine these quantitative values, a kinetic analysis is needed. In many situations, it is also desirable to know the internal joint forces and individual skeletal muscle forces because knowledge of the joint loading encountered by the human body could play a crucial role in determining the possible mechanism and in prevention of injury during occupational and sports activities.

This thesis addresses the problem of determining joint forces and moments, power and energy flows, individual muscle forces and internal joint forces for the upper limb. Such knowledge could provide valuable information for the design of joint implants, prostheses, surgery, and rehabilitation programs. It is hoped that this study will provide a step towards establishing a basis for solving relevant clinical problems.

1.2. RESEARCH OBJECTIVES AND STATEMENT OF THE PROBLEM

There are two major objectives for this research. The first is to do kinetic analysis of the upper limb based on three dimensional motion data. The second is to determine power flows and individual muscle forces based on the kinetic and kinematic variables.

In general, body segments can be studied from two points of view- statically, in which the body is at rest or is moving with uniform motion, or dynamically, in which body segment motion accelerates. The study of dynamic motion, dynamics, is further subdivided into kinematics, a study of motion without considering the forces that produce it, and kinetics, which formulates the relationship between forces and the resulting motion. There are two general problems when kinet-

ics of a rigid body is considered. The first is the direct problem where the applied forcing functions are known and the objective is to determine the resulting motion of the system. The second is the inverse problem in which the motion is completely specified or known and the objective is to find the forcing functions that cause the motion.

This research is concerned with the inverse kinetic analysis of upper limb movement based on motion data. This is done, not only from a theoretical viewpoint, but also with an aim of utilizing the theoretical analysis for clinical applications. To formulate kinetic equations, kinematic variables, i.e., angular and linear displacements, velocities and accelerations, of different points of the body segment should be known. Also, to generate kinetic equations for the upper limb, a link-segment model must first be established. The link-segment model, along with the kinematic variables based on motion data, is used to develop the kinetic equations which govern the dynamic behaviour of a limb. The inverse kinetic analysis is the first objective of this research (Fig. 1.1).

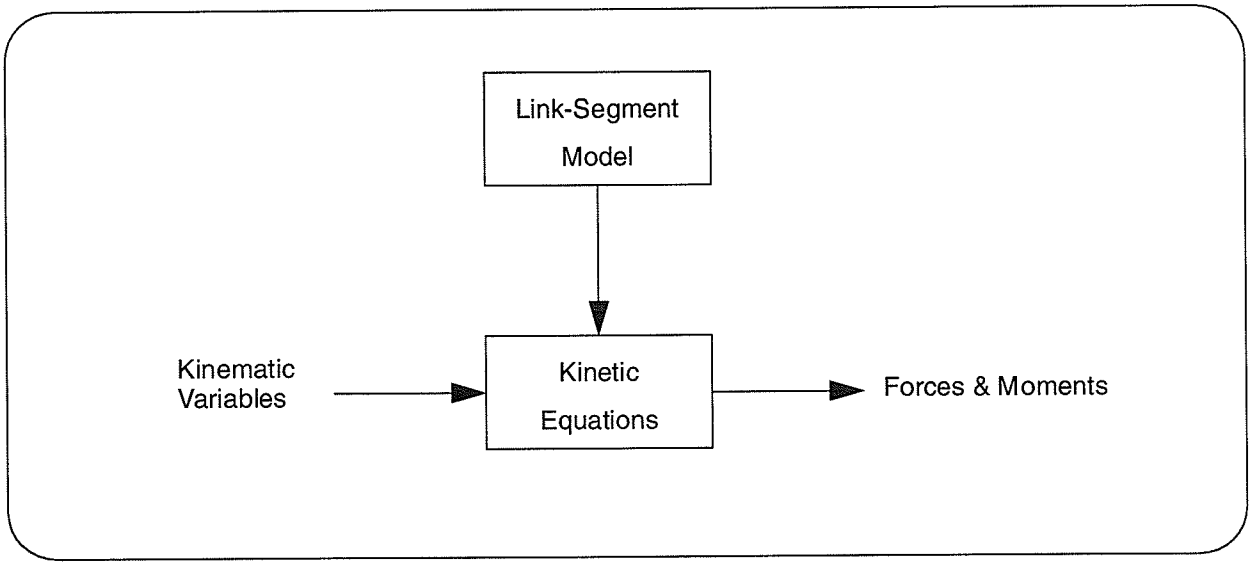

Fig. 1.1 Objective one: inverse kinetic analysis of the upper limb.

The second objective is the determination of the power flows, individual muscle forces and internal joint forces that occur during upper limb motion. A new approach based on fuzzy logic is developed for the force distribution problem, that is, the partitioning of the intersegmental forces and moments to individual muscle forces and moments. To distribute the intersegmental forces during motion, the fuzzy model uses not only the forces and moments extracted from the kinetic equations, but also the kinematic variables of the motion. However, as when any new method is being developed, the fuzzy logic approach was first applied to a straightforward problem; the methodology was developed by considering only the elbow joint, the muscles crossing the anterior aspect of the joint and the one degree of freedom motion (extension/flexion) possible at this joint. The second objective is shown in Fig. 1.2.

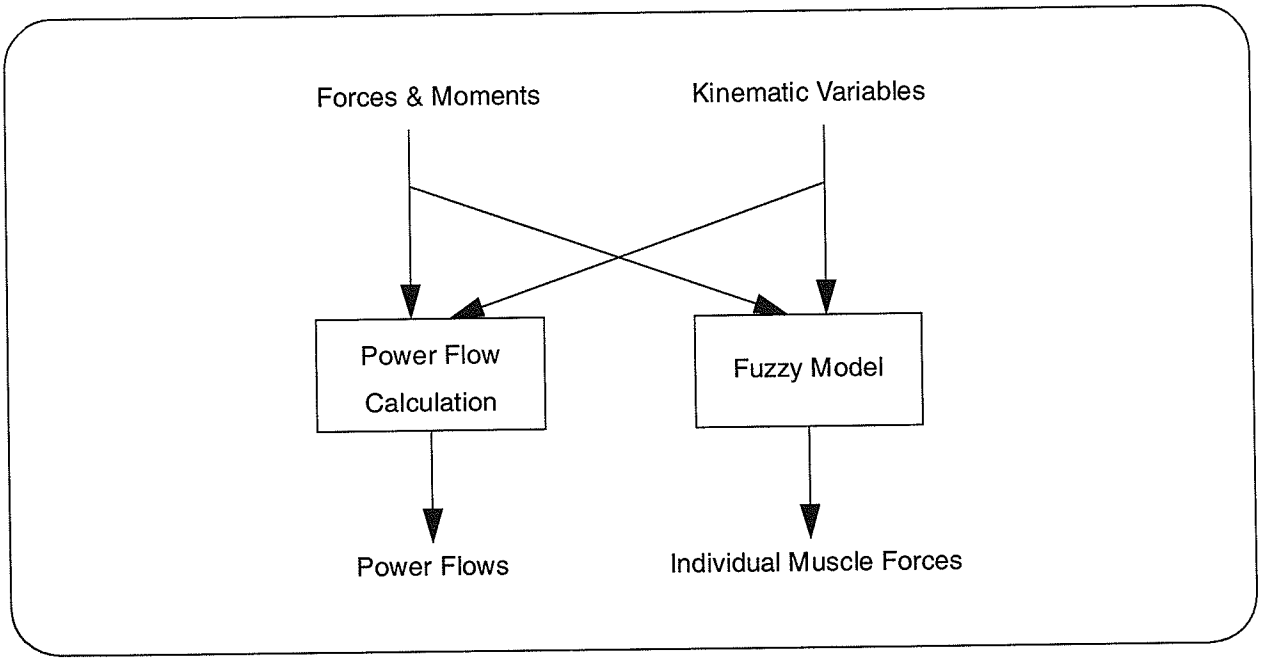

Fig. 1.2 Objective two: determining power flows and individual muscle forces.

As can be seen in Fig. 1.1 and Fig. 1.2, to achieve the research objectives it is necessary to establish a link segment model and to determine kinematic variables. A model consisting of three segments representing the arm, forearm and hand segments has been developed. In this model, the elbow and wrist joints are considered as ball and socket joints, each with two rotational degrees of freedom (DOF). However, because both translation and rotation occur at the shallow gleno-humeral (shoulder) joint, three translational DOF and three rotational DOF for the arm segment are considered. Therefore the model has a total of ten DOF, three translational DOF and seven rotational DOF. The determination of the necessary kinematic variables is shown in Fig. 1.3.

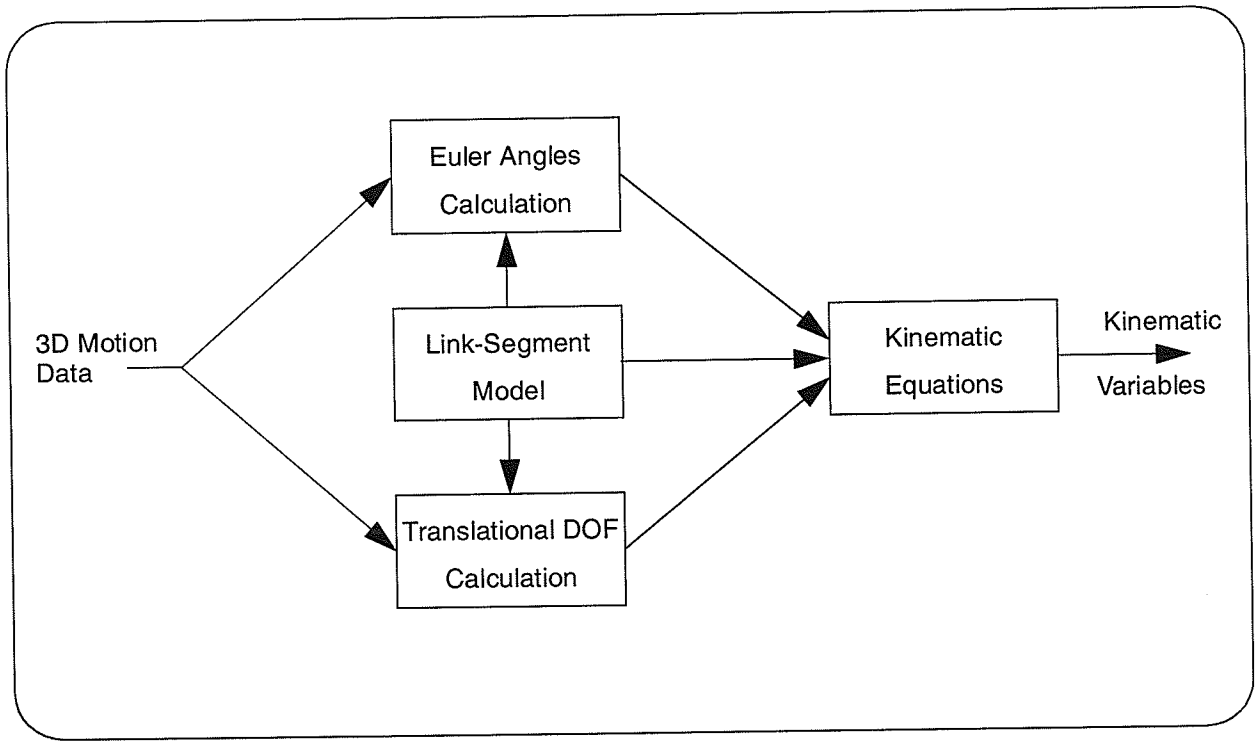

Fig. 1.3 Block diagram of the kinematic analysis.

For kinetic analysis, not only the position but also velocity (first derivative) and acceleration (second derivative) are required. Because the differentiation process amplifies noise, data should be smoothed to prevent error amplification in the system. Therefore a data smoothing block is added to the block diagram of Fig. 1.3. Smoothing can be applied to the motion data or to the inputs to the kinematic equations. To prevent amplification of possible error produced in calculation of the Euler angles and translational DOF it is better to apply smoothing after these calculations (Fig. 1.4). In the other words smoothing should be applied as close as possible to the differentiation process. In addition, motion data in 2D (or 3D) are displacements of different markers over time expressed as xy (or xyz) coordinates. The question then arises whether these data components should be processed independently or not. Known and constant distances between markers might be used as constraints during the smoothing process. Imposing constraints during the smoothing process is not an easy task. Therefore in this work, smoothing is applied to the inputs of the kinematic equations.

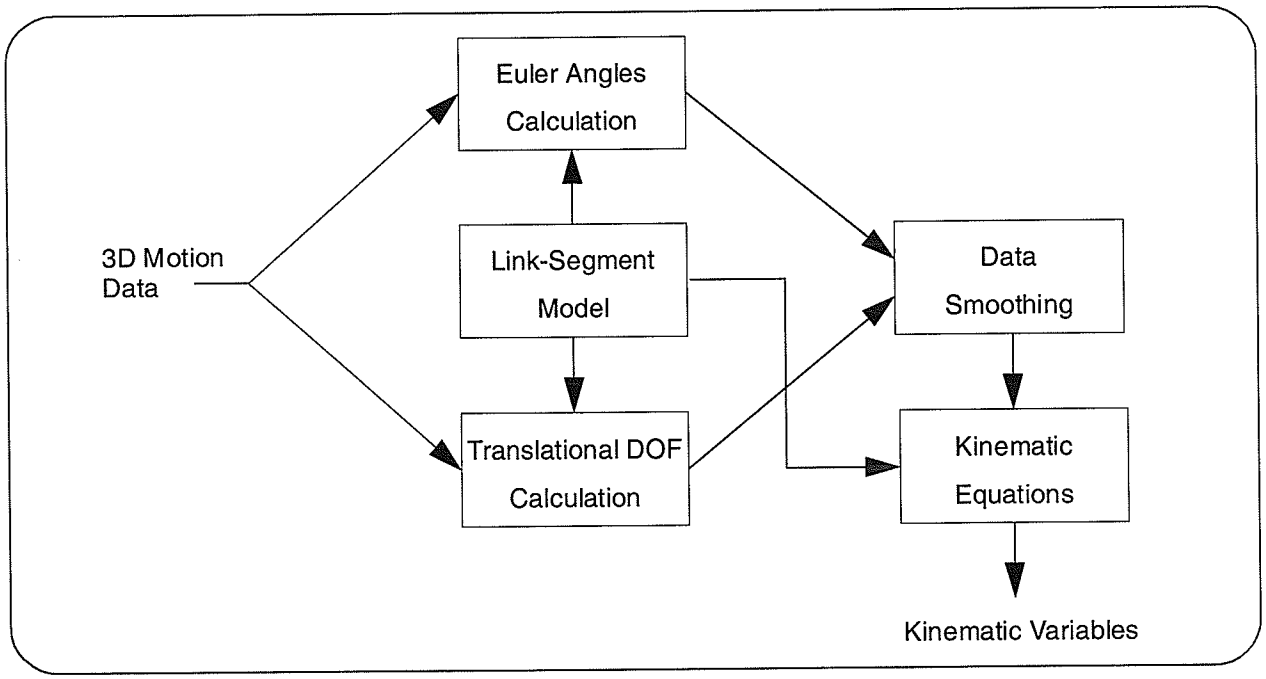

Fig. 1.4 Block diagram for kinematic analysis with data smoothing.

1.3. THESIS ORGANIZATION

The organization of the thesis is shown in Fig. 1.5. As was stated, one of the objectives of this research was to do kinetic analysis which requires development of a link segment model and calculation of kinematic variables. This model, along with the determination of Euler angles, three translational DOF and the resultant kinematic equations, is presented in Chapter 2. In Chapter 3 four different methods for kinematic data smoothing are described and compared. Kinetic equations developed using both Lagrangian and Newtonian methods and an analytical relationship between them for the upper limb are described in Chapter 4. Also equations for obtaining power flows are developed. At the end of the chapter results of experiments to test the model are presented. Chapter 5 describes the fuzzy logic method to determine individual muscle forces. Simulation results are presented and results of experiments to verify the fuzzy logic approach for the force distribution problem are shown at the end of the chapter. The final chapter, Chapter 6, concludes and makes recommendations for future research. Each chapter begins with a review of the relevant literature.

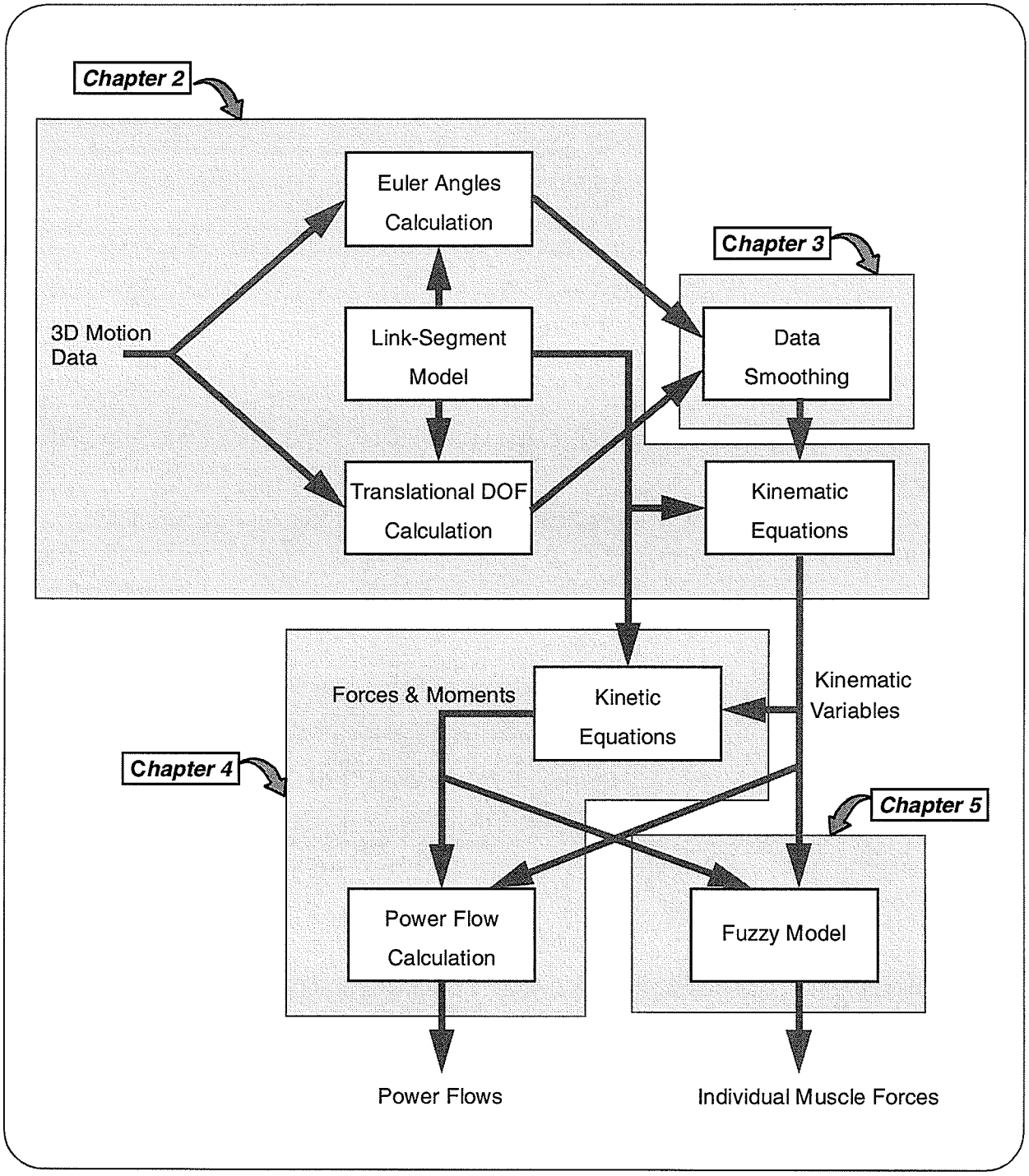

Fig. 1.5 Organization of the thesis.

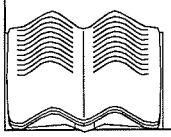

CHAPTER 2. KINEMATIC ANALYSIS

2.1. INTRODUCTION

Many kinematic three dimensional (3D) analyses of body segment movement start with data captured by an imaging device. An exposition on instrumentation for 3D measurements and 3D video-based measuring systems is presented in [1]. Thus description of such systems is not discussed in any detail in this thesis. However, to achieve the research objectives, it is necessary to establish a link segment model and determine kinematic variables, i.e. angular and linear displacements, velocities and accelerations. This model and the determination of the necessary kinematic variables are discussed in this chapter.

The chapter is organized as follows. First, the center of rotation is explained. The general method to determine center of rotation in two dimensional (2D) space is presented and it is shown that this method does not work in 3D space. Therefore a method to determine the center of rotation in 3D space using the screw axis is introduced. Then the link segment model of the upper limb with three translational DOF determined by the screw axis and seven rotational DOF modelled by Euler angles is described. Finally, kinematic equations of the model using homogenous coordinates are presented.

In general, kinematic analysis of the musculo-skeletal system is a challenging task in bioengineering. In biomechanics, models are categorized into three groups [2]:

I) bones II) joints III) body segments

This research is concerned with modelling at the level of body segments with a simple model for

the joint [3]. King [2] has divided the third class of modelling into five major groups: fingers and thumb, the lower extremities, the spinal segment, thorax, and the whole body. It is interesting to note that upper limb modelling was not included. In body segment modelling, the number of links, dimension of space (2D/3D), the number of degrees of freedom (DOF) and consideration of kinetics and/or kinematics are some features of the model. Table 2.1 lists a number of upper limb models and their features.

Ref. #	Year	Model of	# of links	2D / 3D	DOF	Kinematic / Dynamic
[4]	1978	Elbow	3	3D	1	Kinematic
[5]	1978	Upper Limb	2	2D	2	Dynamic
[6]	1979	Elbow	3	3D	2	Kinematic
[7]	1981	Upper Limb	2	3D	6	Kinematic
[8]	1989	Upper Limb	3	2D	3	Dynamic
[9]	1990	Upper Limb	3	3D	7	Kinematic
[10]	1992	Hand & Finger	2	3D	3	Kinematic
[11]	1994	Upper Limb	3	3D	7	Kinematic
[12]	1994	Upper Limb	3	3D	7	Kinematic

Table 2.1 Studies considering a model of the upper limb and their features.

The number of links should be chosen in such a way that the link-segment model represents the physical motion of the bones and also that the position and orientation of points of interest can be found. The number of bones in the shoulder, arm, forearm and hand are respectively 2, 1, 2 and 27 [13]. In this research the objective is to accomplish kinetic analysis of upper limb motion for application in movements typically associated with activities of daily living. Thus the upper limb model has been simplified appropriately and finger movement is not considered. The hand is modelled as a single segment. The final model for the upper limb contains three links each representing the arm, forearm and hand segments, respectively, that move in 3D space.

The outputs of the link-segment model are trajectories of markers attached to defined points on the upper limb. To obtain the orientation and position of different points of the segments, kinematic equations need to be established. Kinematic equations are obtained using a homogeneous coordinate system which can easily incorporate an increase in the number of links.

The number of DOF in a kinematic model is related to the number of joints. Generally, each joint has six DOF, three rotational and three translational [3][14]. The total DOF of the upper limb has been reported to be 42 [15] and 87 [16]. Because of the research objectives, only three joints with ten DOF are considered: three translational and three rotational DOF for the arm segment, two rotational DOF for the forearm segment and two rotational DOF for the hand segment [17]. Three translational DOF are considered for the arm segment because both translation and rotation occur at the shallow glenohumeral (shoulder) joint [18]. To find the translational DOF of the arm segment, the instantaneous center of rotation of the segment must be determined. The center of rotation and its determination in 2D and 3D space are discussed in the next section.

2.2. CENTER OF ROTATION

To obtain the force and moment at a joint, it is necessary to determine rolling and sliding movements at that joint. Therefore the location and trajectory of the joint's center of rotation must be known. The instantaneous center of rotation is defined as the point in space which maintains a constant distance from every point of the moving segment or as the point with zero velocity during an infinitesimally small motion [19]. A moving segment can both translate along and rotate about a fixed segment. Although in many cases translation can be ignored because it is very small, this simplification results in an error when the center of rotation is calculated. In fact, the center of rotation for the moving segment will change throughout the course of motion. Therefore its position must be derived for each instant in time.

Because in experimental measurements it is nearly impossible to determine the instantaneous velocity of different points on a body in motion [20], the center of rotation is usually approximated by two points on the moving segment using two consecutive positions within a short period of time [21]. The methods for determining the center of rotation in 2D and 3D space are quite different. These are discussed in the next two sections.

2.2.1. DETERMINATION OF CENTER OF ROTATION IN 2D

Fig. 2.1 shows graphically the determination of the center of rotation of a moving segment in 2D space. Let the position of two markers on the moving segment in position 1 be M_1 and N_1 and in position 2 be M_2 and N_2. The approximated center of rotation can be found as a intersection of the two lines perpendicular to the lines M_1M_2 and N_1N_2 as shown in Fig. 2.1. Points C_{12} and C_{23} are, respectively, the calculated center of rotation using positions 1,2 and 2,3 of the moving segment.

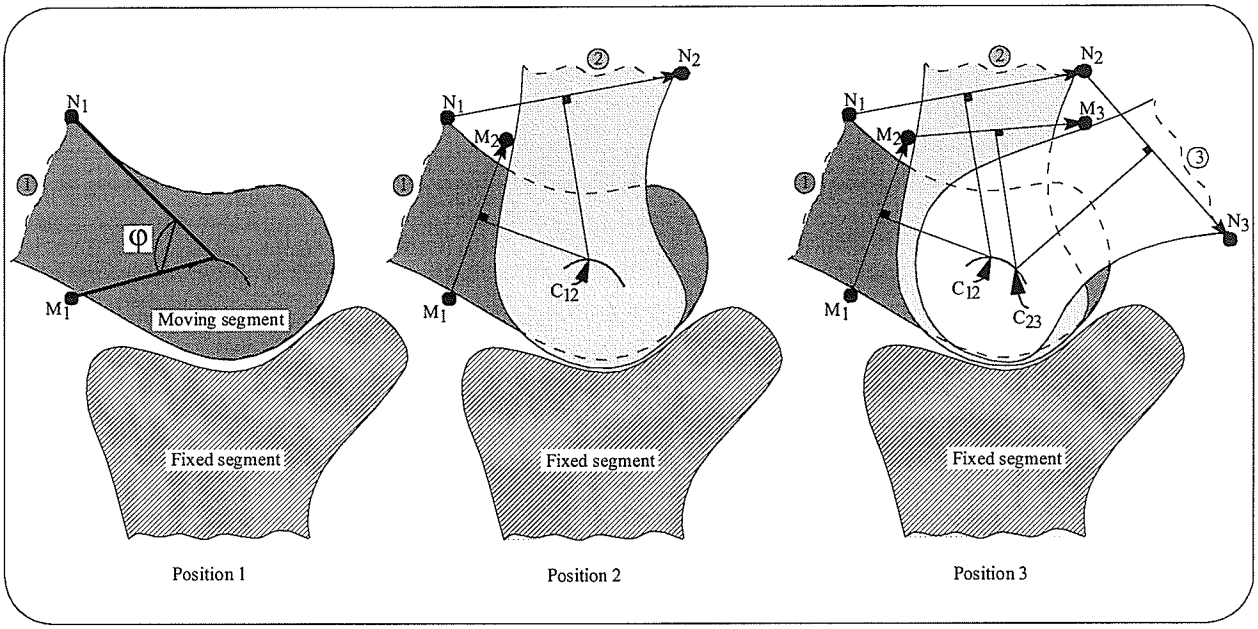

Fig. 2.1 Determination of center of rotation between two positions of a moving segment.

Mathematical determination of the center of rotation is explained in the literature [19][22] [23]. All methods are based on the fact that within an arbitrary plane coordinate system, movement of every point of a rigid body from point $\boldsymbol{X}_1$ to $\boldsymbol{X}_2$ can be expressed as

$$\boldsymbol{X}_2 = R\boldsymbol{X}_1 + \boldsymbol{T} \tag{2-1}$$

where R and $\boldsymbol{T}$ are the rotation matrix and translation vector respectively. If the origin of the coordinate system is chosen at the center of rotation, the translation vector will be zero, that is, the rigid body motion can be written in the following form in an arbitrary coordinate system

$$\boldsymbol{X}_2 - \boldsymbol{C} = R(\boldsymbol{X}_1 - \boldsymbol{C}) \tag{2-2}$$

where $\boldsymbol{C}$ is the center of the rotation vector. Solving Eq (2-2) for $\boldsymbol{C}$, one obtains

$$\boldsymbol{C} = [I - R]^{-1}(\boldsymbol{X}_2 - R\boldsymbol{X}_1) \tag{2-3}$$

The rotation matrix in the 2D coordinate system can be easily found using two markers

(e.g., M and N in Fig. 2.1) on the moving segment. Therefore, to determine the center of rotation of a moving segment in a 2D coordinate system at least two markers on the segment are necessary.

This method does not work in 3D space, because the rank of $[I-R]$ is two. It means that center of rotation in 3D space must be determined by another method.

2.2.2. DETERMINATION OF CENTER OF ROTATION IN 3D USING SCREW AXIS

To overcome the above mentioned difficulty in determining the center of rotation in 3D space, in this research an approach based on the screw axis is developed. For completeness, the determination of the screw axis is described next.

Regardless of how the actual motion takes place in 3D space, the displacement of the moving segment from position 1 to position 2 can always be represented as a rotation about and a translation along a unique axis as shown in Fig. 2.2. This axis is directly analogous to the instant center of rotation for 2D space motion and is called the screw axis [14]. It is used to obtain the three translational DOF of the arm segment. To use the screw axis one needs to determine orientation of the axis in space and also its rotation angle and translation vector, respectively angle ϕ and vector $\mathbf{T}$ in Fig. 2.3. This is done as follows.

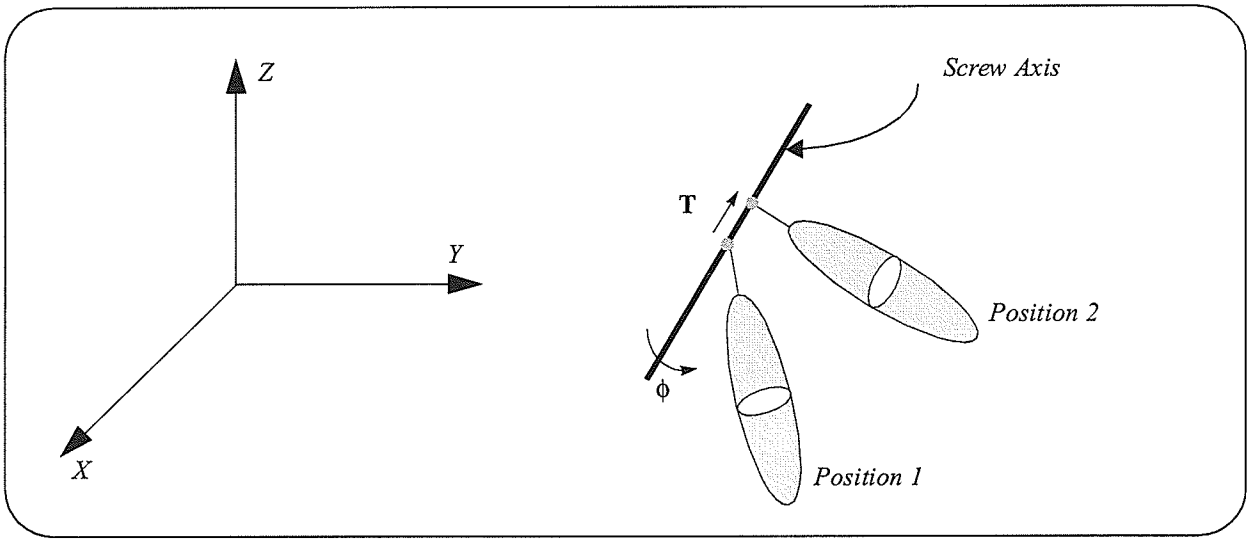

Fig. 2.2 Displacement of a segment as the rotation about and translation along screw axis.

In a homogeneous coordinate system*[24], a point *(x,y,z)* can be represented with respect to a coordinate system *i* by the following vector

$$ {}^{i}\boldsymbol{r}' = [x, y, z, 1]^{T} \tag{2-4} $$

This point with respect to another coordinate system *j* can be written as

$$ {}^{j}\boldsymbol{r}' = {}^{j}H^{i} \cdot {}^{i}\boldsymbol{r}' \tag{2-5} $$

The transformation matrix, ${}^{j}H^{i}$, has the following structure

$$ {}^{j}H^{i} = \begin{bmatrix} {}^{j}R^{i} & {}^{j}\boldsymbol{T}^{i} \\ \mathbf{0}^{T} & 1 \end{bmatrix} \tag{2-6} $$

where ${}^{j}R^{i}$ and ${}^{j}\boldsymbol{T}^{i}$ are respectively the rotation matrix and translation vector of the coordinate system *i* relative to the coordinate system *j* and $\mathbf{0}^{T} = [0, 0, 0]$.

In 3D space, Eq. (2-1) can be written in homogeneous form,

*. In this section every vector with the prime is considered in the homogeneous coordinate system.

$$\begin{bmatrix} \boldsymbol{X}_2 \\ 1 \end{bmatrix} = \begin{bmatrix} R & T \\ 0 & I \end{bmatrix} \begin{bmatrix} \boldsymbol{X}_1 \\ 1 \end{bmatrix} = \begin{bmatrix} a_{11} & a_{11} & a_{13} & T_x \\ a_{21} & a_{22} & a_{23} & T_y \\ a_{31} & a_{32} & a_{33} & T_z \\ 0 & 0 & 0 & 1 \end{bmatrix} \begin{bmatrix} \boldsymbol{X}_1 \\ 1 \end{bmatrix} \tag{2-7}$$

or

$$\boldsymbol{X}'_2 = A'\boldsymbol{X}'_1 \tag{2-8}$$

The matrix A' can be determined if the coordinates of four non-coplanar points $\boldsymbol{M}^{(i)}$ (i = 1, 2, 3, 4) on the moving segment are known in both positions 1 and 2. For four points, Eq. (2-8) can be written in matrix form as follows

$$B'_2 = A'B'_1 \tag{2-9}$$

where matrix B'_i is 4×4 and its four columns are the homogenous coordinates of four points in position i. Therefore the matrix A' is given by

$$A' = (B'_2)\,(B'_1)^{-1} \tag{2-10}$$

Considering ϕ as the rotation angle about the screw axis and $\boldsymbol{T} = K\boldsymbol{u}$ as the translation vector along the axis, where $\boldsymbol{u}$ is a unit vector with components (u_x, u_y, u_z), the rotation matrix in Eq.(2-7) can be written as [14]

$$R = \begin{bmatrix} u_x^2 D + C & u_x u_y D - u_z S & u_z u_x D + u_y S \\ u_x u_y D + u_z S & u_y^2 D + C & u_y u_z D - u_x S \\ u_z u_x D - u_y S & u_y u_z D + u_x S & u_z^2 D + C \end{bmatrix} \tag{2-11}$$

where $S = \sin(\phi)$, $C = \cos(\phi)$ and $D = 1 - \cos(\phi)$.

The submatrix R defines a pure rotation. It has three independent parameters and its elements are independent of where the axis of rotation is actually located. Consider a new axis parallel to the screw axis but passing through the origin. A pure rotation of a point $\boldsymbol{P}$ about this axis is

given by

$$\boldsymbol{P}_2 = R\boldsymbol{P}_1 \tag{2-12}$$

If the point $\boldsymbol{P}$ is located on the axis of rotation, then $\boldsymbol{P}$ is not rotated and $\boldsymbol{P}_1$ and $\boldsymbol{P}_2$ become the same point. Therefore

$$\boldsymbol{P} = R\boldsymbol{P} \Rightarrow [I-R]\,\boldsymbol{P} = \boldsymbol{0} \tag{2-13}$$

As was mentioned in the previous section, the rank of $[I-R]$ is two, therefore there is a non-trivial solution for Eq. (2-13) which is the vector $\boldsymbol{u}$, the direction of the screw axis. Eq. (2-13) can be expressed as

$$\begin{bmatrix} a_{11}-1 & a_{12} & a_{13} \\ a_{21} & a_{22}-1 & a_{23} \\ a_{31} & a_{32} & a_{33}-1 \end{bmatrix} \begin{bmatrix} u_x \\ u_y \\ u_z \end{bmatrix} = \begin{bmatrix} 0 \\ 0 \\ 0 \end{bmatrix} \tag{2-14}$$

Thus one possible solution is

$$\begin{cases} u_x = u_x \\ u_y = \dfrac{u_x\,[a_{23}a_{31} - a_{21}\,(a_{33}-1)\,]}{(a_{22}-1)\,(a_{33}-1) - a_{23}a_{32}} \\ u_y = \dfrac{u_x\,[a_{21}a_{32} - a_{31}\,(a_{22}-1)\,]}{(a_{22}-1)\,(a_{33}-1) - a_{23}a_{32}} \end{cases} \tag{2-15}$$

Since $\boldsymbol{u}$ is a unit vector,

$$u_x^2 + u_y^2 + u_z^2 = 1 \tag{2-16}$$

Eqs. (2-15) and (2-16) are sufficient to determine the direction of the screw axis.

When the direction of the screw axis is known, the rotation angle can be calculated using Eq. (2-11)

$$\phi = \operatorname{acos}\left[\frac{a_{11} - u_x^2}{1 - u_x^2}\right] \tag{2-17}$$

Now let $\boldsymbol{Q}$ be a point located on the screw axis. The position of the point $\boldsymbol{Q}$ from position 1 to 2 can be expressed in homogenous coordinates as

$$\boldsymbol{Q}_2' = A'\boldsymbol{Q}_1' \tag{2-18}$$

But the point is on the screw axis, therefore

$$\boldsymbol{Q}_2' - \boldsymbol{Q}_1' = K\boldsymbol{u}' \tag{2-19}$$

or from Eq. (2-18)

$$[A' - I]\,\boldsymbol{Q}_1' = K\boldsymbol{u}' \tag{2-20}$$

Every parameter in Eq. (2-20) is known, except the three components of the point $\boldsymbol{Q}$ and scaling factor K. But $\boldsymbol{Q}$ is an arbitrary point on the screw axis and, given one component of the point, the two other components and the constant K can be found from the three equations in Eq. (2-20). Therefore, translation along the screw axis can be found using Eq. (2-20).

The screw axis is used to obtain three translational DOF of the link-segment model as follows. Let the moving segment be at position 1, 2, 3 and 4 respectively at times t_1, t_2, t_3 and t_4 as shown in Fig. 2.3. Consider lines $\mathbf{S}_1$, $\mathbf{S}_2$ and $\mathbf{S}_3$ as three screw axes from position 1 to 2, 2 to 3 and 3 to 4, respectively. $\mathbf{T}_1$, $\mathbf{T}_2$ and $\mathbf{T}_3$ are translations along the three axes calculated using equations (2-15) and (2-20). The trajectory of the axis of rotation from position 1 to 4 can be found by connecting vectors $\mathbf{T}_1$, $\mathbf{T}_2$ and $\mathbf{T}_3$, as shown in Fig. 2.3. Using this method to calculate the trajectory of the rotation axis, the three translational DOF of the arm segment are determined during movement.

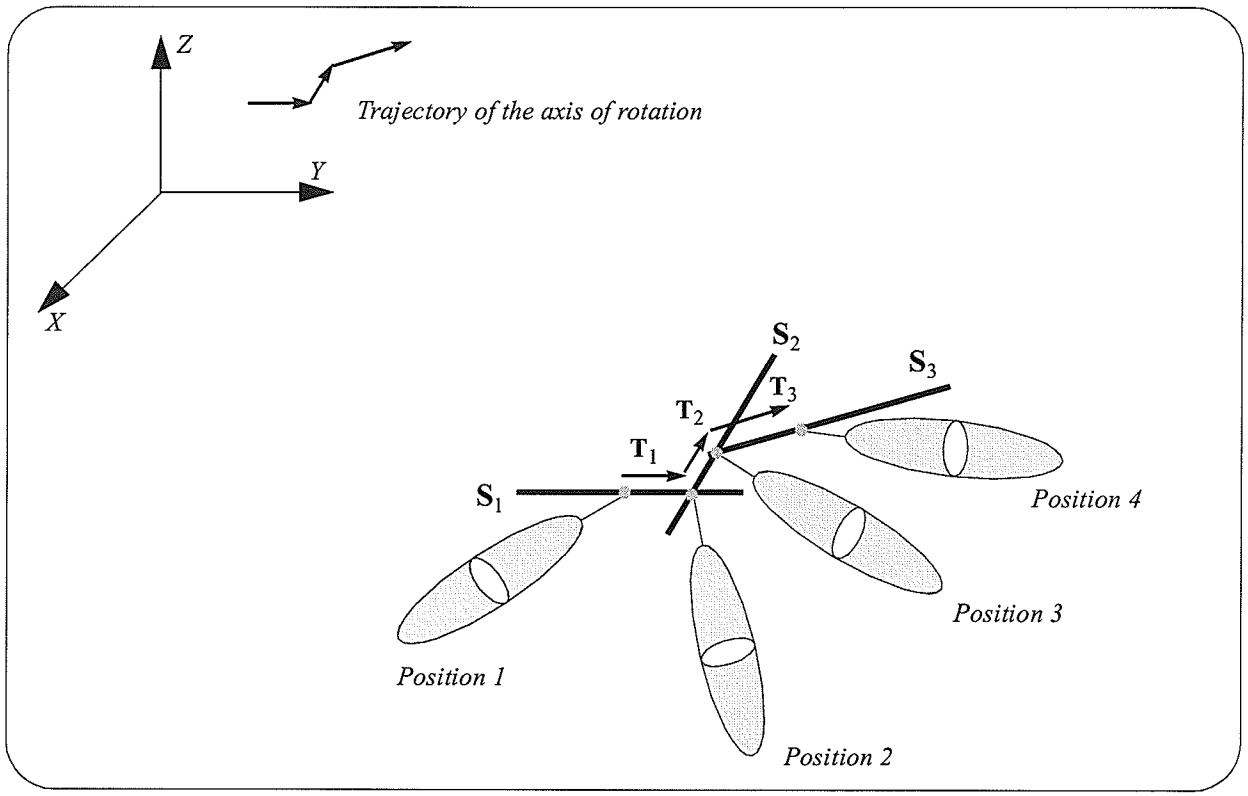

Fig. 2.3 Determination of trajectory of the axis of rotation using screw axis.

2.3. KINEMATIC MODEL OF THE UPPER LIMB

The physical system of the upper limb is represented by a link-segment model composed of three rigid segments representing the arm, forearm and hand as shown in Fig. 2.4A. Points ❶, ❷ and ❸ represent the shoulder, elbow and wrist joints respectively. A coordinate system is associated with each segment. The model contains ten DOF, three translational and three rotational DOF for the shoulder joint, two rotational DOF for the elbow joint and two rotational DOF for the wrist joint. The seven rotational DOF are modelled using nine Euler angles of the three defined coordinate systems of each segment relative to the lab coordinate system with the three translational DOF obtained using the screw axis method described in the previous section.

For experimental purposes, six reflective markers (M_i , i = *1, ..., 6*) are used to define the three coordinate systems of the three segments. Markers M_1, M_2 and M_3 are fixed on the arm, M_4 and M_5 are fixed on the forearm and M_6 is fixed on the hand as shown in Fig. 2.4B. Marker specifications are explained in Appendix A. Let $(\boldsymbol{i}_s,\boldsymbol{j}_s,\boldsymbol{k}_s)$ be the orthogonal basis of the coordinate system (X_s,Y_s,Z_s) s=*1,2,3*, where s represents the segment number. Then three bases for the three segments are defined as follows

$$\begin{cases} \boldsymbol{j}_1 = \overrightarrow{M_1M_2} \\ \boldsymbol{i}_1 = \overrightarrow{M_1M_2} \otimes \overrightarrow{M_1M_3} \\ \boldsymbol{k}_1 = \boldsymbol{i}_1 \otimes \boldsymbol{j}_1 \end{cases} \quad \begin{cases} \boldsymbol{j}_2 = \overrightarrow{M_2M_4} \\ \boldsymbol{i}_2 = \overrightarrow{M_2M_4} \otimes \overrightarrow{M_2M_5} \\ \boldsymbol{k}_2 = \boldsymbol{i}_2 \otimes \boldsymbol{j}_2 \end{cases} \quad \begin{cases} \boldsymbol{j}_3 = \overrightarrow{M_4M_6} \\ \boldsymbol{i}_3 = \overrightarrow{M_4M_6} \otimes \overrightarrow{M_4M_5} \\ \boldsymbol{k}_3 = \boldsymbol{i}_3 \otimes \boldsymbol{j}_3 \end{cases} \tag{2-21}$$

where $\overrightarrow{M_iM_j}$ means the unit vector from marker M_i to M_j and $\otimes$ is the cross product operator.

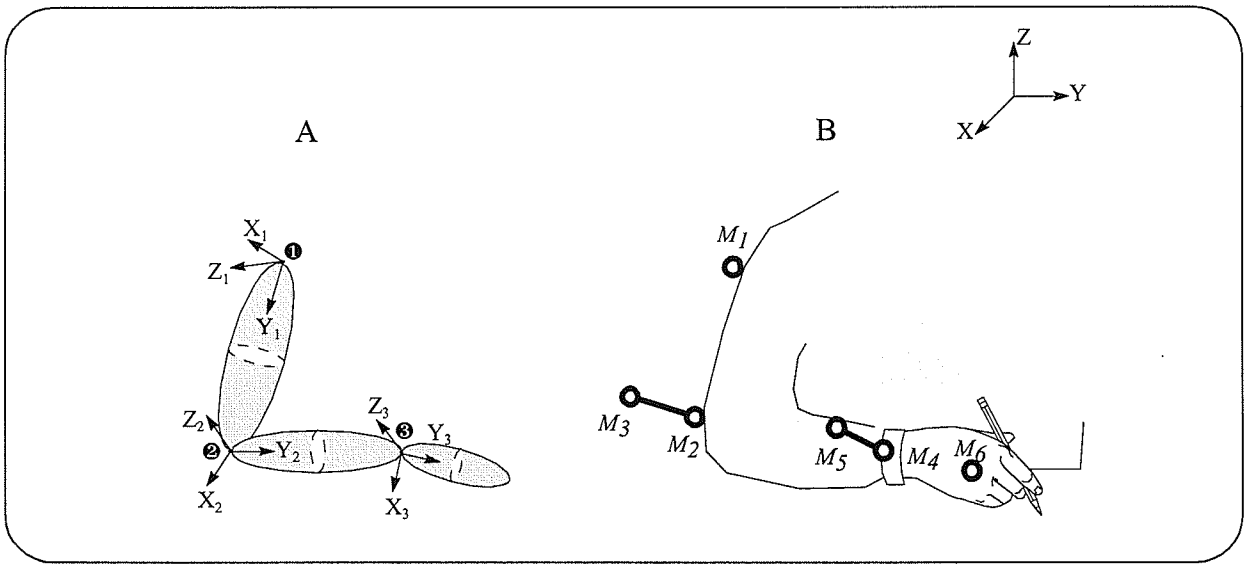

Fig. 2.4 A) Link-segment model of the upper limb consisting of three segments. B) Arrangement of six markers on the upper limb.

The next section explains specifically how the three translational DOF are determined for the upper limb. The section following it shows the derivation of the seven rotational DOF using Euler angles.

2.3.1. DERIVATION OF THREE TRANSLATIONAL DOF

It is assumed that the forearm and hand are connected respectively to the arm and forearm using a joint with two DOF [3]. However for the arm segment, six DOF, three translational and three rotational DOF, are considered [18].

In Section 2.2.2., it was explained that at least four points are necessary to find all parameters of the screw axis, but there are only three markers (M_1, M_2, M_3) on the arm segment as shown in Fig. 2.4B. It appears that one extra marker should be added to the arm segment for this purpose. However an imaginary marker, discussed below, was used for all calculations of the screw axis. Consider matrices R_a and R_f respectively as the rotation matrix of the arm and forearm relative to the lab coordinate system. The rotation matrix can be found using three Euler angles of the segment and is independent of the arm translation. An imaginary marker, M_4^I, of the arm segment can be found using the following equation

$$M_4^I = M_2 + R_a R_f^{-1} (M_4 - M_2) \tag{2-22}$$

where M_4 and M_2 are vectors of the physical markers as shown in Fig. 2.4B and $R_a R_f^{-1}$ is the rotation matrix of the forearm coordinate system relative to the arm segment. M_4^I along with the first three markers (M_1, M_2, M_3) is used to find screw axis of the arm segment.

Having described how to determine analytically the three translational DOF of the arm segment, it is of interest to see how large they are in a typical upper limb movement. Therefore an illustrative experiment was performed where a subject was asked to pick up a bottle from a table while sitting on a chair. Three dimensional motion data were collected using the University of Manitoba Motion Analysis System (UM^{2}AS) [9][25] (Appendix A). Fig. 2.5 shows the three translational DOF of the arm segment for this experiment. Fig. 2.6 shows the trajectory of the translational DOF in 3D space. Although it appears that the magnitude of the trajectory vector is

small relative to the range of motion which is on the order of 30 cm and can be ignored, it is shown in Chapter 4, which considers kinetic analysis, that these small translational DOF are very important for kinetic analysis purposes. This is because the three translational DOF of the arm segment are used as the coordinates of a point upon which the displacement of all points in the link-segment model depends. Also in kinetic analysis not only displacements but also the first and second derivatives of the kinematic variables are used. Therefore any small error is magnified and it is important that the translational DOF be considered.

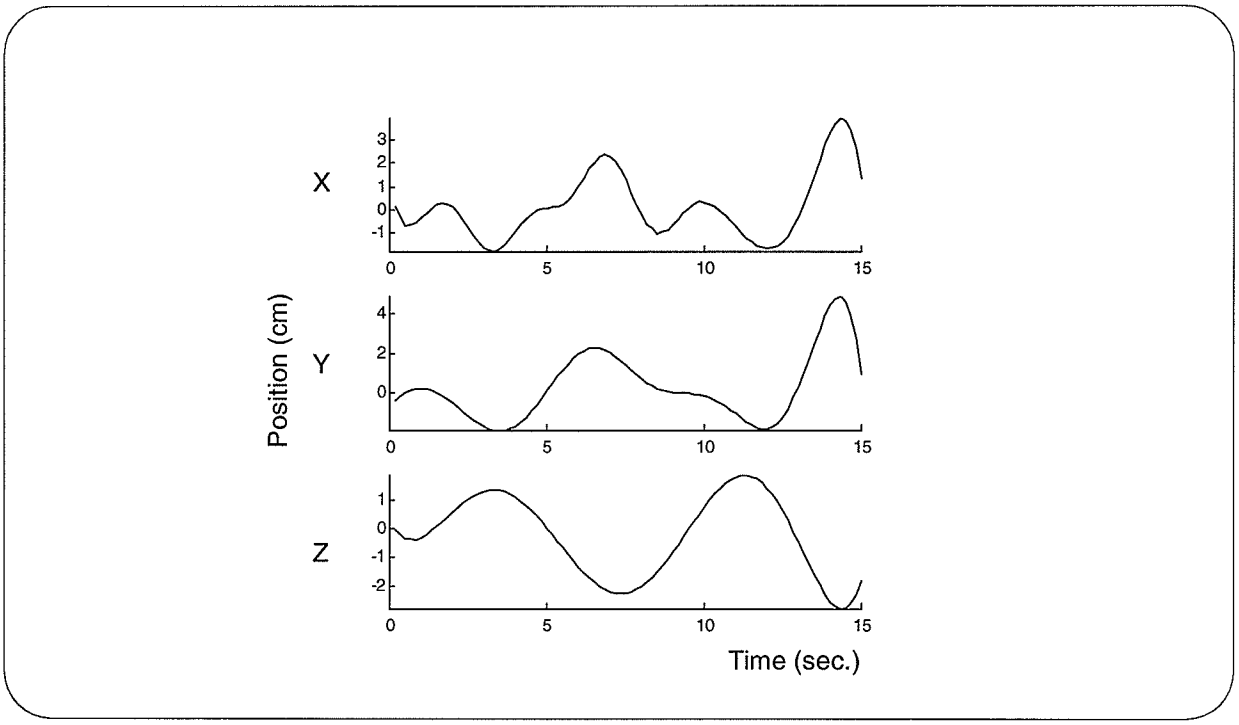

Fig. 2.5 Three components of the translational DOF of the arm segment in lab coordinate system.

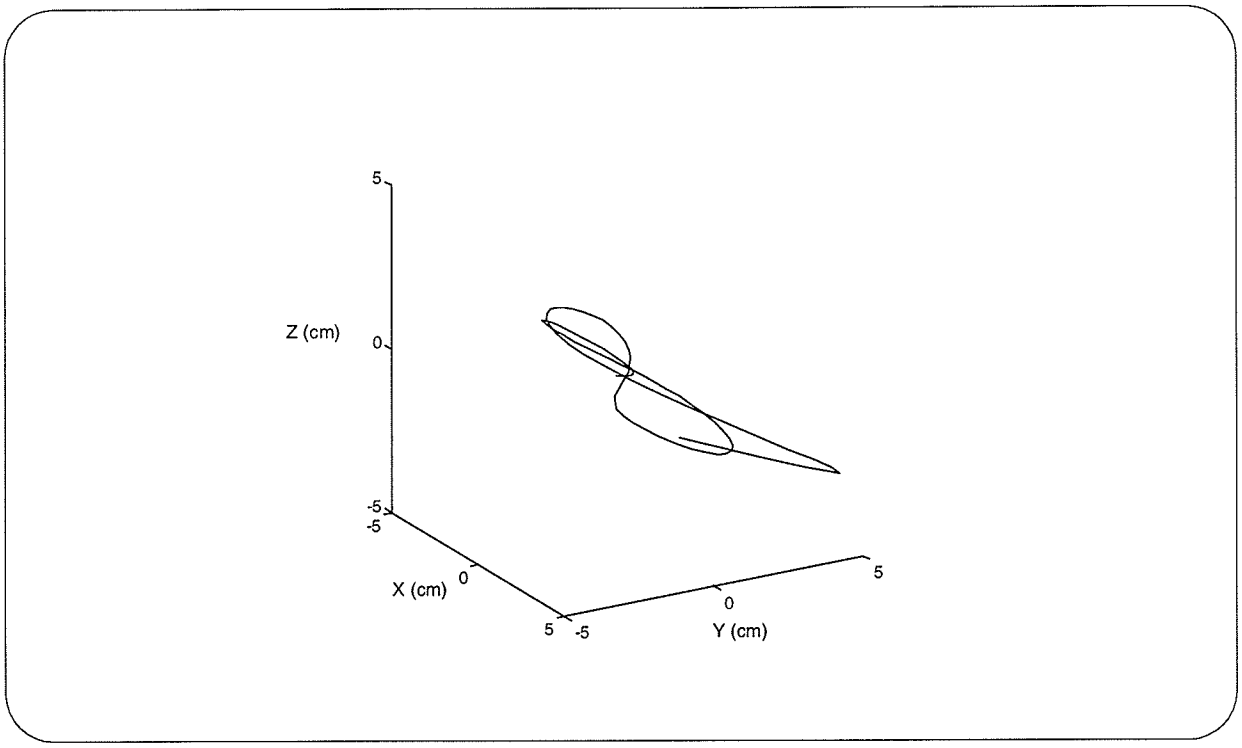

Fig. 2.6 Translational DOF of the arm segment in lab coordinate system.

2.3.2. DERIVATION OF SEVEN ROTATIONAL DOF

Using the three segment coordinate systems defined in Eq. (2-21), the Euler angles of each joint can be determined. Let the rotation sequence of Euler angles for a segment be *XYZ*. Rotation through angle Eu_{s1} about the *X* axis, angle Eu_{s2} about the *Y* axis and angle Eu_{s3} about the *Z* axis can be written as follows

$$\begin{bmatrix} \boldsymbol{I} \\ \boldsymbol{J} \\ \boldsymbol{K} \end{bmatrix} = \begin{bmatrix} 1 & 0 & 0 \\ 0 & C_1 & -S_1 \\ 0 & S_1 & C_1 \end{bmatrix} \begin{bmatrix} \boldsymbol{i}_1 \\ \boldsymbol{j}_1 \\ \boldsymbol{k}_1 \end{bmatrix}, \quad \begin{bmatrix} \boldsymbol{i}_1 \\ \boldsymbol{j}_1 \\ \boldsymbol{k}_1 \end{bmatrix} = \begin{bmatrix} C_2 & 0 & S_2 \\ 0 & 1 & 0 \\ -S_2 & 1 & C_2 \end{bmatrix} \begin{bmatrix} \boldsymbol{i}_2 \\ \boldsymbol{j}_2 \\ \boldsymbol{k}_2 \end{bmatrix}, \quad \begin{bmatrix} \boldsymbol{i}_2 \\ \boldsymbol{j}_2 \\ \boldsymbol{k}_2 \end{bmatrix} = \begin{bmatrix} C_3 & -S_3 & 0 \\ S_3 & C_3 & 0 \\ 0 & 0 & 1 \end{bmatrix} \begin{bmatrix} \boldsymbol{i}_3 = \boldsymbol{i} \\ \boldsymbol{j}_3 = \boldsymbol{j} \\ \boldsymbol{k}_3 = \boldsymbol{k} \end{bmatrix} \quad (2\text{-}23)$$

where the symbols C_i and S_i denote respectively cosine and sine functions of angle Eu_{si} and $(\boldsymbol{I}, \boldsymbol{J}, \boldsymbol{K})$ and $(\boldsymbol{i}_s, \boldsymbol{j}_s, \boldsymbol{k}_s), s = 1, 2, 3$, are bases for the corresponding coordinate system. The total

rotation of the coordinate system i relative to the lab coordinate system is given by

$$\begin{bmatrix} \boldsymbol{I} \\ \boldsymbol{J} \\ \boldsymbol{K} \end{bmatrix} = {}^{0}R^{i} \begin{bmatrix} \boldsymbol{i} \\ \boldsymbol{j} \\ \boldsymbol{k} \end{bmatrix} \quad \text{where} \quad {}^{0}R^{i} = \begin{bmatrix} C_2C_3 & -C_2S_3 & S_2 \\ C_1S_3 - S_1S_2C_3 & C_1C_3 - S_1S_2S_3 & -S_1C_2 \\ S_1S_3 + C_1S_2C_3 & S_1C_3 - C_1S_2S_3 & C_1C_2 \end{bmatrix} \tag{2-24}$$

Euler angles $(Eu_{s1}, Eu_{s2}, Eu_{s3})$ of coordinate system s, $s = 1, 2, 3$, with $(\boldsymbol{i}_s, \boldsymbol{j}_s, \boldsymbol{k}_s)$ as a basis, relative to the lab coordinate system XYZ with $(\boldsymbol{I}, \boldsymbol{J}, \boldsymbol{K})$ as a basis (considering an XYZ rotation sequence) are

$$\begin{cases} Eu_{s2} = Sin^{-1}(\boldsymbol{I} \cdot \boldsymbol{k}_s) \\ Eu_{s1} = Cos^{-1}(\boldsymbol{K} \cdot \boldsymbol{k}_s / Cos(Eu_{s2})) \\ Eu_{s3} = Cos^{-1}(\boldsymbol{I} \cdot \boldsymbol{i}_s / Cos(Eu_{s2})) \end{cases} \qquad s=1,2,3 \tag{2-25}$$

The objective of determining the Euler angles of the link-segment model in this section is not to provide the joint's anatomical rotations, but to have a mathematical model of the segment's rotation that can be used in kinetic analysis. Therefore, slight variation of the placement of markers only changes the direction of the corresponding coordinate system. This results in an equivalent set of Euler angles, equivalent in the sense that both sets describe mathematically the motion and the kinetic variables are the same.

A total of nine Euler angles represent the seven rotational DOF of the upper limb. To conclude, it is important to note that in the link segment model presented in this research, the number of DOF are less than the number of Euler angles and that the Euler angles do not necessarily correspond to common anatomical terminology used to describe upper limb movements.

Euler angles for the illustrative experiment described in the previous section were also found. The nine Euler angles, shown in Fig. 2.7, Fig. 2.8 and Fig. 2.9, represent seven rotational DOF of the three segments. It should be noted that for the elbow and wrist joints with two DOF,

all three Euler angles are non zero (Fig. 2.8 and Fig. 2.9). While these angles can not be considered as anatomical movement, e.g., flexion/extension, there is a mapping between Euler angles and anatomical angles. Finding this mapping or arranging the markers in such a way that the mapping is an identity is an interesting and challenging subject for research [10]. However in order to perform a kinetic analysis of the upper limb, Euler angles are sufficient and appropriate.

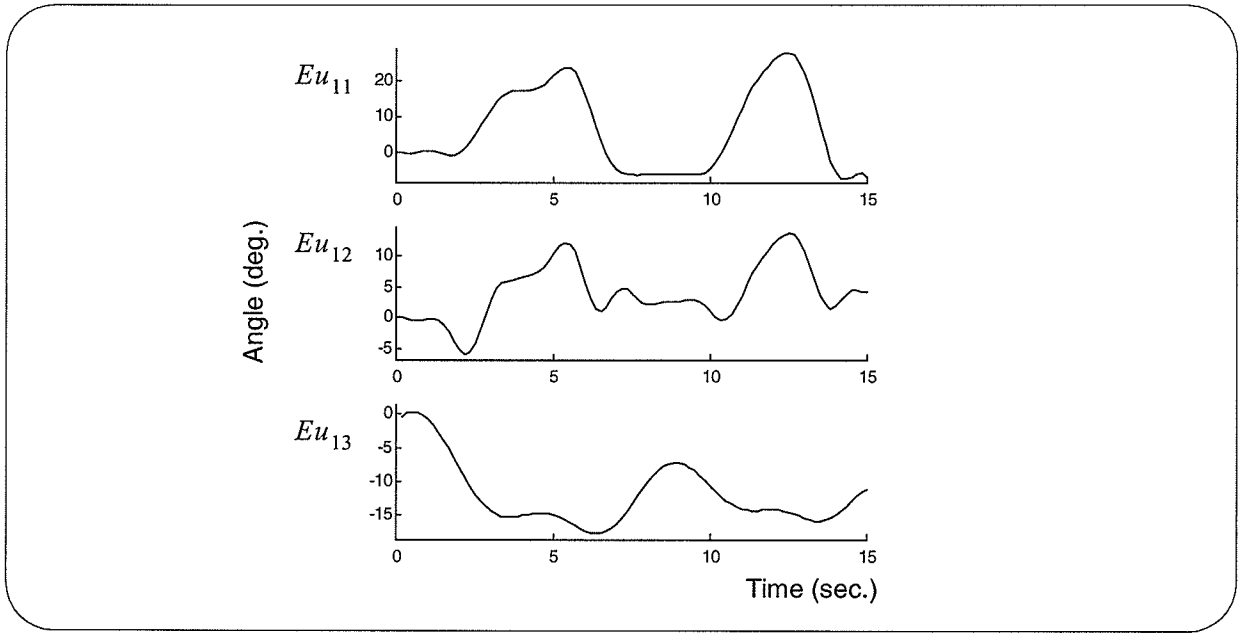

Fig. 2.7 Three Euler angles of the first coordinate system attached to the arm segment relative to the lab coordinate system.

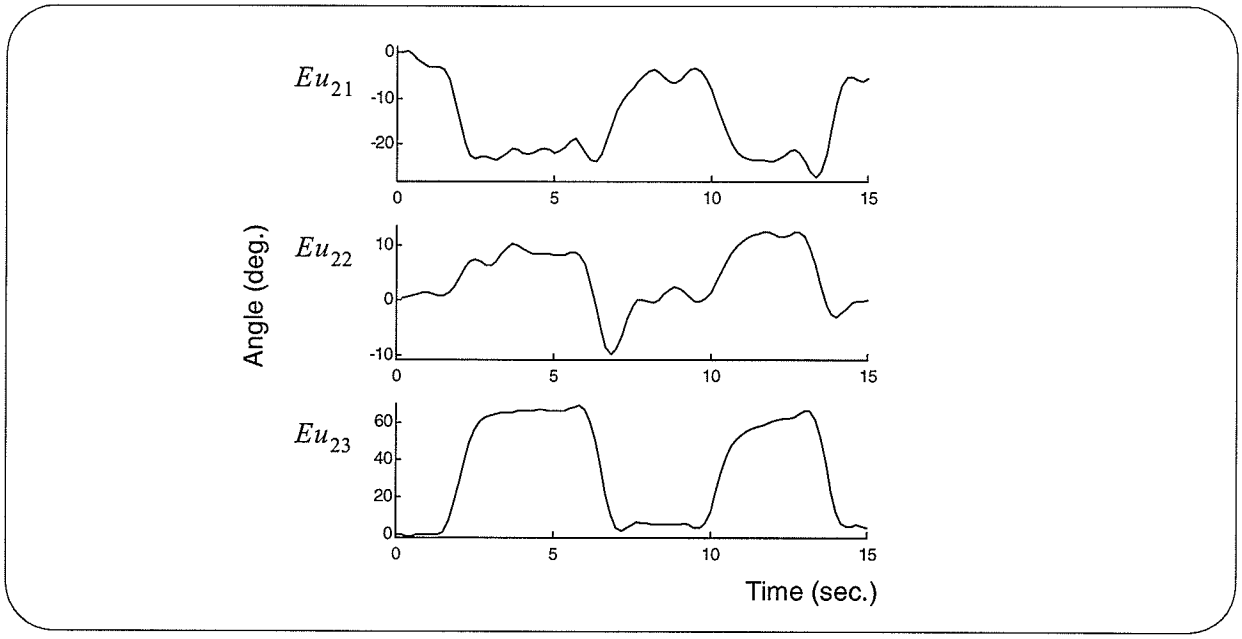

Fig. 2.8 Three Euler angles of the second coordinate system attached to the forearm segment relative to the first coordinate system attached to the arm segment.

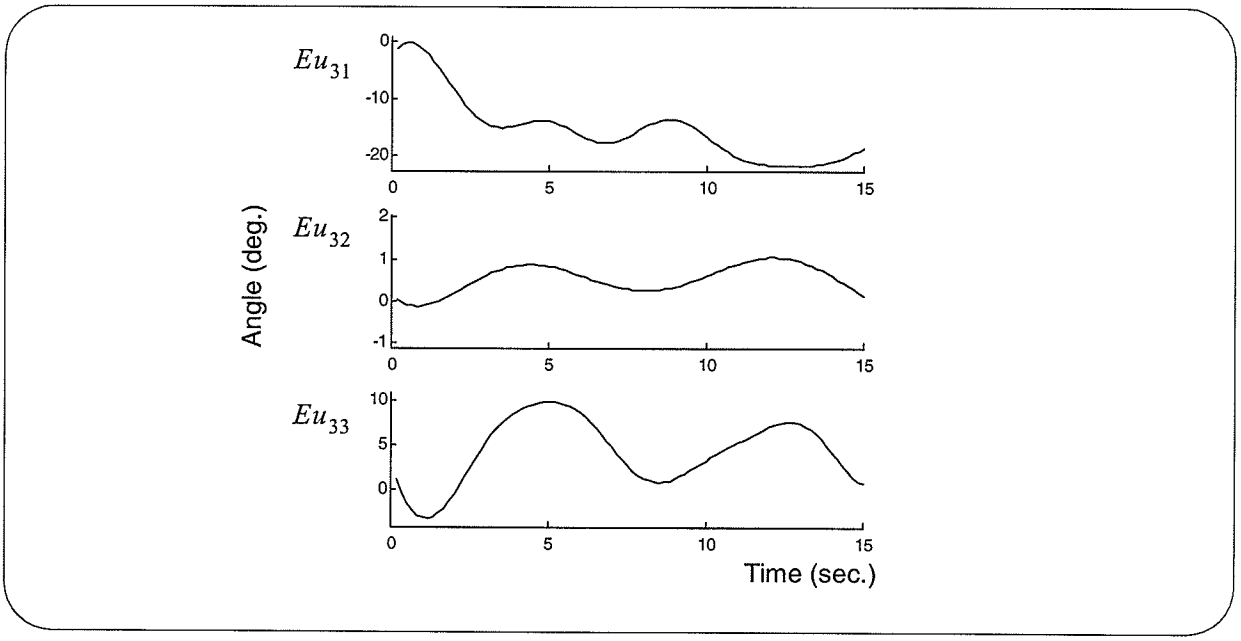

Fig. 2.9 Three Euler angles of the third coordinate system attached to the hand segment relative to the second coordinate system attached to the forearm segment.

2.4. ESTABLISHMENT OF THE KINEMATIC EQUATIONS FOR THE UPPER LIMB

To determine kinematic variables, i.e., angular and linear displacements, velocities and accelerations, of different points of the upper limb segments, kinematic equations must be established. To do so, anthropometric parameters are required. Determination of these parameters is described followed by a derivation of the kinematic equations.

For the model shown in Fig. 2.10, let L_1, L_2 and L_3 be respectively the length and m_1, m_2 and m_3 be the mass and G_1, G_2 and G_3 be the mass center of the arm, forearm and hand. From [26], these variables can be calculated on the basis of the height, H, and weight, W, of the subject:

$$\begin{cases} L_1 = 0.173H \\ L_2 = 0.16H \\ L_3 = 0.0575H \end{cases} \qquad \begin{cases} m_1 = 0.028W \\ m_2 = 0.016W \\ m_3 = 0.06W \end{cases} \tag{2-26}$$

The distances between the mass center (G_i) and the proximal joint of the segments can be calculated using the following equations [26]

$$\begin{cases} O_1G_1 = 0.463L_1 \\ O_2G_2 = 0.430L_2 \\ O_3G_3 = 0.506L_3 \end{cases} \tag{2-27}$$

Let ${}^0H^1$, ${}^1H^2$ and ${}^2H^3$ be homogeneous transformation matrices of respectively the arm, forearm and hand coordinate systems relative to the lab arm and forearm coordinate systems. They can be written as follows

$${}^0H^1 = \begin{bmatrix} {}^0R^1 & \boldsymbol{T}_1 \\ \mathbf{0}^T & 1 \end{bmatrix}, \; {}^1H^2 = \begin{bmatrix} ({}^0R^2)\,({}^0R^1)^{-1} & \boldsymbol{T}_2 \\ \mathbf{0}^T & 1 \end{bmatrix} \text{ and } {}^2H^3 = \begin{bmatrix} ({}^0R^3)\,({}^0R^2)^{-1} & \boldsymbol{T}_3 \\ \mathbf{0}^T & 1 \end{bmatrix} \tag{2-28}$$

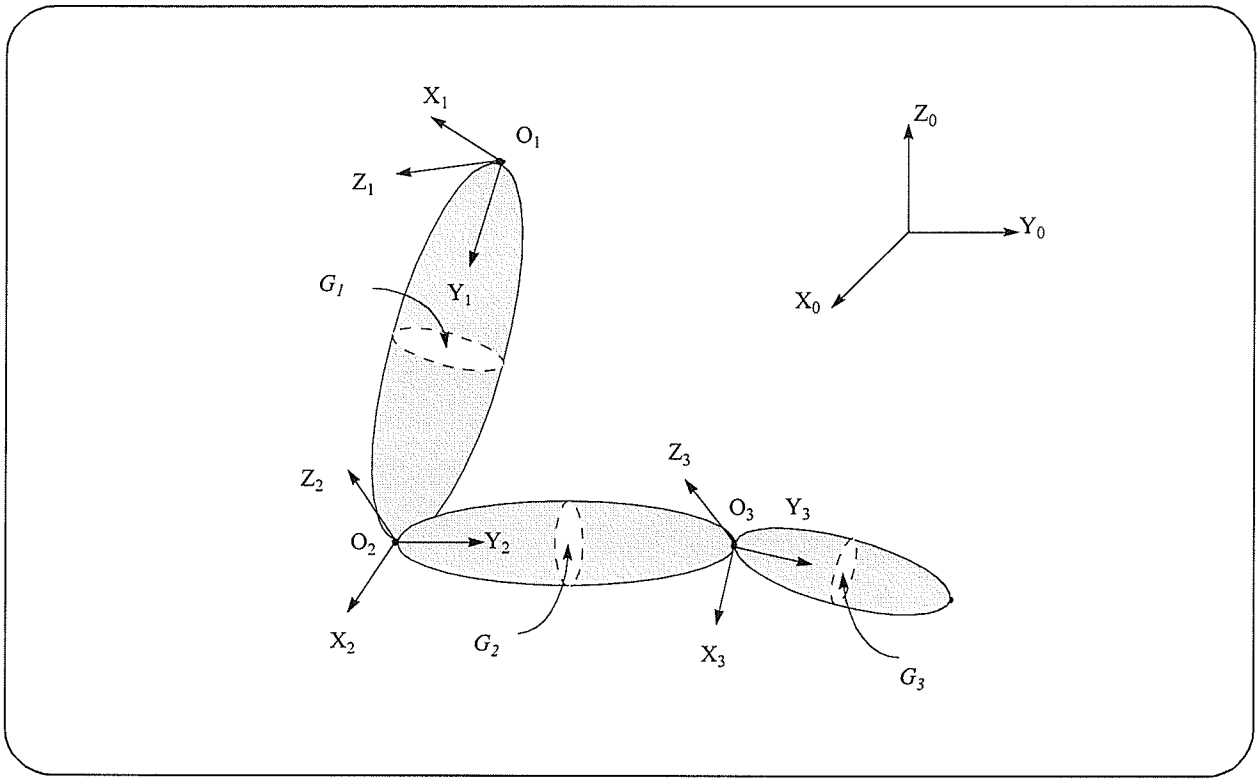

Fig. 2.10 Link-segment model of the upper limb.

where $\boldsymbol{T}_1$ is the trajectory vector of the axis of rotation of the arm segment determined using the screw axis equations given in Section 2.3.1. and

$$\begin{cases} \boldsymbol{T}_2 = [0 \quad L_1 \quad 0]^T \\ \boldsymbol{T}_3 = [0 \quad L_2 \quad 0]^T \end{cases} \tag{2-29}$$

Finally the position of the joints and mass centers in the homogenous lab coordinate system can be written as follows

$$\begin{cases} \boldsymbol{O'}_1 = \boldsymbol{T}_1 \\ \boldsymbol{G'}_1 = {}^0H^1 [0 \quad O_1G_1 \quad 0 \quad 1]^T \\ \boldsymbol{O'}_2 = {}^0H^1 [0 \quad L_1 \quad 0 \quad 1]^T \\ \boldsymbol{G'}_2 = ({}^0H^1)({}^1H^2) [0 \quad O_2G_2 \quad 0 \quad 1]^T \\ \boldsymbol{O'}_3 = ({}^0H^1)({}^1H^2) [0 \quad L_1 \quad 0 \quad 1]^T \\ \boldsymbol{G'}_2 = ({}^0H^1)({}^1H^2)({}^2H^3) [0 \quad O_3G_3 \quad 0 \quad 1]^T \end{cases} \tag{2-30}$$

The angular velocity of a segment s can be expressed as follows

$$\omega_s = \dot{Eu}_{s1}\boldsymbol{i}_1 + \dot{Eu}_{s2}\boldsymbol{j}_2 + \dot{Eu}_{s3}\boldsymbol{k}_3 = \omega_{sx}\boldsymbol{i} + \omega_{sy}\boldsymbol{j} + \omega_{sz}\boldsymbol{k} \tag{2-31}$$

where

$$\begin{cases} \omega_{sx} = C_2C_3\dot{Eu}_{s1} + S_3\dot{Eu}_{s2} \\ \omega_{sy} = -C_2S_3\dot{Eu}_{s1} + C_3\dot{Eu}_{s2} \\ \omega_{sz} = S_2\dot{Eu}_{s1} + \dot{Eu}_{s3} \end{cases} \tag{2-32}$$

Velocity and acceleration of an arbitrary point A in a segment relative to another point, e.g., B, of the segment are as follows

$$\begin{cases} \boldsymbol{V}_A = \boldsymbol{V}_B + \omega_s \otimes \boldsymbol{r}_{BA} \\ \boldsymbol{a}_A = \boldsymbol{a}_B + \dot{\omega}_s \otimes \boldsymbol{r}_{BA} + \omega_s \otimes (\omega_s \otimes \boldsymbol{r}_{BA}) \end{cases} \tag{2-33}$$

where $\otimes$ represents the cross product operator.

These velocities and accelerations are used in the kinetic equations to determine intersegmental forces and moments.

2.5. SUMMARY

In this chapter the link segment model is presented and determination of the kinematic variables necessary to do kinetic analysis is discussed. First, the center of rotation in 2D and 3D space is explained. A method to determine the trajectory of the axis of the rotation in 3D space is introduced.

A kinematic model for the upper limb in 3D space is described. The model contains ten DOF: three translational and seven rotational DOF. Using the screw axis, determination of the three translational DOF for the upper limb is explained. The seven rotational DOF are represented by nine Euler angles of the three defined coordinate systems of each segment relative to lab coordinate system. The chapter ends with the establishment of kinematic equations.

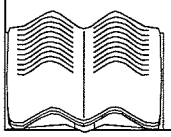

CHAPTER 3. KINEMATIC DATA SMOOTHING

3.1. INTRODUCTION

All kinematic studies utilize data obtained from some type of measurement. Most equipment for kinematic movement analysis measures position of markers affixed to body segments. Modelling errors (e.g., a joint is not a point but a surface in three dimensional space) and measurement errors (e.g., systematic errors in measurement equipment) affect the measured variables [1].

To perform dynamic analysis, the first and second derivatives of the kinematic data have to be estimated. Because the differentiation process amplifies noise, kinematic data should be smoothed before differentiation. Though error propagation effects in the calculations can be considerable, special measures can be taken to minimize them. It is necessary to include constraints to achieve meaningful derivative estimates and minimize error propagation. A suitable criterion is to assume that the movement is sufficiently smooth, i.e., it does not contain ordinarily high frequency components since this would entail extremely high inertial forces [27].

A common approach to model error is to assume that the data are corrupted by additive noise, thus the observations can be considered to be samples of a continuous random variable Y. Let Y_n be the value of Y at times t_n. The following equation

$$Y_n = f(t_n) + \varepsilon_n \qquad n = 1, 2, \ldots, N \tag{3-1}$$

is known as the regression model where $f(t_n)$ is the value of a unknown function and ε_n is a zero mean, uncorrelated random variable with variance σ^2. The function f is usually referred to as the regression function [28].

In general, there are two approaches for regression analysis, parametric and nonparametric regression. A parametric regression assumes that the form of f is known except for finitely many unknown parameters [28]. In this case the function f can be linear or nonlinear. Polynomial curve fitting is an example of linear parametric regression analysis. Parametric methods require very specific quantitative information about the regression function. Nonparametric regression analysis, such as the splines method, gives an estimate of f that allows great flexibility in the form of the regression function, relies on the qualitative information about it and lets the data speak for itself concerning the actual form of the regression function [29].

Kinematic data smoothing can be applied to the "raw" 2D motion data, to the 3D reconstructed data, or to the inputs of the kinematic equations. However as mentioned previously, due to the noise-amplification characteristic of the differentiation process it is better to perform data smoothing as close as possible to the differentiation process. In addition, kinematic data in 2D (or 3D) are expressed as xy (or xyz) coordinates of different markers over time. The question then arises whether these data components should be processed independently or not. Known and constant distances between markers might be used as constraints during the smoothing process. Imposing constraints during the smoothing process is not an easy task. Therefore in this thesis, smoothing is applied to the inputs of the kinematic equations.

For the kinematic data smoothing, four different methods were investigated: Butterworth filter as an example of a classic linear filter and one which is widely used in biomechanics; the median filter which is a simple digital technique; curve fitting representing the linear parametric regression approach; and the splines method, a nonparametric regression method. Although these are not the only methods found in the literature that could or have been applied to the kinematic data, they represent the most commonly used ones, particularly the Butterworth filter and the

splines approach. The objective of comparing these methods is to determine somewhat heuristically which approach is best suited for kinetic analysis purposes.

3.2. FOUR METHODS OF SMOOTHING

In this section the four methods of smoothing: Butterworth filter, median filter, polynomial curve fitting technique and splines method, and their characteristics are briefly explained.

The basic concept of a linear filter, of which the Butterworth filter is a classic example, is the separation of signals based on their nonoverlapping frequency content. The Butterworth filter considered here is one which has been used for biomechanical signal smoothing [26]. It is a low pass second order filter with zero-phase. Its difference equation when the sampling frequency and cutoff frequency are respectively 60 Hz and 6 Hz is

$$f(t_n) = a_1 f(t_{n-1}) + a_2 f(t_{n-2}) + b_0 Y_n + b_1 Y_{n-1} + b_2 Y_{n-2} \tag{3-2}$$

where

$$\begin{cases} a_1 = 1.1429 \\ a_2 = -0.4129 \end{cases} \qquad \begin{cases} b_0 = 0.0675 \\ b_1 = 0.135 \\ b_2 = 0.0675 \end{cases} \tag{3-3}$$

The second filter considered is the median filter which is a simple digital technique for smoothing signals. The implementation of a median filter requires a very simple digital nonlinear operation [30]. It slides a window that spans $2W+1$ points across the data with the filter output set equal to the median value of these $2W+1$ samples. Only the center point of the window is affected.

To account for start up and end effects at the two end points, W samples each are appended at the beginning and at the end of the sequence [31]. For data to pass through a median filter

unchanged means that central sample value for each window position is itself the median of the samples within the window. The only parameter of the filter is the size of window (W). Note that the output of the filter when the window size is equal to one will be the same as its input.

As an example of a commonly used linear parametric approach consider the regression function f to be approximated by a polynomial as follows

$$f(t_n) = a_0 + a_1 t_n + a_2 t_n^2 + \ldots + a_p t_n^p \tag{3-4}$$

The parameters $a_0, a_1, a_2, \ldots, a_p$ of this linear parametric regression can be selected to give the best fit using a criterion such as minimum square error (SE).

$$SE = \sum_{n=1}^{N} \left| Y_n - f(t_n) \right|^2 \tag{3-5}$$

The SE is decreased by increasing the degree of the polynomial (p). For best smoothness, not best fit, p should be chosen carefully.

The last approach is spline smoothing which is a nonparametric regression method. In this method, the goal is to find a good fit for the data which at the same time has some degree of smoothness. The natural measure of roughness (lack of smoothness) associated with a function f, is the roughness penalty [28][29] given by

$$R_m = \sum_{n=1}^{N} \left| f^{(m)}(t_n) \right|^2 \tag{3-6}$$

where $f^{(m)}$ represents *mth* derivative of the function f.

Spline smoothing is based on the weighted combination of the two criteria as follows

$$Min \{ SE + \mu R_m \} \tag{3-7}$$

for a suitably selected $m>0$ where μ is a weighting factor. The value $m=0$ results in an interpolat-

ing spline. The spline consists of local polynomials of degree not greater than *2m-1*. These polynomials are piecewise continuous at the knots (t_n) up to and including the *(2m-2)nd* derivative [27]. The case *m=2* corresponds to cubic splines, *m=3* to quintic splines, *m=4* to heptic splines and *m=5* to nonic splines [27][29]. Because in kinetic analysis only first and second derivatives of the data are necessary cubic splines are used in this research.

To obtain some feel for the efficacy of the four methods they were applied to experimental data. Fig. 3.1 shows a typical example of the raw data along with the filtered data. First and second derivatives of the filtered data are shown in Fig. 3.2. Although the outputs of four methods for the raw data (Fig. 3.1) are similar, the differences of the outputs for the derivatives (Fig. 3.2) are obvious visually. However, because the raw data is corrupted with unknown noise, it is not clear which filter produces an output that is closest to the actual values of the derivatives of the data. Thus it was decided to use a simulation model to compare these methods in order to determine which approach is best suited for the purpose of kinetic analysis.

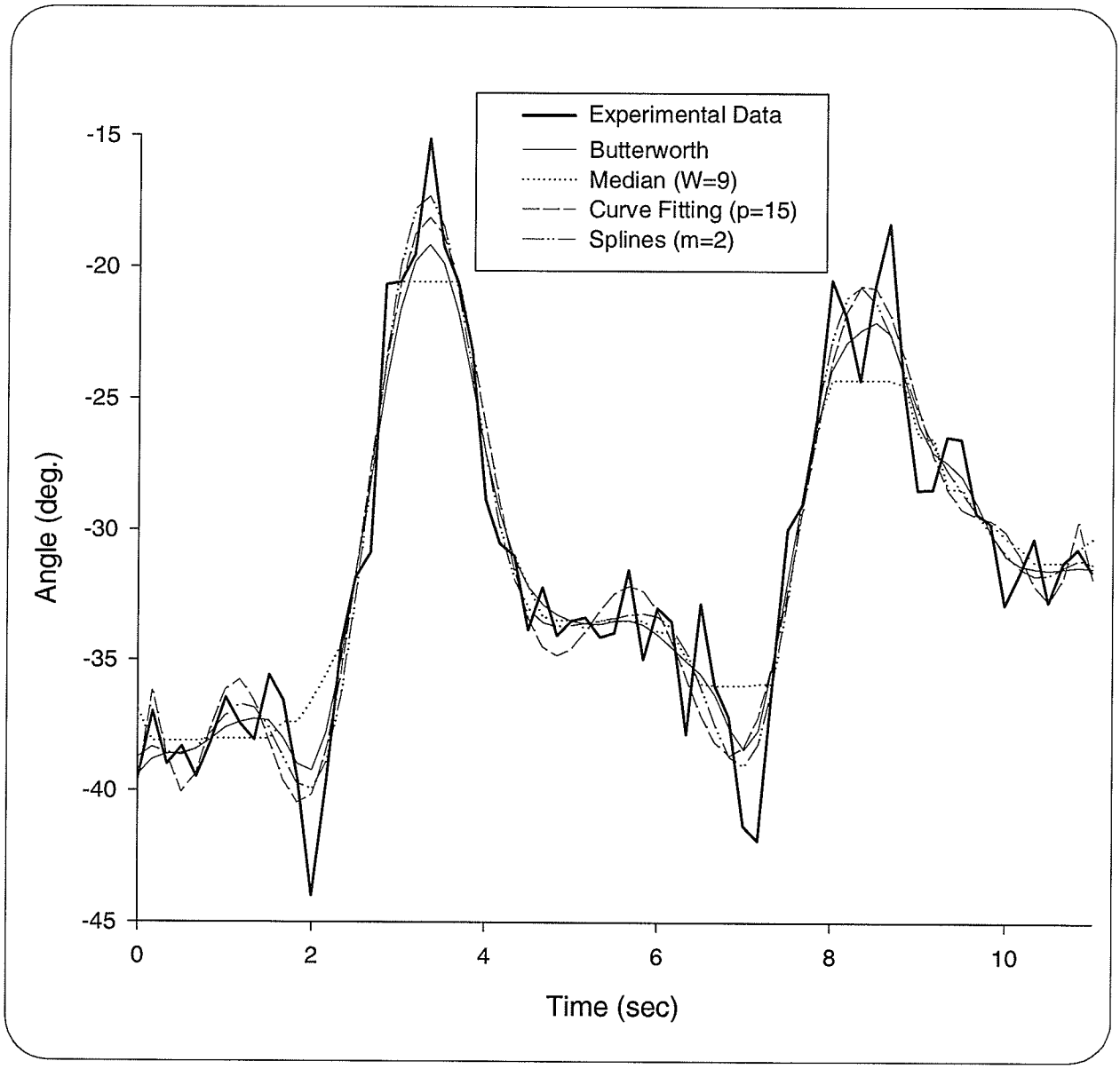

Fig. 3.1 Experimental data and smoothed data using four methods.

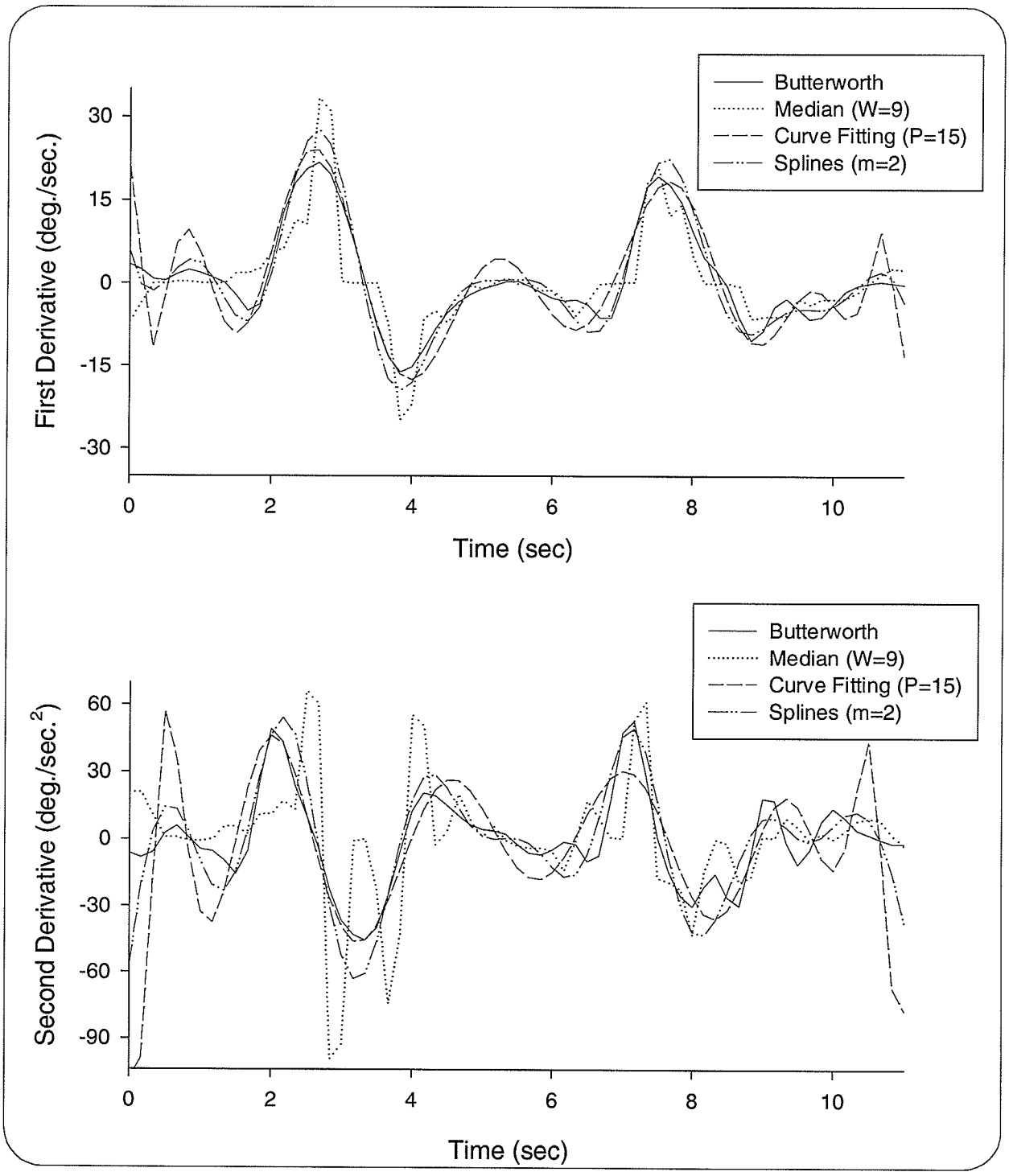

Fig. 3.2 First and second derivatives of the smoothed data using four methods.

3.3. COMPARISON AMONG FOUR METHODS OF SMOOTHING

To compare the four methods especially at the level of first and second derivatives of the data [32][33], exact values of the raw data before corruption with noise need to be known. Because the source of the noise is unknown, this is not possible to do with experimental data. However an experimental signal can be simulated. The simulated or test signal cannot be any signal, but should be a suitable representation of the class of experimental data. The next section discusses the generation of test signals to represent the class of kinematic data.

3.3.1. GENERATING THE TEST SIGNALS

A simple method to generate a test signal is to sum sinusoidal signals of different amplitude, frequency and phase as follows

$$s(t) = \sum_{i=1}^{N} A_i \sin(2\pi f_i t + \theta_i) \tag{3-8}$$

It should be noted that although this formula looks like a Fourier series, it is not necessarily a Fourier series of $s(t)$. In a Fourier series, the frequencies, f_i, are harmonically related, but here they can be any real number. Having chosen $s(t)$ to be the representation of kinematic data the first issue that needs to be resolved is what is a reasonable choice of N. Four experimental signals $z_i(t)$; $i = 1, 2, 3, 4$ were considered, and for $N = 2, 3, 4, 5, 6$, the parameters A_i, f_i and θ_i were determined using a nonlinear optimization program with a least square criterion*. The initial conditions for the A_i, f_i and θ_i were chosen as the random variables with uniform distribution over the range of $[0, 1]$, $[0, 1]$ and $[0, 2\pi]$ respectively. The range for the phase ($[0, 2\pi]$) covers all

*. "Curvefit.m" function in optimization toolbox of MATLAB package (Version 5.1) was used.

possible values. The range of $[0, 1]$ for the amplitude and frequency is a normalized range, normalized by the maximum value.

To compare the different fits the normalized mean square measure was used

$$E(z_i)\% = \frac{\int_0^T [z_i(t) - s(t)]^2 dt}{\int_0^T [z_i(t)]^2 dt} \times 100 \tag{3-9}$$

The results are tabulated in Table 3.1. The average value of the error versus N is shown in Fig. 3.3. This figure shows that after reaching $N = 3$ the error curve is almost flat and it is less than 8% which is considered to be reasonable. Therefore $N = 3$ was used for the generation of the test signals.

	$N = 2$	$N = 3$	$N = 4$	$N = 5$	$N = 6$
$E(z_1)\%$	97.3%	12.2%	9.1%	8.2%	8.0%
$E(z_2)\%$	95.3%	7.2%	6.6%	5.3%	5.2%
$E(z_3)\%$	85.3%	7.6%	7.3%	6.3%	6.2%
$E(z_4)\%$	89.1%	4.9%	3.7%	3.3%	3.0%
Average	91.7%	7.9%	6.7%	5.7%	5.6%

Table 3.1 Error of fitting test signal to four experimental data.

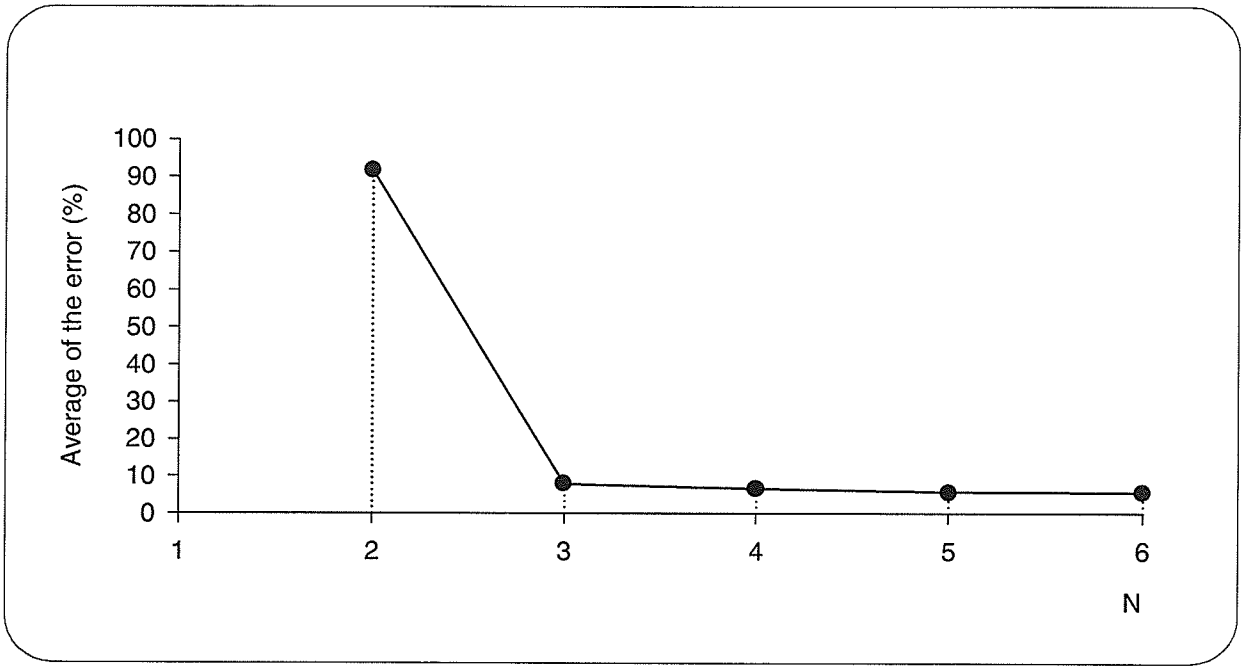

Fig. 3.3 Average value of the error versus N

3.3.2. METHOD OF COMPARISON

Ten test signals were generated as described in the previous section ($N = 3$), where A_i, f_i and θ_i are considered to be random variables with uniform distribution over the range of $[0, 1]$, $[0, 1]$ and $[0, 2\pi]$ respectively. Then noise, $n(t)$, was added to the test signal, $s(t)$.

$$x(t) = s(t) + n(t) \tag{3-10}$$

Two different noise models were chosen: Gaussian noise which, because of the central limit theorem, occurs frequently in nature, and uniform noise which in some sense is noise that is most difficult to be filtered. A signal to noise ratio of 10dB was considered, felt to be a typical experimental situation. Two other ratios were also considered: 3dB less, a doubling of noise power, and 3dB more, a halving of noise power. Therefore three different signal to noise ratios, 7dB, 10dB, 13dB were used.

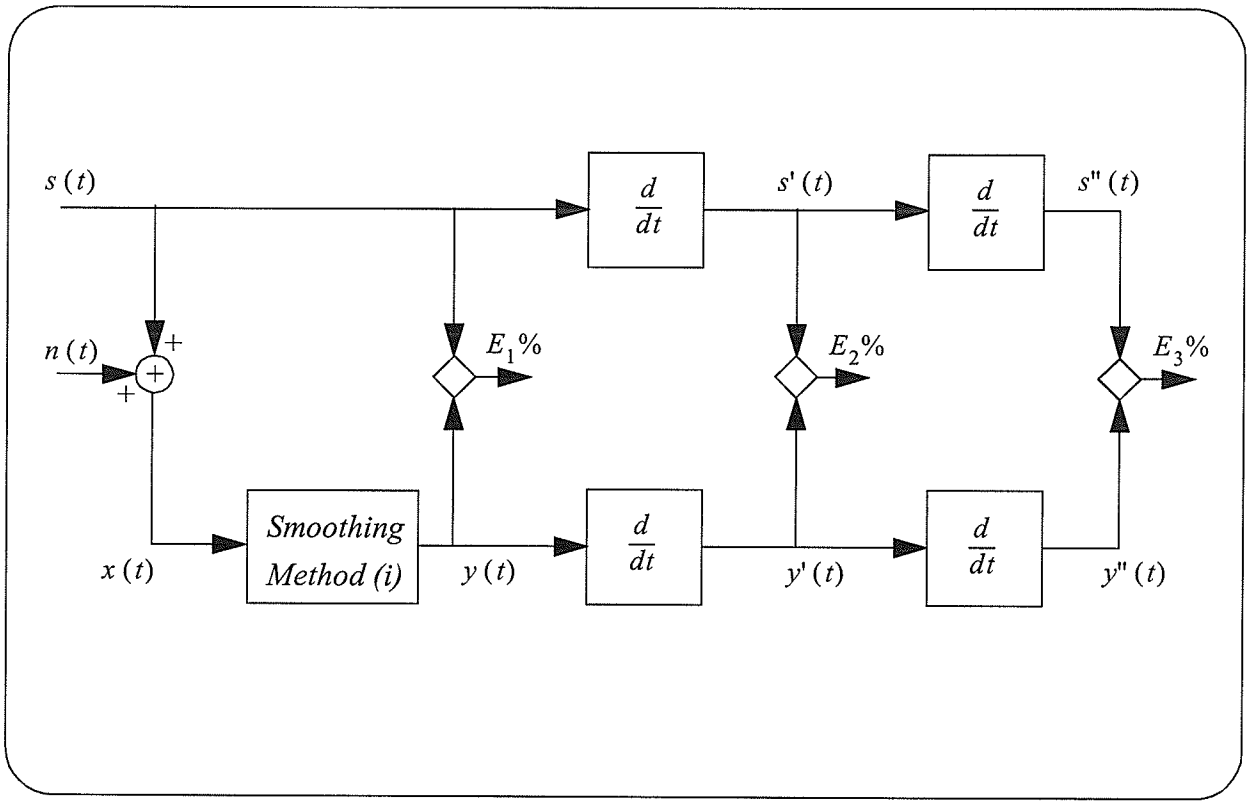

Fig. 3.4 Comparison of four smoothing methods at three levels.

Then the resultant signal, $x(t)$ was filtered using the four different approaches and compared with the test signal at three levels; raw, first derivative and second derivative of the signal as shown in Fig. 3.4. The resultant errors at each level (E_1, E_2 and E_3) were calculated using Eq. (3-9) for the ten generated test signals.

3.3.3. RESULTS OF COMPARISON

The mean and standard deviation of error at three levels of comparison are illustrated in Fig. 3.5 (first level comparison), Fig. 3.6 (second level comparison) and Fig. 3.7 (third level comparison). The numerical values of mean and standard deviation are given in Appendix B. Two things can be concluded from a visual inspection of these three figures. The first is that the median filter performs considerably poorer than any of the other three methods. The second is that for all three levels of comparison, all considered types of noise and noise levels the spline method produces the smallest error. However the difference is some situations is not that striking. Consider Fig. 3.5, with Gaussian noise and a signal to noise ratio of 13dB. The performance of splines and curve fitting is very close.

To further confirm whether the observed differences were significant or not a statistical comparison was performed. The statistical test was a two way analysis of variance (ANOVA) with a post-hoc Student-Newman-Keuls Multiple Range Test for multiple comparisons [34][35]. The level of significance was set *a priori* as $p \leq 0.05$. At the first level there was no significant difference between the splines method and the curve fitting approach (Table 3.2). At this level the splines method performed significantly better than the Butterworth filter except for the case of Gaussian noise at a signal to noise ratio of 13dB. However the results of comparison at the second and third levels (Table 3.3 and Table 3.4 respectively) showed that the performance of the splines method was significantly better than the other methods for all types of noise and noise levels. Therefore the splines method was used in this research for smoothing of kinematic data.

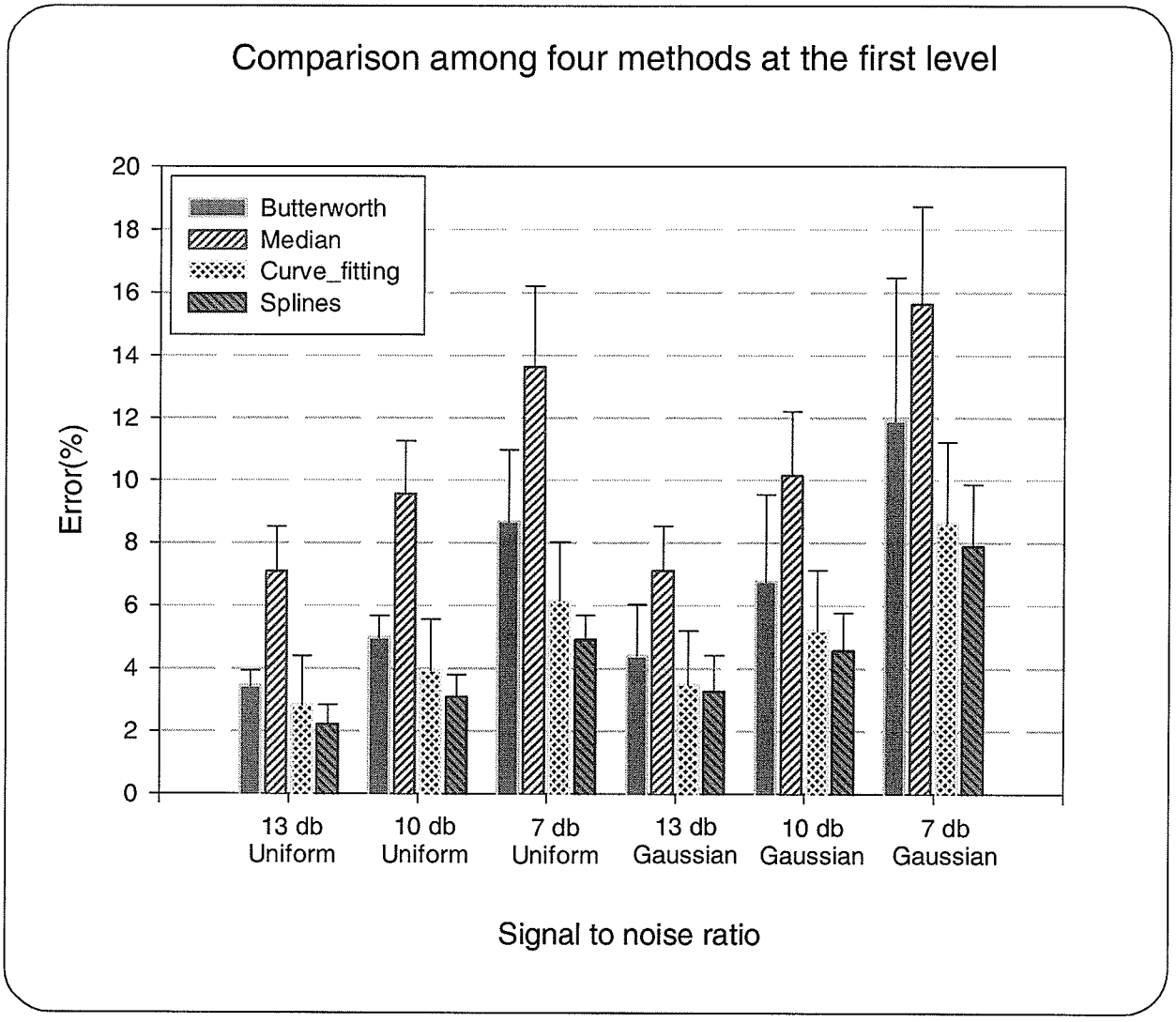

Fig. 3.5 Mean and standard deviation of error for four methods at the first level.

	Butterworth	Median	Curve Fitting
Splines	✓ ✓ ✓ ✗ ✓ ✓	✓ ✓ ✓ ✓ ✓ ✓	✗ ✗ ✗ ✗ ✗ ✗

Table 3.2 ANOVA comparison of the splines method with the other three approaches at the first level. A (✓) indicates that the splines method was significantly different. An (✗) indicates that there was no significant difference. The order here is the same as in Fig. 3.5.

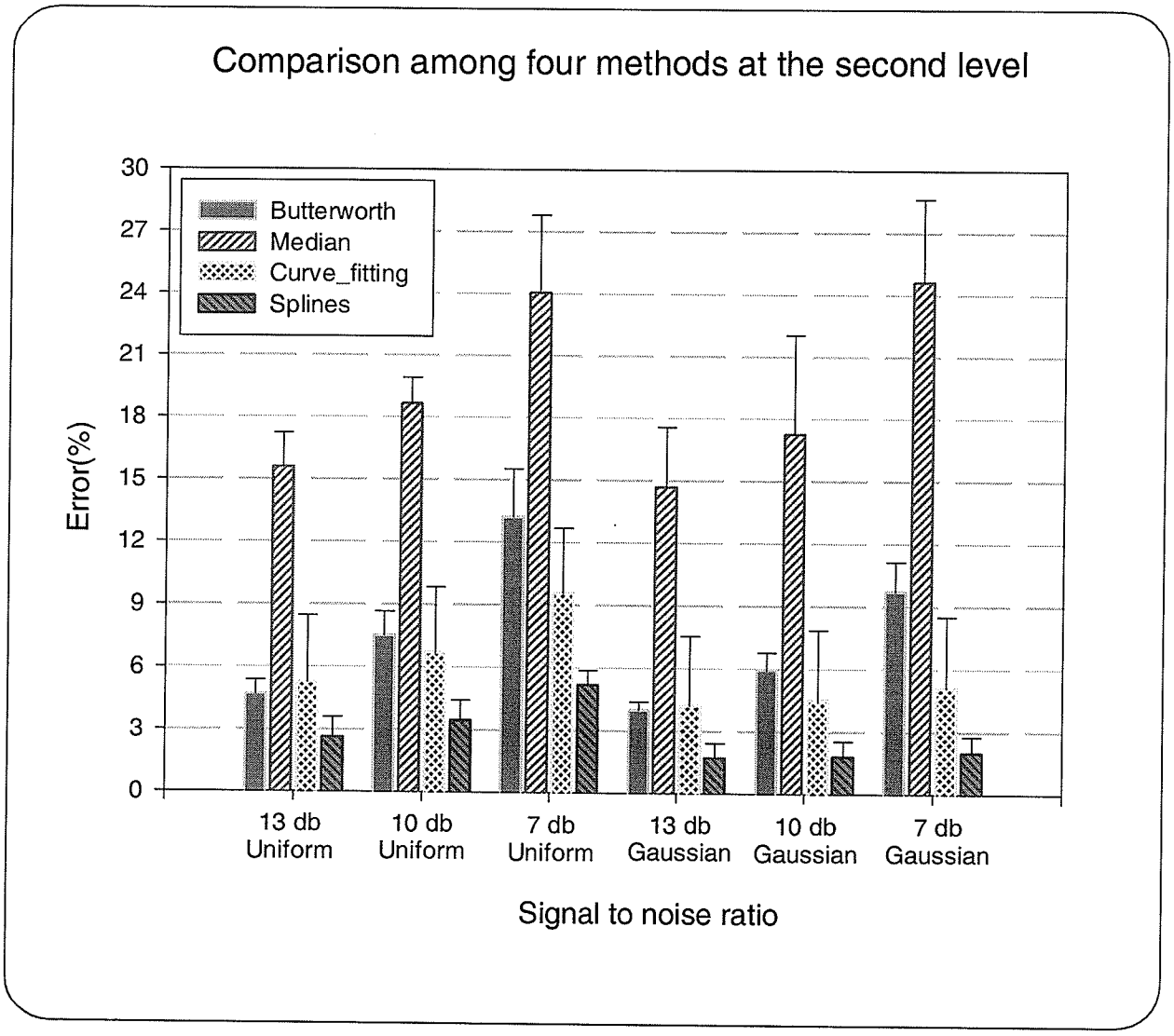

Fig. 3.6 Mean and standard deviation of error for four methods at the second level.

	Butterworth	Median	Curve Fitting
Splines	✓✓✓✓✓✓	✓✓✓✓✓✓	✓✓✓✓✓✓

Table 3.3 ANOVA comparison of the splines method with the other three approaches at the second level. A (✓) indicates that the splines method was significantly different.

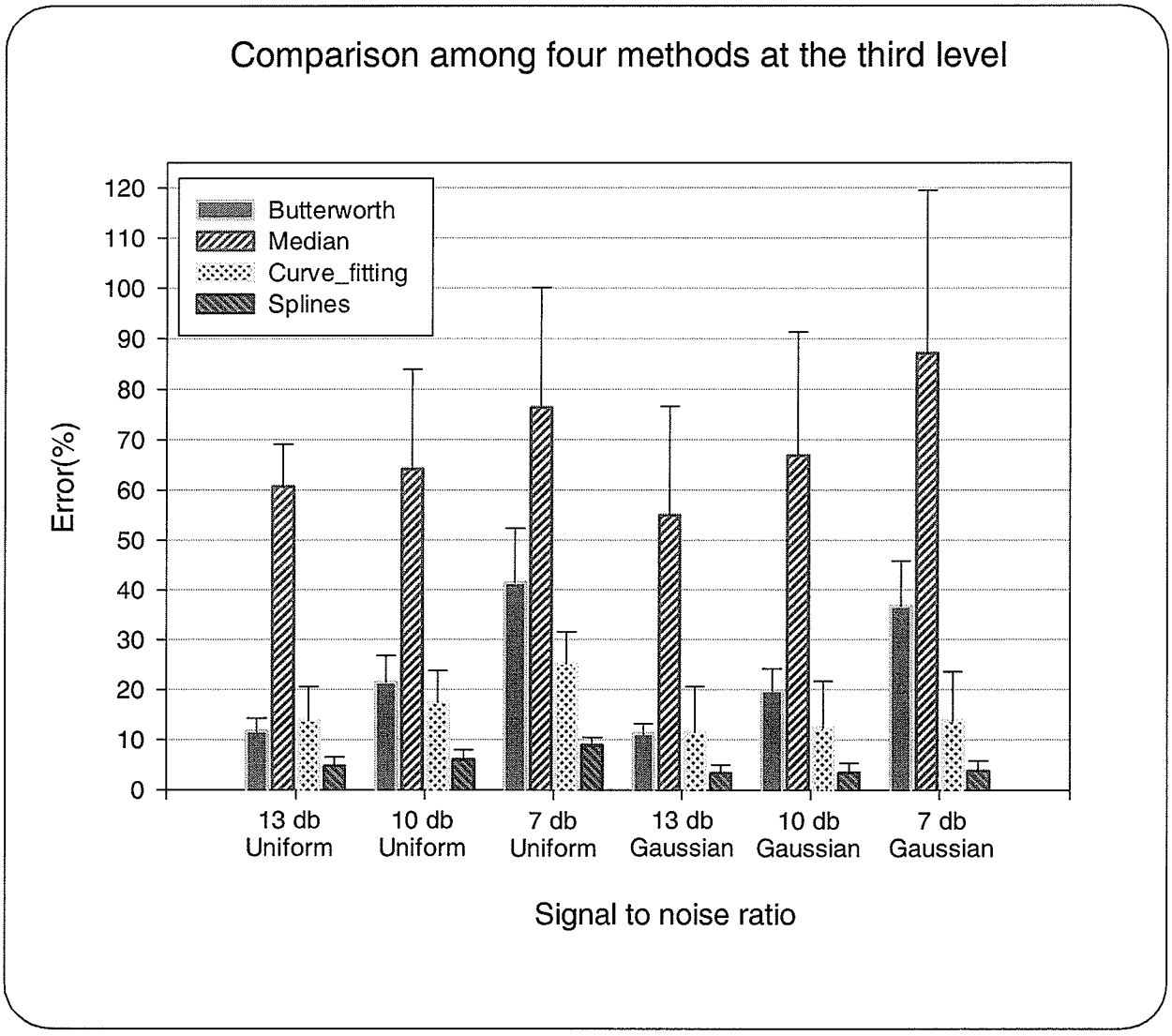

Fig. 3.7 Mean and standard deviation of error for four methods at the third level.

	Butterworth	Median	Curve Fitting
Splines	✓✓✓✓✓✓	✓✓✓✓✓✓	✓✓✓✓✓✓

Table 3.4 ANOVA comparison of the splines method with the other three approaches at the third level. A (✓) indicates that the splines method was significantly different.

3.4. SUMMARY

In kinetic analysis, not only the displacement data provided by a motion system, but also velocity (first derivative) and acceleration (second derivative) are required. Since differentiation is a process that amplifies the error in the data, it is necessary to smooth the measured data. There are no generally accepted models either for the class of signals or for computing noise. Thus a heuristic approach is necessary to design and/or evaluate the smoothing process.

This approach was adopted in this chapter where four common methods of smoothing were investigated. A heuristic model of the class of signals was determined. Based on this the performance of the four smoothing methods was investigated under two noise models via simulation.

The results indicate that overall the splines method offered the best performance, particularly at the second and third levels. Therefore for the experimental portions of the research the splines method was used.

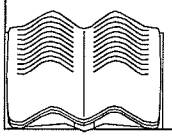

CHAPTER 4. KINETIC ANALYSIS

4.1. INTRODUCTION

There are two general problems when kinetics of a rigid body is considered [36]. The first is the direct problem where the applied forcing functions are known and one wants to determine the resultant motion of the system. The second type, the one of interest in this research, is the inverse problem. Here the motion is completely specified or known and the forcing functions that cause the motion are to be determined. In both cases, the kinetic equations of the motion may be formulated using either the Lagrangian or the Newtonian method. This chapter describes the process of generating upper limb kinetic equations. To avoid error and for confidence, the kinetic equations are developed using both methods. The two methods are, of course, related and this relationship is developed in the chapter. Formulation of the kinetic equations allows one to determine the inter-segmental forces and moments at three upper limb joints, one of the research objectives.

The kinetic equations along with the kinematic variables are also used to determine energy and power flows in the upper limb. Power can be calculated by using either the time derivative of total energy, i.e., the sum of the kinetic and potential energies or by considering the power generated or absorbed by muscles and transmitted between segments through the joints. Both methods are described later in the chapter where it is shown that if the body segments are considered to be rigid bodies then the two methods always yield the same power. Thus, contrary to some literature, discrepancies between the output of the two methods cannot be used to test the validity of the model [37] or be attributed to errors in modelling, experimental errors, kinematic errors resulting from digitizing cinefilm, movement of the markers on skin or anthropometric data [37][38][44].

The difference between the two methods only reflects computational error. The other possibility to reach different results is the wrong supination, i.e., body segments are not rigid bodies.

4.2. GOVERNING EQUATIONS

In order to develop the kinetic equations of the upper limb, the governing equations of a single segment must first be considered. For a single segment as shown in Fig. 4.1, the angular momentum about the mass center denoted by $\boldsymbol{H}_G$ is given by

$$\boldsymbol{H}_G = I\omega \tag{4-1}$$

where I is the moment of inertia matrix and ω is the angular velocity of the segment. The total force ($\boldsymbol{F}_T$) and total moments about mass center ($\boldsymbol{M}_T$) are given by

$$\begin{cases} \boldsymbol{F}_T = \boldsymbol{F}_P + \boldsymbol{F}_D - m\boldsymbol{g} \\ \boldsymbol{M}_T = \boldsymbol{M}_P + \boldsymbol{M}_D + \boldsymbol{r} \otimes \boldsymbol{F}_P + \boldsymbol{r}' \otimes \boldsymbol{F}_D \end{cases} \tag{4-2}$$

where $\otimes$ denotes cross product and

$$\boldsymbol{g} = [0 \quad 0 \quad g]^T, \quad g = 9.8\,(N/Kg) \tag{4-3}$$

The kinetic energy (KE) can be written

$$KE = TKE + RKE \tag{4-4}$$

where

$$\begin{cases} TKE = \frac{1}{2} \times m\,(\boldsymbol{V}_G \cdot \boldsymbol{V}_G) \\ RKE = \frac{1}{2} \times \omega \cdot \boldsymbol{H}_G = \frac{1}{2} \times I\omega \cdot \omega \end{cases} \tag{4-5}$$

and $\cdot$ denotes inner product. The potential energy of the segment is given by

$$PE = m\boldsymbol{g} \cdot \boldsymbol{G} \tag{4-6}$$

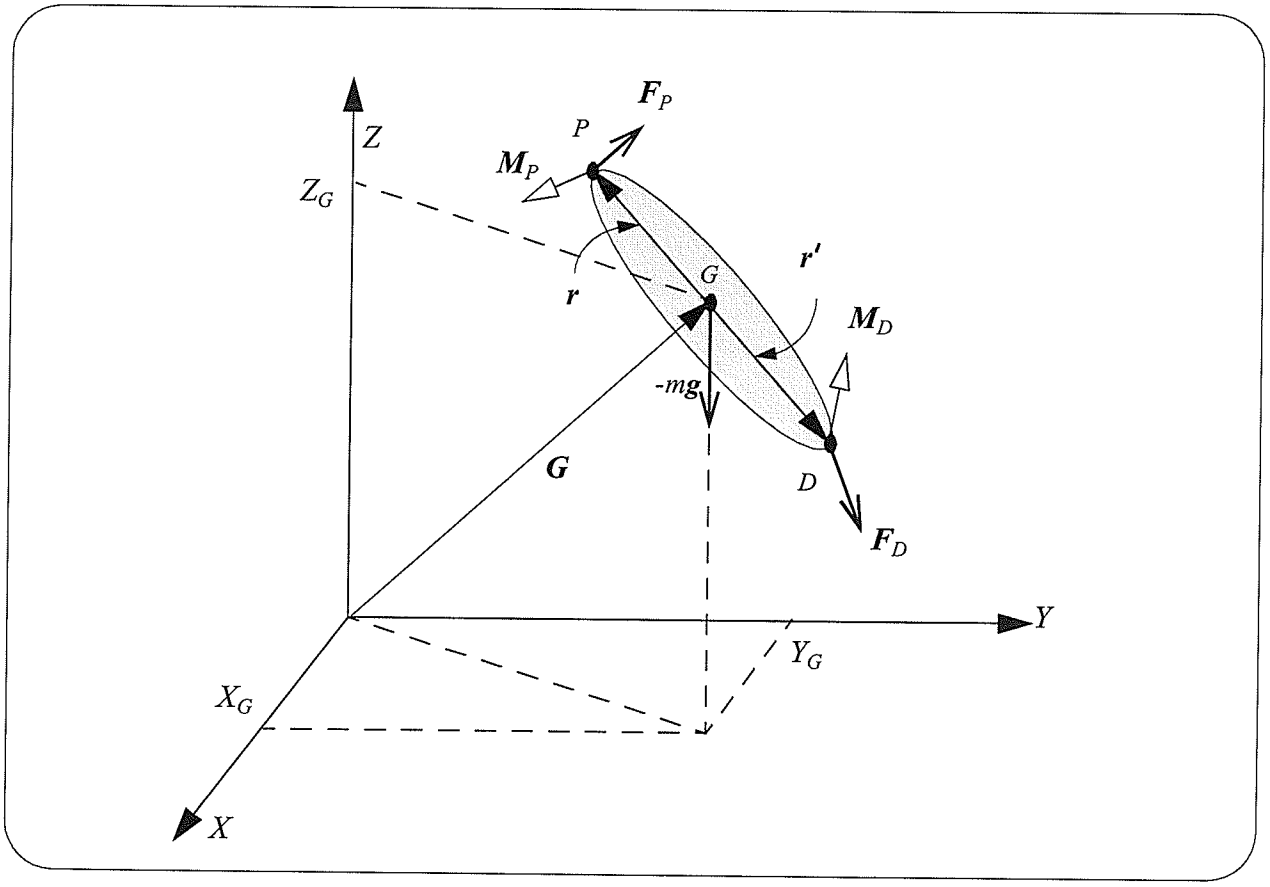

Fig. 4.1 Single segment model.

4.2.1. LAGRANGIAN METHOD

For a single segment the associated Lagrangian equation is defined as

$$L = KE - PE \tag{4-7}$$

where KE and PE are the kinetic and potential energy given by Eqs. (4-4) and (4-6). The generalized force, $\boldsymbol{Q}$, for a segment with six degrees of freedom, $\boldsymbol{q}$, (i.e., three Euler angles and three coordinates of mass center)

$$\boldsymbol{q} = [q_1 \quad q_2 \quad q_3 \quad q_4 \quad q_5 \quad q_6]^T \tag{4-8}$$

is $$\boldsymbol{Q} = [Q_1 \quad Q_2 \quad Q_3 \quad Q_4 \quad Q_5 \quad Q_6]^T \tag{4-9}$$

given by $$\boldsymbol{Q} = \sum_i \left[\left(D_{X_i}\right)^T \boldsymbol{F}_{X_i}\right] + \sum_j \left[(J)^T \boldsymbol{M}_{X_j}\right] \tag{4-10}$$

where X_i and X_j are the points where, respectively, the external forces and moments are applied. D_{X_i} and J can be found using the following set of equations

$$\begin{cases} \boldsymbol{V}_{X_j} = D_{X_j}\dot{\boldsymbol{q}} \\ \omega = J\dot{\boldsymbol{q}} \end{cases} \tag{4-11}$$

Lagrange's equations are expressed by

$$\frac{\partial}{\partial t}\left(\frac{\partial L}{\partial \dot{q}_i}\right) - \frac{\partial L}{\partial q_i} = Q_i \qquad i = 1, 2, \ldots, 6 \tag{4-12}$$

For the upper limb model shown in Fig. 4.2, let $\boldsymbol{p}_1$, $\boldsymbol{p}_2$ and $\boldsymbol{p}_3$ be the Euler angle vectors respectively related to the arm, forearm and hand be written as follows

$$\begin{cases} \boldsymbol{p}_1 = [Eu_{11} \quad Eu_{12} \quad Eu_{13}]^T \\ \boldsymbol{p}_2 = [Eu_{21} \quad Eu_{22} \quad Eu_{23}]^T \\ \boldsymbol{p}_3 = [Eu_{31} \quad Eu_{32} \quad Eu_{33}]^T \end{cases} \tag{4-13}$$

Using Eqs. (4-4), (4-6) and (4-7), the left hand side of Lagrange's equations can be written

$$\frac{\partial}{\partial t}\left(\frac{\partial L}{\partial \dot{\boldsymbol{p}}_s}\right) - \frac{\partial L}{\partial \boldsymbol{p}_s} = \Re(\omega_s)\boldsymbol{I}_s + \Re(\boldsymbol{V}_s)\boldsymbol{m}_s + \aleph_s \qquad s = 1, 2, 3 \tag{4-14}$$

The operators $\Re$ and $\aleph$ are defined as

$$\Re(\boldsymbol{u}_s) \equiv \begin{bmatrix} L(u_x, Eu_{s1}) & L(u_y, Eu_{s1}) & L(u_z, Eu_{s1}) \\ L(u_x, Eu_{s2}) & L(u_y, Eu_{s2}) & L(u_z, Eu_{s2}) \\ L(u_x, Eu_{s3}) & L(u_y, Eu_{s3}) & L(u_z, Eu_{s3}) \end{bmatrix} \tag{4-15}$$

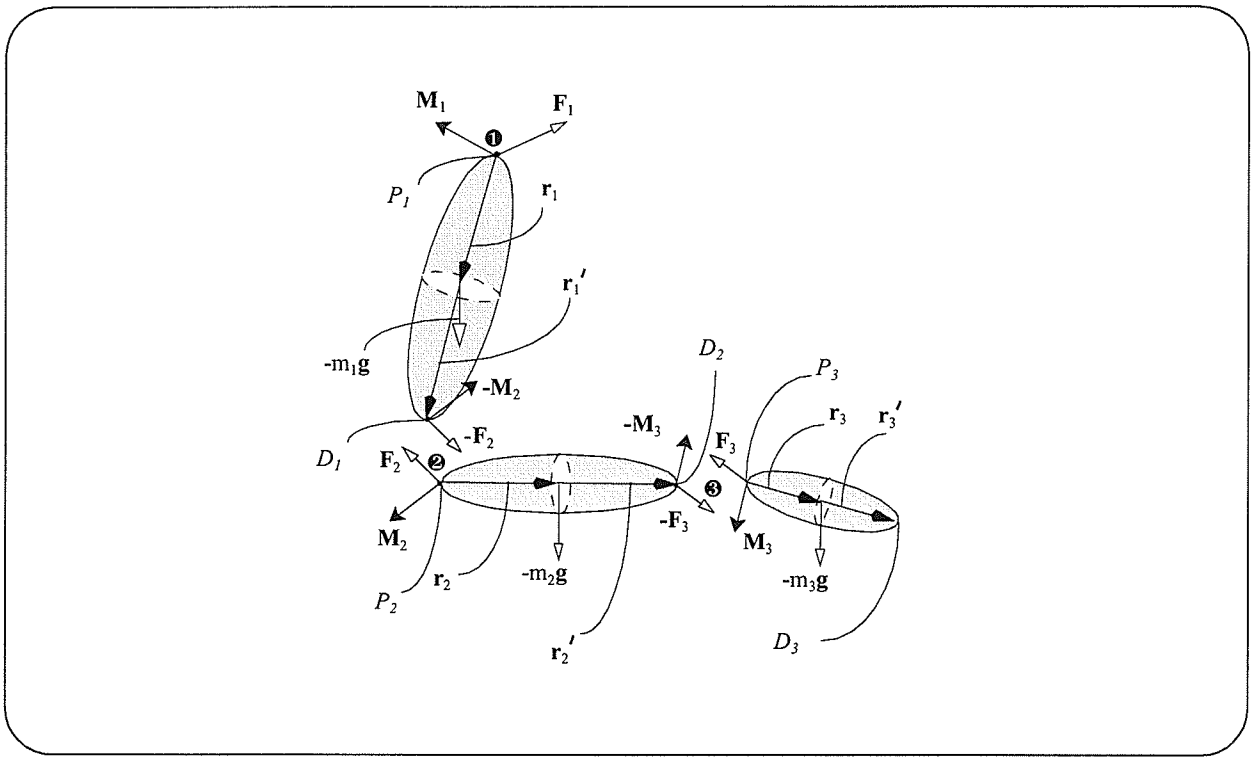

Fig. 4.2 The upper limb model consisting of three segments.

$$\aleph_s \equiv m_s \left(\frac{\partial \boldsymbol{r}_s}{\partial \boldsymbol{p}_s} \right)^T \boldsymbol{g} \tag{4-16}$$

where

$$L(v, Eu_{ij}) \equiv \frac{\partial^2 v}{\partial t \partial Eiu_{ij}} v + \frac{\partial v}{\partial Eiu_{ij}} \dot{v} - \frac{\partial v}{\partial Eu_{ij}} v \tag{4-17}$$

In Eq. (4-14) $\boldsymbol{I}_s = [I_{sx} \quad I_{sy} \quad I_{sz}]^T$, $\boldsymbol{m}_s = [m_s \quad m_s \quad m_s]^T$ where I_{sx}, I_{sy}, I_{sz} and m_s are respectively the moment of inertia about the x, y, z axes and the mass of segment s.

Using Eq. (4-10), the generalized forces which are the right hand side of the Lagrange's equations for each segment, can be written as follows

$$\begin{cases} \boldsymbol{Q}_1 = J_1^T(\boldsymbol{M}_1 - \boldsymbol{M}_2) \\ \boldsymbol{Q}_2 = J_2^T(\boldsymbol{M}_2 - \boldsymbol{M}_3) \\ \boldsymbol{Q}_3 = J_3^T\boldsymbol{M}_3 \end{cases} \tag{4-18}$$

Finally the total moments about shoulder joint, elbow joint and wrist joint can be written

$$\boldsymbol{M}_3 = \bar{J}_3^T\{\Re(\omega_3)\boldsymbol{I}_3 + \Re(\boldsymbol{V}_3)\boldsymbol{m}_3 + \aleph_3\} \tag{4-19}$$

$$\boldsymbol{M}_2 = \boldsymbol{M}_3 + \bar{J}_2^T\{\Re(\omega_2)\boldsymbol{I}_2 + \Re(\boldsymbol{V}_2)\boldsymbol{m}_2 + \aleph_2\} \tag{4-20}$$

$$\boldsymbol{M}_1 = \boldsymbol{M}_3 + \boldsymbol{M}_2 + \bar{J}_1^T\{\Re(\omega_1)\boldsymbol{I}_1 + \Re(\boldsymbol{V}_1)\boldsymbol{m}_1 + \aleph_1\} \tag{4-21}$$

where $\bar{J}_n^T = \left(J_n^{-1}\right)^T$.

4.2.2. NEWTONIAN METHOD

Newton's first and second laws are expressed by

$$\begin{cases} \boldsymbol{F}_T = \dfrac{d\boldsymbol{P}}{dt} \\ \boldsymbol{M}_T = \dfrac{d\boldsymbol{H}}{dt} \end{cases} \text{ where } \begin{cases} \boldsymbol{P} = m\boldsymbol{V}_G \\ \boldsymbol{H} = I\omega \end{cases} \tag{4-22}$$

where $\boldsymbol{V}_G$ is the velocity of mass center and

$$\frac{d\boldsymbol{H}}{dt} = \frac{\partial}{\partial t}(I\omega) = I\dot{\omega} + \omega \otimes I\omega \tag{4-23}$$

Considering the three link-segment model shown in Fig. 4.2 and Eq. (4-22), Newton's equations for the hand are given by

$$\begin{cases} \boldsymbol{F}_{T_3} = m_3\boldsymbol{a}_{G_3} \\ \boldsymbol{M}_{T_3} = \dot{\boldsymbol{H}}_3 \end{cases} \tag{4-24}$$

where

$$\begin{cases} \boldsymbol{F}_{T_3} = \boldsymbol{F}_3 - m_3\boldsymbol{g} \\ \boldsymbol{M}_{T_3} = \boldsymbol{M}_3 - \boldsymbol{r}_3 \otimes \boldsymbol{F}_3 \end{cases} \tag{4-25}$$

Using Eqs. (4-23), (4-24) and (4-25), the moment about the wrist joint can be written as

$$\boldsymbol{M}_3 = I_3\dot{\omega}_3 + \omega_3 \otimes I_3\omega_3 + \boldsymbol{r}_3 \otimes m_3\boldsymbol{a}_{G_3} + \boldsymbol{r}_3 \otimes m_3\boldsymbol{g} \tag{4-26}$$

For the elbow, Newton's equations are

$$\begin{cases} \boldsymbol{F}_{T_2} = m_2\boldsymbol{a}_{G_2} \\ \boldsymbol{M}_{T_2} = \dot{\boldsymbol{H}}_2 \end{cases} \tag{4-27}$$

where

$$\begin{cases} \boldsymbol{F}_{T_2} = \boldsymbol{F}_2 - \boldsymbol{F}_3 - m_2\boldsymbol{g} \\ \boldsymbol{M}_{T_2} = \boldsymbol{M}_2 - \boldsymbol{M}_3 - \boldsymbol{r}_2 \otimes \boldsymbol{F}_2 - \boldsymbol{r'}_2 \otimes \boldsymbol{F}_3 \end{cases} \tag{4-28}$$

Using Eqs. (4-24), (4-25), (4-26), (4-27) and (4-28), the moment about the elbow joint is expressed by

$$\begin{aligned} \boldsymbol{M}_2 &= \boldsymbol{M}_3 + I_2\dot{\omega}_2 + \omega_2 \otimes I_2\omega_2 + \boldsymbol{r}_2 \otimes m_2\boldsymbol{a}_{G_2} + \boldsymbol{r}_2 \otimes m_2\boldsymbol{g} + \boldsymbol{r'}_2 \otimes m_3\boldsymbol{a}_{G_3} + \boldsymbol{r'}_2 \otimes m_3\boldsymbol{g} \\ &= I_3\dot{\omega}_3 + \omega_3 \otimes I_3\omega_3 + \boldsymbol{r}_3 \otimes m_3\boldsymbol{a}_{G_3} + \boldsymbol{r}_3 \otimes m_3\boldsymbol{g} + \\ &\quad I_2\dot{\omega}_2 + \omega_2 \otimes I_2\omega_2 + \boldsymbol{r}_2 \otimes m_2\boldsymbol{a}_{G_2} + \boldsymbol{r}_2 \otimes m_2\boldsymbol{g} + \boldsymbol{r'}_2 \otimes m_3\boldsymbol{a}_{G_3} + \boldsymbol{r'}_2 \otimes m_3\boldsymbol{g} \end{aligned} \tag{4-29}$$

In the same way, the generated moment about the shoulder joint can be written as follows

$$\begin{aligned} \boldsymbol{M}_1 &= \boldsymbol{M}_3 + \boldsymbol{M}_2 + I_1\dot{\omega}_1 + \omega_1 \otimes I_1\omega_1 + \boldsymbol{r}_1 \otimes m_1\boldsymbol{a}_{G_1} + \boldsymbol{r}_1 \otimes m_1\boldsymbol{g} + \boldsymbol{r'}_1 \otimes m_2\boldsymbol{a}_{G_2} + \boldsymbol{r'}_1 \otimes m_2\boldsymbol{g} \\ &= I_3\dot{\omega}_3 + \omega_3 \otimes I_3\omega_3 + \boldsymbol{r}_3 \otimes m_3\boldsymbol{a}_{G_3} + \boldsymbol{r}_3 \otimes m_3\boldsymbol{g} + \\ &\quad I_2\dot{\omega}_2 + \omega_2 \otimes I_2\omega_2 + \boldsymbol{r}_2 \otimes m_2\boldsymbol{a}_{G_2} + \boldsymbol{r}_2 \otimes m_2\boldsymbol{g} + \boldsymbol{r'}_2 \otimes m_3\boldsymbol{a}_{G_3} + \boldsymbol{r'}_2 \otimes m_3\boldsymbol{g} + \\ &\quad I_1\dot{\omega}_1 + \omega_1 \otimes I_1\omega_1 + \boldsymbol{r}_1 \otimes m_1\boldsymbol{a}_{G_1} + \boldsymbol{r}_1 \otimes m_1\boldsymbol{g} + \boldsymbol{r'}_1 \otimes m_2\boldsymbol{a}_{G_2} + \boldsymbol{r'}_1 \otimes m_2\boldsymbol{g} \end{aligned} \tag{4-30}$$

Next, it is shown that the Eqs. (4-28), (4-29) and (4-30) (Newtonian method) are equivalent to Eqs. (4-19), (4-20) and (4-21) (Lagrangian method), as one would expect.

4.2.3. RELATIONSHIP BETWEEN NEWTON'S AND LAGRANGE'S EQUATIONS

First, the relationship between the cross product in "Newtonian space" and the derivative with respect to the generalized coordinates in "Lagrangian space" needs to be found. Consider two vectors $\boldsymbol{X}$ and $\boldsymbol{Y}$ fixed in a coordinate system rotating with angular velocity ω with respect to a global coordinate system with rotation matrix J. The angular velocity, ω, can be expressed as follows

$$\omega = J\dot{\boldsymbol{p}} \tag{4-31}$$

where for the XYZ sequence rotation, matrix J is

$$J = \begin{bmatrix} C_2C_3 & S_3 & 0 \\ -C_2S_3 & C_3 & 0 \\ S_2 & 0 & 1 \end{bmatrix} \tag{4-32}$$

Now, consider the cross product of the two vectors $\boldsymbol{X}$ and $\boldsymbol{Y}$

$$\begin{aligned}
\boldsymbol{X}\otimes\boldsymbol{Y} &= (\omega\omega^T)^{-1}\omega\omega^T(\boldsymbol{X}\otimes\boldsymbol{Y}) \\
&= [(\omega\omega^T)^{-1}\omega]\,\omega^T(\boldsymbol{X}\otimes\boldsymbol{Y}) \\
&= [(\omega\omega^T)^{-1}\omega]\,\omega\cdot(\boldsymbol{X}\otimes\boldsymbol{Y}) \\
&= [(\omega\omega^T)^{-1}\omega]\,(\omega\otimes\boldsymbol{X})\cdot\boldsymbol{Y} \\
&= [(\omega\omega^T)^{-1}\omega]\,\dot{\boldsymbol{X}}\boldsymbol{Y} \\
&= [(\omega\omega^T)^{-1}\omega]\left(\frac{\partial\boldsymbol{X}}{\partial\boldsymbol{p}}\dot{\boldsymbol{p}}\right)^T\boldsymbol{Y} \\
&= [(\omega\omega^T)^{-1}\omega]\left(\frac{\partial\boldsymbol{X}}{\partial\boldsymbol{p}}J^{-1}\omega\right)^T\boldsymbol{Y} \\
&= [(\omega\omega^T)^{-1}\omega]\,\omega^TJ^{-T}\left(\frac{\partial\boldsymbol{X}}{\partial\boldsymbol{p}}\right)^T\boldsymbol{Y} \\
&= [(\omega\omega^T)^{-1}(\omega\omega^T)]J^{-T}\left(\frac{\partial\boldsymbol{X}}{\partial\boldsymbol{p}}\right)^T\boldsymbol{Y} \\
&= J^{-T}\left(\frac{\partial\boldsymbol{X}}{\partial\boldsymbol{p}}\right)^T\boldsymbol{Y}
\end{aligned} \tag{4-33}$$

Therefore, $$J^T(\boldsymbol{X}\otimes\boldsymbol{Y}) = \left(\frac{\partial \boldsymbol{X}}{\partial \boldsymbol{p}}\right)^T \boldsymbol{Y} \tag{4-34}$$

Let $\boldsymbol{X} = \omega$

$$\left(\frac{\partial \boldsymbol{X}}{\partial \boldsymbol{p}}\right)^T \boldsymbol{Y} = \left(\frac{\partial \omega}{\partial \boldsymbol{p}}\right)^T \boldsymbol{Y} = \left[\frac{\partial}{\partial \boldsymbol{p}}(J\dot{\boldsymbol{p}})\right]^T \boldsymbol{Y} = \left(\frac{\partial J}{\partial \boldsymbol{p}}\dot{\boldsymbol{p}}\right)^T \boldsymbol{Y} = \dot{J}^T \boldsymbol{Y} \tag{4-35}$$

and using Eq. (4-34)

$$J^T(\omega\otimes\boldsymbol{Y}) = \dot{J}^T \boldsymbol{Y} \tag{4-36}$$

Consider the moment about the wrist joint obtained by the Lagrangian method (Eq. (4-19), page 52) and that obtained by the Eulerian method (Eq. (4-26), page 53).

$$\boldsymbol{M}_3 = \bar{J}_3^T\{\Re(\omega_3)\boldsymbol{I}_3 + \Re(\boldsymbol{V}_3)\boldsymbol{m}_3 + \aleph_3\} \qquad \text{[from page 52] (4-19)}$$

$$\boldsymbol{M}_3 = I_3\dot{\omega}_3 + \omega_3\otimes I_3\omega_3 + \boldsymbol{r}_3\otimes m_3\boldsymbol{a}_{G_3} + \boldsymbol{r}_3\otimes m_3\boldsymbol{g} \qquad \text{[from page 53] (4-26)}$$

After some algebric manipulation, the first term in Eq. (4-19) can be written as follows

$$\bar{J}_3^T\Re(\omega_3)\boldsymbol{I}_3 = I_3\dot{\omega}_3 + \bar{J}_3^T\dot{J}^T{}_3 I_3\omega_3 - \bar{J}_3^T\left(\frac{\partial \omega_3}{\partial \boldsymbol{p}_3}\right)^T \omega_3\boldsymbol{I}_3 \tag{4-37}$$

Note that boldface $\boldsymbol{I}_3 = [I_x \quad I_y \quad I_z]^T$, whereas I_3 is a 3×3 matrix of moment of inertia.

In Eq. (4-36), let $\boldsymbol{Y} = I_3\omega_3$, then

$$\omega_3\otimes[I_3\omega_3] = \bar{J}_3^T\dot{J}^T{}_3 I_3\omega_3 \tag{4-38}$$

The right hand side of Eq. (4-38) is the same as second term on the right hand side of Eq. (4-37).

In Eq. (4-34), if $\boldsymbol{X} = \omega_3$ and $\boldsymbol{Y} = \omega_3$, it follows that

$$J_3^{-T}\left(\frac{\partial \omega_3}{\partial \dot{p}_3}\right)^T \omega_3 = [0]_{3\times 1} \tag{4-39}$$

By substitution of Eqs. (4-38) and (4-39) in Eq. (4-37), the first term of Eq. (4-19) equals the first and second term of Eq. (4-26).

Now consider the second term in Eq. (4-19).

$$\begin{aligned} \Re(V_3)\, m_3 &= \Re(\dot{r}_3)\, m_3 = m_3\left(\frac{\partial^2 \dot{r}_3}{\partial t \partial \dot{p}_3}\right)^T \dot{r}_3 + m_3\left(\frac{\partial \dot{r}_3}{\partial \dot{p}_3}\right)^T \ddot{r}_3 - m_3\left(\frac{\partial \dot{r}_3}{\partial p_3}\right)^T \dot{r}_3 \\ &= m_3\left\{\frac{\partial}{\partial t}\left[\left(\frac{\partial \dot{r}_3}{\partial \dot{p}_3}\right)^T \dot{r}_3\right] - \left(\frac{\partial \dot{r}_3}{\partial p_3}\right)^T \dot{r}_3\right\} \end{aligned} \tag{4-40}$$

Using Eq. (4-34), it is obvious that

$$\left(\frac{\partial \dot{r}_3}{\partial p_3}\right)^T \dot{r}_3 = [0]_{3\times 1} \tag{4-41}$$

$$\dot{r}_3 = \omega_3 \otimes r_3 = J_3 \dot{p}_3 \otimes r_3 = -r_3 \otimes J_3 \dot{p}_3 \tag{4-42}$$

In the Eq. (4-40), let $-r_3 = X$ and $J_3\dot{p}_3 = Y$. Therefore, using Eq. (4-34), one can write Eq. (4-40) as follows

$$J_3^T \dot{r}_3 = -\left(\frac{\partial r_3}{\partial p_3}\right)^T \left(J_3 \dot{p}_3\right) \tag{4-43}$$

Then

$$J_3^T \frac{\partial \dot{r}_3}{\partial \dot{p}_3} = -\left[\left(\frac{\partial r_3}{\partial p_3}\right)^T J_3\right]^T = -J_3^T \frac{\partial r_3}{\partial p_3} \tag{4-44}$$

Therefore,

$$\frac{\partial \dot{\boldsymbol{r}}_3}{\partial \dot{\boldsymbol{p}}_3} = -\frac{\partial \boldsymbol{r}_3}{\partial \boldsymbol{p}_3} \tag{4-45}$$

and Eq. (4-40) can be written as follows

$$\Re(\boldsymbol{V}_3)\,\boldsymbol{m}_3 = -m_3\left(\frac{\partial \boldsymbol{r}_3}{\partial \boldsymbol{p}_3}\right)^T \ddot{\boldsymbol{r}}_3 \tag{4-46}$$

and using (4-34)

$$J_3^T \Re(\boldsymbol{V}_3) = -m_3\left(\boldsymbol{r}_3 \otimes \ddot{\boldsymbol{r}}_3\right) \tag{4-47}$$

Finally, the second term of Eq. (4-19) can be written

$$J_3^T \Re(\boldsymbol{V}_3)\,\boldsymbol{m}_3 = m_3 \boldsymbol{r}_3 \otimes \ddot{\boldsymbol{r}}_{G_3} \tag{4-48}$$

which is equal to the third term in Eq. (4-26).

Using $\boldsymbol{X} = \boldsymbol{G}$ and $\boldsymbol{Y} = \boldsymbol{g}$ the third term in Eq. (4-19) is

$$\aleph_3 = \left(\frac{\partial \boldsymbol{r}_3}{\partial \boldsymbol{p}_3}\right)^T m_3 \boldsymbol{g} = \boldsymbol{r}_3 \otimes m_3 \boldsymbol{g} \tag{4-49}$$

the same as the last term in Eq. (4-26).

Therefore, as one would expect, Newton's equations for the upper limb are equivalent to Lagrange's equations.

4.3. POWER FLOWS

Power analysis of human movement has been an area of interest for many years [39][40][41]. A number of investigations have been performed to estimate total power and its components during different activities [37][38][42][43]. Two basic methods are used for this purpose [38][44]. One uses the time derivative of total energy, i.e., the sum of the kinematic and potential energies. The other considers the power generated or absorbed by muscles and transmitted between segments through the joints.

Discrepancies between results obtained by the two methods have been reported. The sources of the discrepancy have been attributed to errors in the modelling, experimental errors, kinematic errors resulting from digitizing cinefilm, movement of the markers on skin and of anthropometric data [37][38][44]. The existence of a discrepancy between the methods has been proposed as a test for validity of the underlying model [37]. The analysis presented here shows that if the body segments are considered to be rigid bodies, then the two methods always yield the same power. The implication is that the results of these two methods cannot be used to draw a conclusion about the validity of the model or data.

To calculate the rate of work done (power) in each segment, the first method takes the time derivative of the total energy, the sum of the kinetic and potential energies, i.e.,

$$P_{es} = \frac{dE_s}{dt} = \frac{d(KE_s + PE_s)}{dt} \qquad s = 1, 2, 3 \tag{4-50}$$

where s is the segment number and kinetic (KE_s) and potential (PE_s) energies are defined in Eqs. (4-5) and (4-6).

In the second method the power generated or absorbed by the muscles (PM_s) and the power

transmitted between segments through joints (PJ_s) are used, i.e.,

$$P_{ps} = PJ_s + PM_s \qquad s = 1, 2, 3 \tag{4-51}$$

$$\begin{cases} PJ_s = \sum_{j=P,D} (\boldsymbol{F}_{js} \cdot \boldsymbol{V}_{js}) \\ PM_s = \sum_{j=P,D} (\boldsymbol{M}_{js} \cdot \omega_s) \end{cases} \tag{4-52}$$

where $\boldsymbol{F}_{js}$ is the intersegmental force vector at joint j (P: proximal joint, D: distal joint) in segment s, $\boldsymbol{V}_{js}$ is the linear velocity vector of joint j (P: proximal joint, D: distal joint) in segment s, $\boldsymbol{M}_{js}$ is the generated moment vector about joint j (P: proximal joint, D: distal joint) in segment s and ω_s is the angular velocity vector of segment s.

PJ_{js} reflects power delivered to or taken from segment s due to work done by the joint intersegmental force ($\boldsymbol{F}_{js}$). If PJ_{js} is positive, power is delivered to the segment and if it is negative, power is taken from this segment and delivered to the adjacent segment. Joint powers therefore show only the rate of transfer of energy between segments. It is easy to show that

$$\sum_{s=1}^{3} PJ_s = 0 \tag{4-53}$$

PM_{js} shows the power delivered to or taken from segment s and its joint j due to the work done by muscles.

4.3.1. EQUIVALENCE OF THE TWO METHODS

In this section it is shown that the two methods produce the same output. For the single segment shown in Fig. 4.1, using Eqs. (4-22), and (4-52), PJ_s can be written as follows

$$PJ_s = \sum_{j=P,D} PJ_{js} = \boldsymbol{F}_D \cdot \boldsymbol{V}_D + m\boldsymbol{g} \cdot \boldsymbol{V}_P + m\boldsymbol{a}_G \cdot \boldsymbol{V}_P - \boldsymbol{F}_D \cdot \boldsymbol{V}_P \tag{4-54}$$

Since

$$\begin{cases} \boldsymbol{V}_P = \boldsymbol{V}_G + \boldsymbol{r} \otimes \omega_s \\ \boldsymbol{V}_D = \boldsymbol{V}_G - \boldsymbol{r}' \otimes \omega_s \end{cases} \tag{4-55}$$

Eq. (4-54) can be written as

$$\begin{aligned} PJ_s = {} & \boldsymbol{F}_D \cdot \boldsymbol{V}_G + \boldsymbol{F}_D \cdot \boldsymbol{r} \otimes \omega_s + m\boldsymbol{g} \cdot \boldsymbol{V}_G + m\boldsymbol{g} \cdot \boldsymbol{r} \otimes \omega_S \\ & + m\boldsymbol{a}_G \cdot \boldsymbol{V}_G + m\boldsymbol{a}_G \cdot \boldsymbol{r} \otimes \omega_s - \boldsymbol{F}_D \cdot \boldsymbol{V}_G + \boldsymbol{F}_D \cdot \boldsymbol{r}' \otimes \omega_s \end{aligned} \tag{4-56}$$

Using Eqs. (4-2), (4-52) and (4-55), PM_s can be written as follows

$$\begin{aligned} PM_s = {} & \sum_{j=P,D} PM_{js} \\ = {} & \boldsymbol{M}_D \cdot \omega_s + \boldsymbol{r} \otimes \boldsymbol{F}_P \cdot \omega_s + \boldsymbol{r}' \otimes \boldsymbol{F}_D \cdot \omega_s + I_s \dot{\omega}_s \cdot \omega_s + \omega_s \otimes I_s \omega_s \cdot \omega_s - \boldsymbol{M}_D \cdot \omega_s \\ = {} & \boldsymbol{r} \otimes \boldsymbol{F}_D \cdot \omega_s + \boldsymbol{r} \otimes m_i \boldsymbol{g} \cdot \omega_s + \boldsymbol{r} \otimes m\boldsymbol{a}_G \cdot \omega_s + \boldsymbol{r}' \otimes \boldsymbol{F}_D \cdot \omega_s \\ & + I_s \dot{\omega}_s \cdot \omega_s + \omega_s \otimes I_s \omega_s \cdot \omega_s \end{aligned} \tag{4-57}$$

By adding Eqs. (4-56) and (4-57), P_{ps} can be written as

$$\begin{aligned} P_{ps} = {} & m\boldsymbol{g} \cdot \boldsymbol{V}_G + m\boldsymbol{a}_G \cdot \boldsymbol{V}_G + I_s \dot{\omega}_s \cdot \omega_s \\ = {} & \frac{d}{dt} m\boldsymbol{g} \cdot \boldsymbol{G} + \frac{1}{2} m_i \boldsymbol{V}_G \cdot \boldsymbol{V}_G + \frac{1}{2} I_s \omega_s \cdot \omega_s \\ = {} & \frac{dPE_s + KE_s}{dt} = \frac{dE_s}{dt} = P_{es} \end{aligned} \tag{4-58}$$

The above shows that both methods of power analysis give identical results. Any discrepancy between the results of the two methods must be solely attributable to the numerical accuracy of the algorithms that implement the two approaches. A discrepancy is not an indication of erroneous kinematic data or of a link segment model that does not represent the physical situation prop-

erly. Therefore a high correlation between the results cannot be assumed to indicate that kinematic data are accurate or that the model necessarily represents physical reality [37]. It only indicates that the precision of the numerical algorithms is sufficiently reasonable. Verification of the data or model accuracy needs to be done by other independent methods. Although theoretical analysis showed that the two methods for determining power flows are identical, for completeness a small experiment was carried out. The results are shown in Appendix C.

4.4. EFFECT OF TRANSLATIONAL DOF

Having discussed the calculation of power, this section considers the effect of ignoring translational DOF on power in an actual situation. An experiment was performed where kinematic data were obtained from the upper limb during the performance of a drinking from a cup. The three dimensional reconstructed data were smoothed using the splines method. Then three Euler angles of each segment and the screw axis of the arm were calculated. Three Euler angles and three translational DOF of the arm segment are shown respectively in Fig. 4.3 and Fig. 4.4. It is important to note that nine Euler angles represent only seven DOF. Total arm power was calculated for two cases; considering only 7 rotational DOF (ignoring translational DOF) and considering all 10 DOF as shown in Fig. 4.5.

As discussed in Section 2.3.1, the three translational DOF considered in the 10 DOF model (Fig. 4.4) are small relative to the range of motion which is about 30 cm. However by looking at the temporal patterns of the two powers calculated using two models shown in Fig. 4.5, considerable difference between them can be seen. The cross correlation between the two powers is 0.79. Also maximum percentage deviation (*MPD*) calculated using the following formula is 215%.

$$MPD\% = \frac{Max(|P(DOF=10)-P(DOF=7)|)}{Max(P(DOF=10))} \times 100 \quad (4\text{-}59)$$

Therefore, it is important to consider translational DOF in kinetic analysis. This is because the three translational DOF of the arm segment are the coordinates of a point on which the displacement of all points in the link-segment model depends. Also in kinetic analysis not only displacements, but also the first and second derivatives of the kinematic variables are used. Therefore any small error is magnified and it is important that the translational DOF be considered.

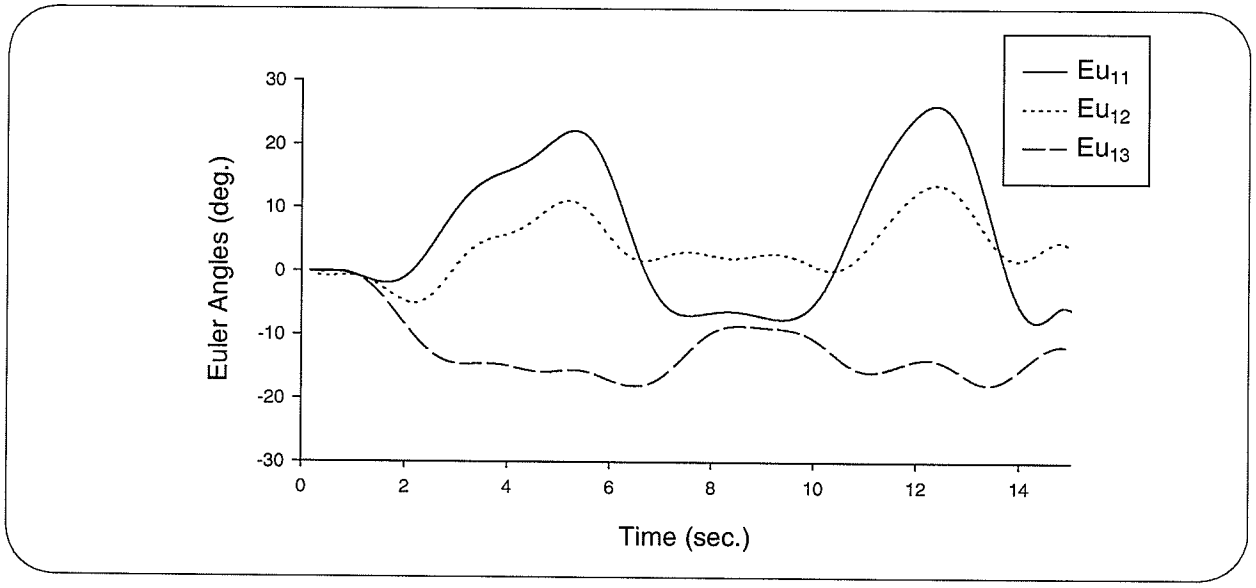

Fig. 4.3 Three Euler angles of the arm segment.

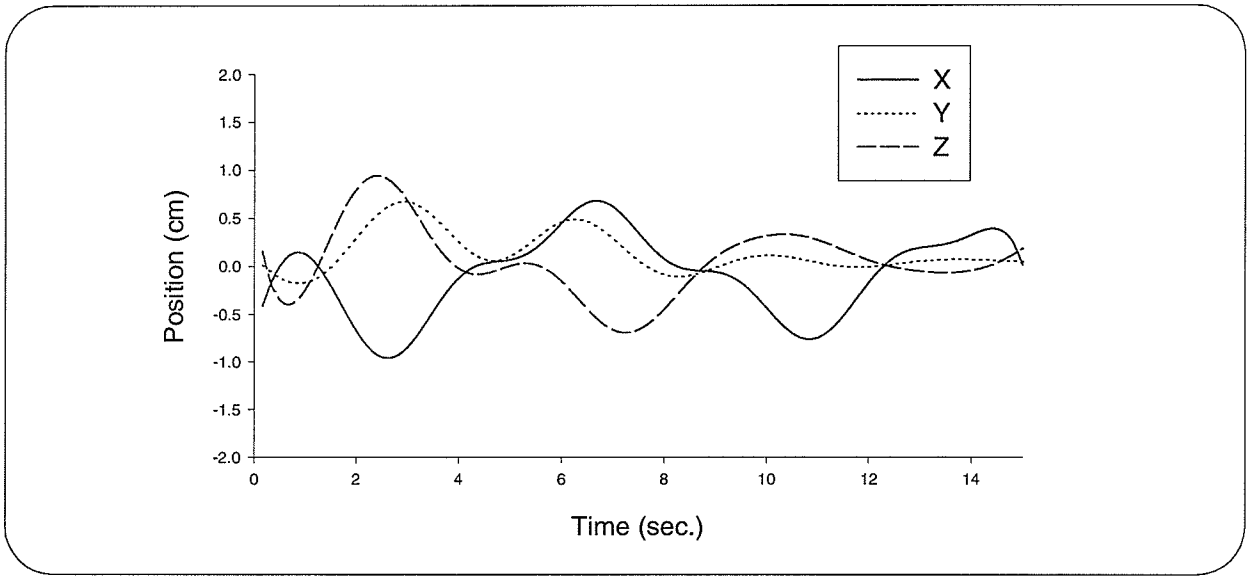

Fig. 4.4 Three translational DOF of the arm segment.

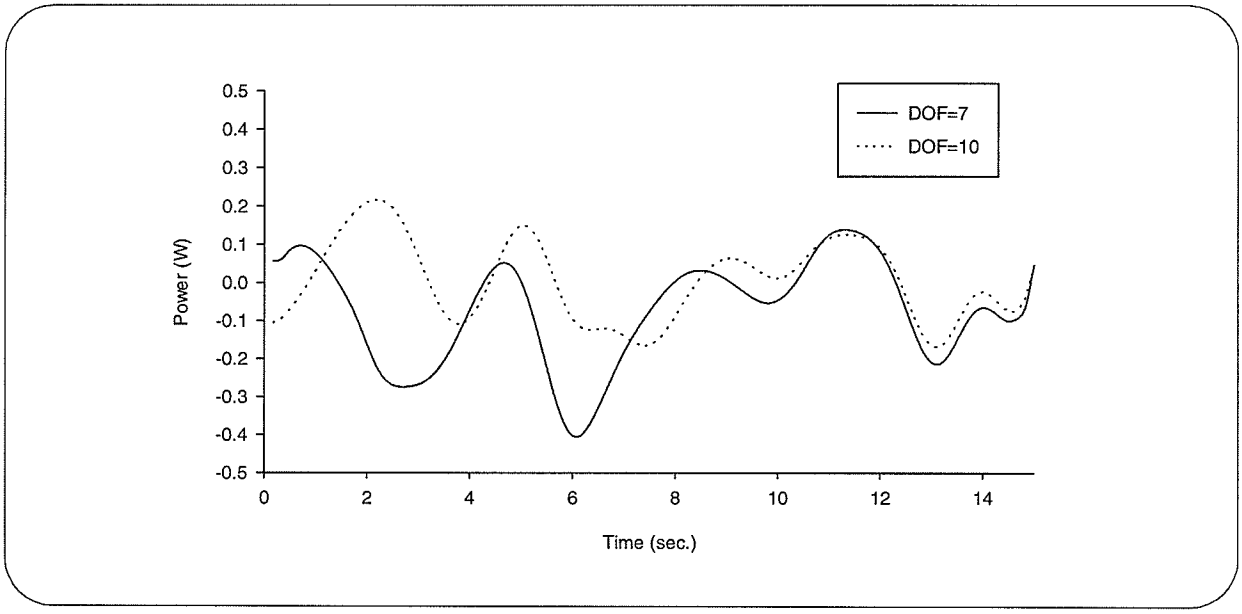

Fig. 4.5 Power calculated in arm segment when DOF=7 and DOF=10.

4.5. POTENTIAL OF KINETIC ANALYSIS TO EVALUATE RHEUMATOID ARTHRITIS

Patterns of upper limb movement required to perform certain independent living tasks may be affected by rheumatoid arthritis (RA) of the shoulder. A kinetic analysis was performed on the data collected by Ripat [45]. The purpose of this analysis is to investigate whether there is a difference between the kinematic/kinetic variables of normal and RA subjects [46][47]. Subjects were ten normal (NR) and ten subjects with rheumatoid arthritis (RA) who had shoulder joint involvement. Subject demographics are presented in Appendix D. More information about subjects can be found in [45].

In Ripat's experiment [45], subjects were asked to perform five different functional tasks. All tasks were performed five times; data from the three middle repetitions were analysed. The starting position for all tasks was with the hand on the thigh.

In task #1, subjects seated on a stool at a comfortable height were asked to lift up a bottle from a shelf. The height of the shelf was adjusted relative to the height of the subject and it was at a distance from the stool which was comfortable for the subject to reach. To perform the experiment, the subject flexed the shoulder, extended the elbow to set the bottle momentarily on the top of the shelf without releasing it. After this the bottle was then returned to the starting position. Task #2 was similar to task #1, except that subjects were asked to lift up an object (tin can) of different weight. In task #3, subjects were asked to comb their hair. The comb was drawn through the hair from front to back; the hand then was returned to the starting position. Task #4 was to touch the sacrum. Subjects brought their hand backwards from the starting position to place the palm on the sacrum, the hand then was returned to the starting position. The last task (task #5) was to reach across the body to touch opposite scapula and to return to the starting position.

4.5.1. RESULTS AND DISCUSSION

From the data collected by Ripat [45], some kinematic and kinetic variables of the upper limb for both normal and RA subjects during the performance of the five tasks were calculated. Maximum values of the Euler angles, angular velocities and accelerations of the three segments, the magnitude of intersegmental forces and moments at three joints and power flows in the three segments were calculated. Two-tailed unpaired *t*-tests [34][35] were used to determine if a significant difference existed between calculated variables of normal and RA subjects (Table 4.1). In this test, the level of significance was set *a priori* as $p \leq 0.05$. The third Euler angles of the forearm and hand segments are not reported because they were small. In this study and in [45], no significant difference was found between maximum angular velocities and acceleration in most cases, therefore these values are not reported.

Fig. 4.6 shows the comparison of the mean of maximum Euler angles for normal and RA subjects. It can be seen that only in three cases (Eu_{11} in task #5 ($p = 0.009$), Eu_{12} in task #1 ($p = 0.01$) and Eu_{22} in task #4 ($p = 0.03$)) the difference was significant ($p \leq 0.05$). It can be concluded that the maximum value of Euler angles is not a good measure to distinguish between two groups of normal and RA subjects [45].

Table 4.1 shows p values of $|\boldsymbol{F}_1|$, $|\boldsymbol{F}_2|$ and $|\boldsymbol{F}_3|$ ($|\boldsymbol{M}_1|$, $|\boldsymbol{M}_2|$ and $|\boldsymbol{M}_3|$) respectively maximum intersegmental forces (moments) at shoulder, elbow and wrist joints. For the first three tasks no significant difference ($p \leq 0.05$) was found. However for the last two tasks, the difference in most cases is significant. This might be because motion at the shoulder joint is the principal motion required to accomplish task #4 and #5. These differences are also reflected in the p values of the maximum power flow at the arm, forearm and hand segment (P_1, P_2, P_3).

Variable	Task #1	Task #2	Task #3	Task #4	Task #5
Euler Angles					
Eu_{11}	0.76	0.36	0.82	0.50	***0.009***
Eu_{12}	***0.01***	0.19	0.25	0.53	0.07
Eu_{13}	0.36	0.29	0.34	0.52	0.34
Eu_{21}	0.65	0.89	0.63	0.98	0.11
Eu_{22}	0.42	0.72	0.53	***0.03***	0.26
Eu_{31}	0.08	0.91	0.55	0.52	0.23
Eu_{32}	0.27	0.81	0.71	0.08	0.07
Forces					
$\lvert F_1 \rvert$	0.47	0.75	0.07	***0.01***	0.45
$\lvert F_2 \rvert$	0.24	0.50	0.10	***0.004***	0.29
$\lvert F_3 \rvert$	0.16	0.35	0.20	***0.005***	0.24
Moments					
$\lvert M_1 \rvert$	0.2	0.14	0.54	***0.05***	***0.02***
$\lvert M_2 \rvert$	0.15	0.59	0.28	***0.03***	***0.05***
$\lvert M_3 \rvert$	0.08	0.20	0.44	***0.007***	0.25
Power Flows					
P_1	0.52	0.20	0.10	0.10	***0.01***
P_2	0.39	0.36	0.17	0.22	0.15
P_3	0.57	0.35	0.15	***0.03***	0.13
P_t	0.60	0.28	0.11	***0.04***	***0.04***

Table 4.1 Results of statistical comparisons of kinematic/kinetic variables between normal and RA subjects.

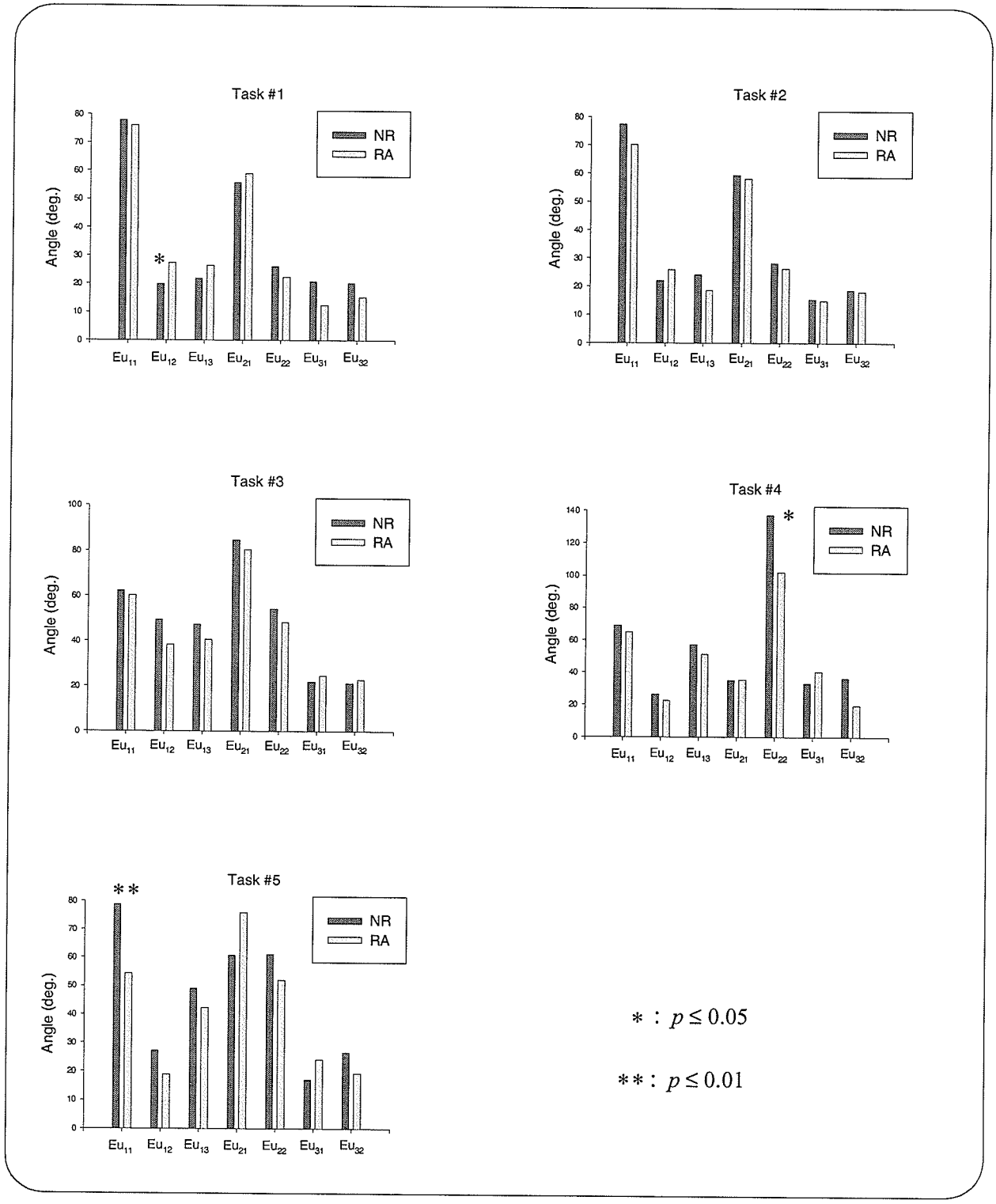

Fig. 4.6 Mean of maximum Euler angles for normal (NR) and RA subjects.

In the final row of the table, p value of the maximum total power, P_t, is shown. It shows that there is a significant difference, $p = 0.04 \leq 0.05$, between total power of normal and RA subjects in tasks #4 and #5. Although the differences between forces and powers in task #5 are not significant (except P_1), the total powers are significantly different. The reason is because of the way the total power is calculated.

$$P_t = \sum_{s=1}^{3} P_s = \sum_{s=1}^{3} (PJ_s + PM_s) \tag{4-60}$$

where PJ_s is the power transmitted between segments and PM_s reflects the power generated or absorbed by muscles,

$$\begin{cases} PJ_s = \sum_{j=P,D} (\boldsymbol{F}_{js} \cdot \boldsymbol{V}_{js}) \\ PM_s = \sum_{j=P,D} (\boldsymbol{M}_{js} \cdot \omega_s) \end{cases} \tag{4-61}$$

However, as was mentioned in Section 4.3., Eq. (4-53), the sum of power transmitted between segments is zero. Therefore the first term in Eq. (4-60) is zero, i.e.,

$$P_t = \sum_{s=1}^{3} P_s = \sum_{s=1}^{3} (PJ_s + PM_s) = \sum_{s=1}^{3} PM_s \tag{4-62}$$

Thus in P_t only moments make contribution not forces. Fig. 4.7 shows the p values of the power flows for different tasks. The p value from task # 1 to task #5, in general, decreases. For the last two tasks total powers of normal subjects are significantly different from those of RA subjects ($p \leq 0.04$).

It can be concluded that the kinetic variables are more sensitive to differences between normal and RA subjects than the kinematic variables.

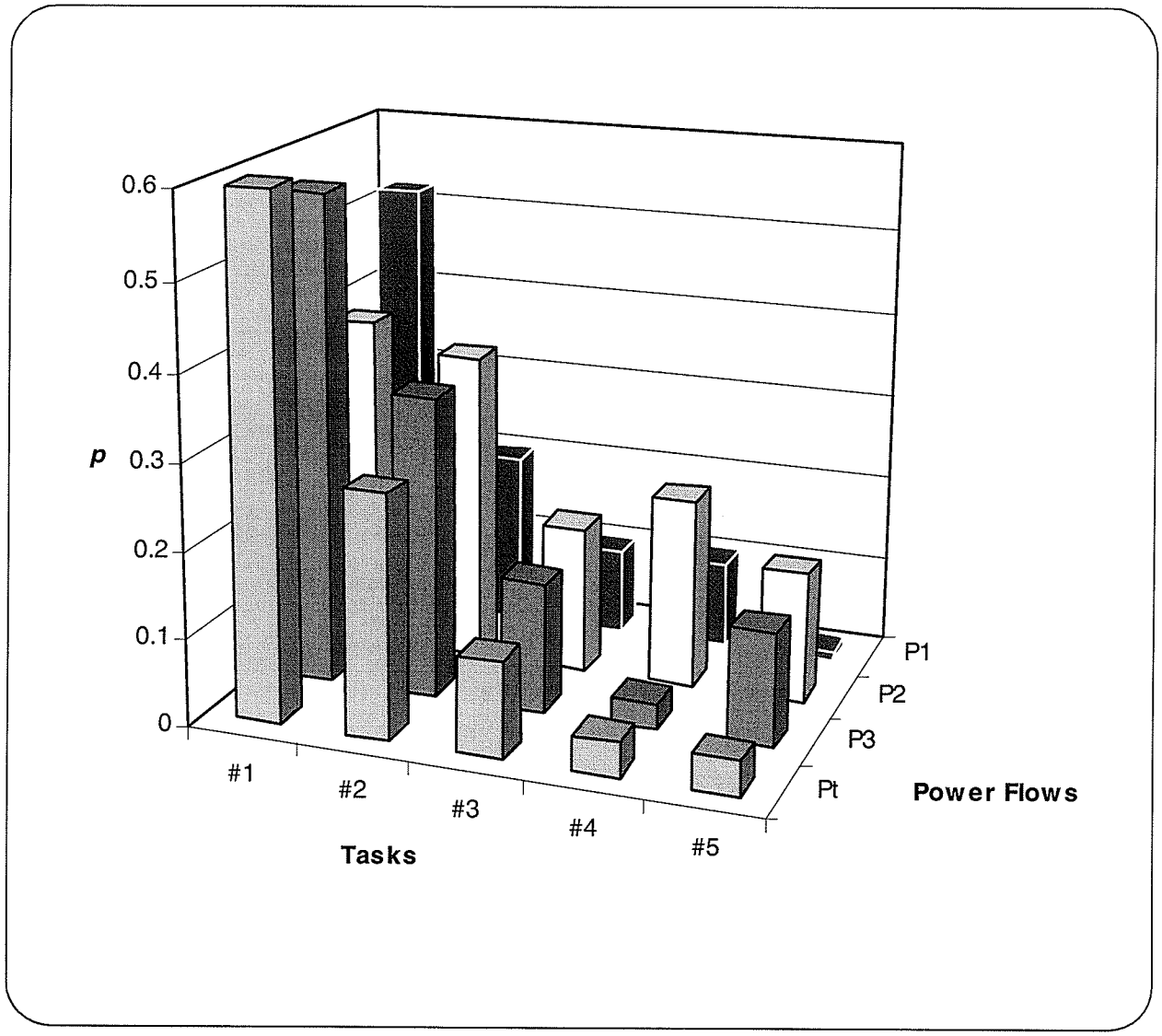

Fig. 4.7 Probability p for power flows in different tasks.

4.6. SUMMARY

To determine muscle forces and joint moments, kinetic equations must be established. In this chapter Newton's and Lagrange's equations for the upper limb movement are developed and the relationship between them is shown. Also two methods to calculate power flows are explained and it is shown that both methods give identical results. Therefore, any discrepancy between the results of the two methods must be solely attributable to the numerical accuracy of the algorithms that implement the two approaches. Experimental results of applying kinetic analysis to two groups of subjects, RA and normal are presented in this chapter. It is shown that kinetic variables are a better measure to distinguish between normal and RA subjects.

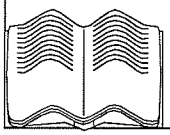

CHAPTER 5. FORCE DISTRIBUTION PROBLEM

5.1. INTRODUCTION

Application of the kinetic and kinematic analyses of the previous chapters allows determination of the net force and moment acting at and across a joint. However situations may arise in which the area of interest is the way muscles in a group share the load; in these cases it is desirable also to determine the individual skeletal muscle forces. In general, this is an indeterminate problem, since the number of unknowns exceeds the number of equations. This can be easily seen from the equilibrium equations. For a given joint crossed by N muscles, the dynamic force and moment equilibrium equations are

$$\begin{cases} \boldsymbol{F}_T = \sum_{m=1}^{N} \boldsymbol{F}_m + \boldsymbol{F}_j \\ \boldsymbol{M}_T = \sum_{m=1}^{N} \boldsymbol{M}_m + \boldsymbol{M}_j \end{cases} \tag{5-1}$$

where $\boldsymbol{F}_T$ and $\boldsymbol{M}_T$ are the intersegmental force and moment, $\boldsymbol{F}_m$ and $\boldsymbol{M}_m$ are the force and moment produced by muscle m, $\boldsymbol{F}_j$ and $\boldsymbol{M}_j$ are the joint constraint force and moment. The intersegmental force and moment, $\boldsymbol{F}_T$ and $\boldsymbol{M}_T$, are the net kinetic effects that adjoining body segments have on each other. The number of unknown variables, i.e., $\boldsymbol{F}_m$ and $\boldsymbol{M}_m$ $(m = 1, \ldots, N)$, usually exceeds the number of equations where the difference represents the degree of redundancy. Mathematically, this produces an indeterminate problem that has no unique solution. The most commonly used approach found in the literature to overcome this problem is the optimization

technique [48][49][50][51][52][53][54][55][56]. This approach is based on the assumption that the load sharing between the muscles is more or less unique during learned motor activities, and that the neural control of the muscle action is governed by certain physiological criteria that guarantee efficient muscle actions. This allows setting up an objective function to be optimized (Appendix E). A major difficulty with the optimization method is that the physiological criteria are presently unknown [57]. Therefore, in the literature objective functions have been chosen for their simplicity and computational tractability. In this research, a new approach based on fuzzy logic is developed which does not suffer from this disadvantage.

5.2. FORCE DISTRIBUTION PROBLEM AT THE ELBOW JOINT

The distribution of the muscle forces at the elbow joint was chosen for the development of the proposed approach. As mentioned, a straightforward problem was considered- one degree of freedom motion (flexion/extension) possible at the elbow joint. A schematic description of the physical model considering one segment for the forearm and hand segments is shown in Fig. 5.1. Because the goal is to distribute the force at the elbow joint, the muscles crossing the anterior aspect of the joint are considered. Three muscles, biceps brachii (Bic), brachialis (Bra) and brachioradialis (Brd), are the major flexor muscles of the elbow joint [58]. In Fig. 5.1, F_{Bic}, F_{Bra} and F_{Brd} represent respectively force produced by Bic, Bra and Brd muscles, m_1, m_2 and m_L denote respectively the mass of the arm segment, sum of the masses of the forearm and hand segments, and the external load. There are two coordinate systems, one for the shoulder (X_S, Y_S) and one for the elbow (X_e, Y_e) where angles α and β are the angle of the arm and forearm with respect to the corresponding coordinate system. In this model the muscle forces are unknowns. In order to

develop the fuzzy logic method, the functional behaviour of the three flexor muscles must be understood.

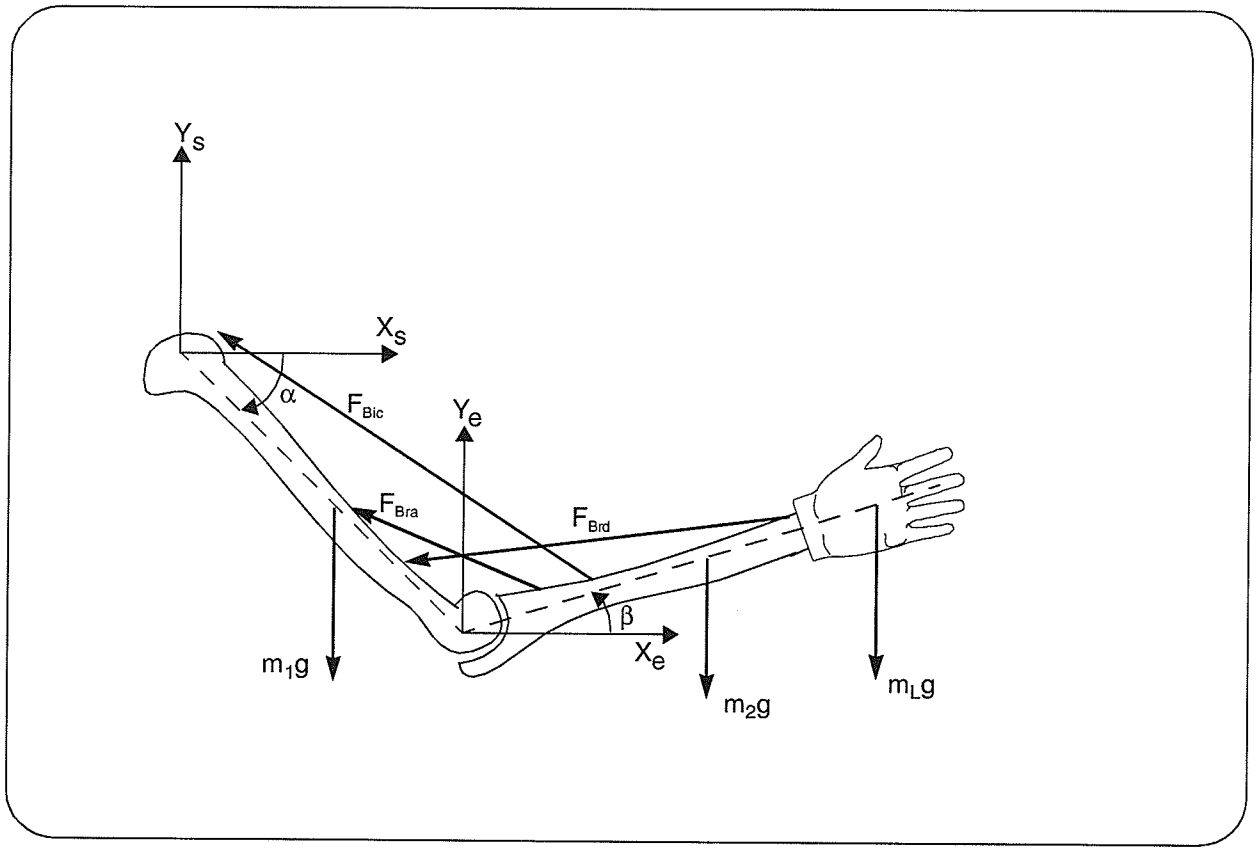

Fig. 5.1 A schematic description of the physical model for force distribution at the elbow joint; (X_S, Y_S): shoulder joint coordinate system, (X_e, Y_e): elbow joint coordinate system.

The biceps brachii is a two headed arm muscle and consists of the long and short head. It extends from the scapula to the proximal aspect of the radius. The biceps is generally active during flexion of the supine forearm under all conditions and during flexion of the semiprone forearm when a load of about 1 kg is lifted. However with the forearm prone, in the majority of instances the biceps plays little if any role in elbow flexion, in the maintenance of elbow flexion, or in antagonistic action during elbow extension, even under load. Biceps is particularly active

during quick extension with an added load likely, providing a protective function for the elbow joint [58].

The brachialis is a flat muscle that lies deep to the biceps arising from the distal anterior aspect of the humerus and inserting in the proximal aspect of the ulna. Maintenance of a specific flexed posture of the elbow, i.e., isometric contraction, or slow extension when the flexors must act as antigravity muscles are situations which generally bring the brachialis into activity in all positions of the forearm [58].

The brachioradialis originates two-thirds of the way down the lateral aspect of the humerus between the triceps and the brachialis and inserts on the thumb side of the distal aspect of the radius. Depending upon the speed of forearm movement, the amount of external load and the rotation angle of the forearm, its role in flexion/extension of the forearm changes [58]. The brachioradialis does not play any appreciable role during maintenance of the elbow position or during slow flexion and extension when the movement is carried out without a external resistance. When a weight is lifted during elbow flexion, the brachioradialis is generally moderately active in the semiprone or prone position of the forearm and is slightly active in the supine position. There is no comparable increase in activity with added load during maintenance of flexion and during slow extension. In most instances brachioradialis is active in all three positions of the forearm during quick flexion and extension. It follows that the muscle is reserved for occasions when rapid movement is required and when weight is to be lifted, especially in the semiprone and the prone forearm positions [58].

In the next section, the architecture of the fuzzy logic model for force distribution is presented and the different components, input interface, output interface and fuzzy rules based on the above discussion are described.

5.3. FUZZY SET THEORY

Fuzzy set theory, a generalization of conventional or Boolean set theory, was introduced by Zadeh [59] as a natural and possible way to represent vagueness in everyday life. A central generalization of fuzzy set theory [60] is the extension of the notation of the elementhood from the discrete set of $\{0,1\}$ to the entire interval [0 1]. Consider an example where the universe of discourse is the set of real numbers and set, A, defined as the set of numbers that are "approximately zero".

$$A = \{x \in \Re | x \cong 0\} \tag{5-2}$$

Using a conventional definition for this set, one must first define the upper and lower crisp limits for its set. These limits are domain specific, e.g., ± 0.5.

$$A = \{x \in \Re | -0.5 < x < 0.5\} \tag{5-3}$$

Equivalently, this boolean set may also be described by its membership function, $A(x)$

$$A(x) = \begin{cases} 1 & \text{if} \quad (-0.5 < x < 0.5) \\ 0 & \text{otherwise} \end{cases} \tag{5-4}$$

Every real number, x, is either in A or it is not. $A(x)$ maps all real numbers onto the two points $\{0,1\}$. Hence, x is "approximately zero" if and only if $A(x) = 1$. Fig. 5.2 illustrates the above mapping which may be considered to be a special case of a membership function. Note that if $x = 0.5$, $A(x) = 0$, hence x is not "approximately zero". However, if $x = 0.4999$, $A(x) = 1$, therefore x is "approximately zero".

In fuzzy set theory, the value of the membership function, $F(x)$, is known as the grade of membership of x in F. There is no unique membership function for F. However, there are some properties [61]. The first property is normality; at least one point in the grade of membership

function should equal to one. A fuzzy set should also satisfy the criterion of monotonicity, i.e., it has only one local maximum. Although not necessary, a fuzzy set may also satisfy the criterion of symmetry. Different possible membership functions for our example are shown in Fig. 5.3.

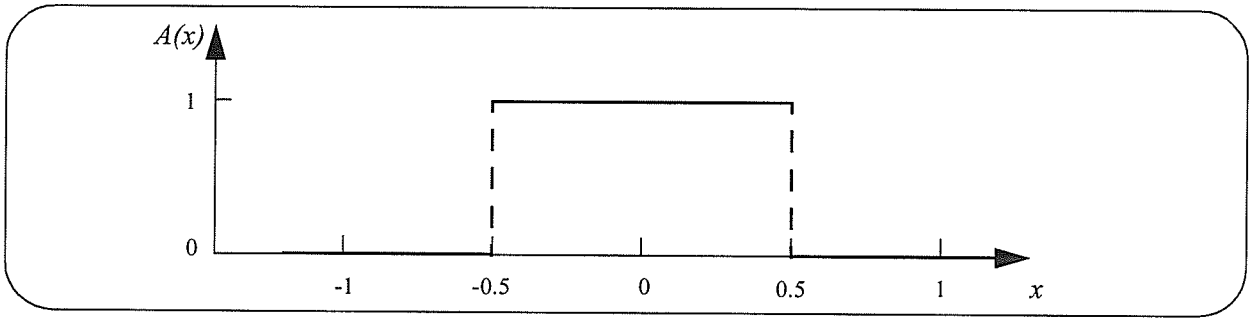

Fig. 5.2 Membership function for the crisp definition of "approximately zero".

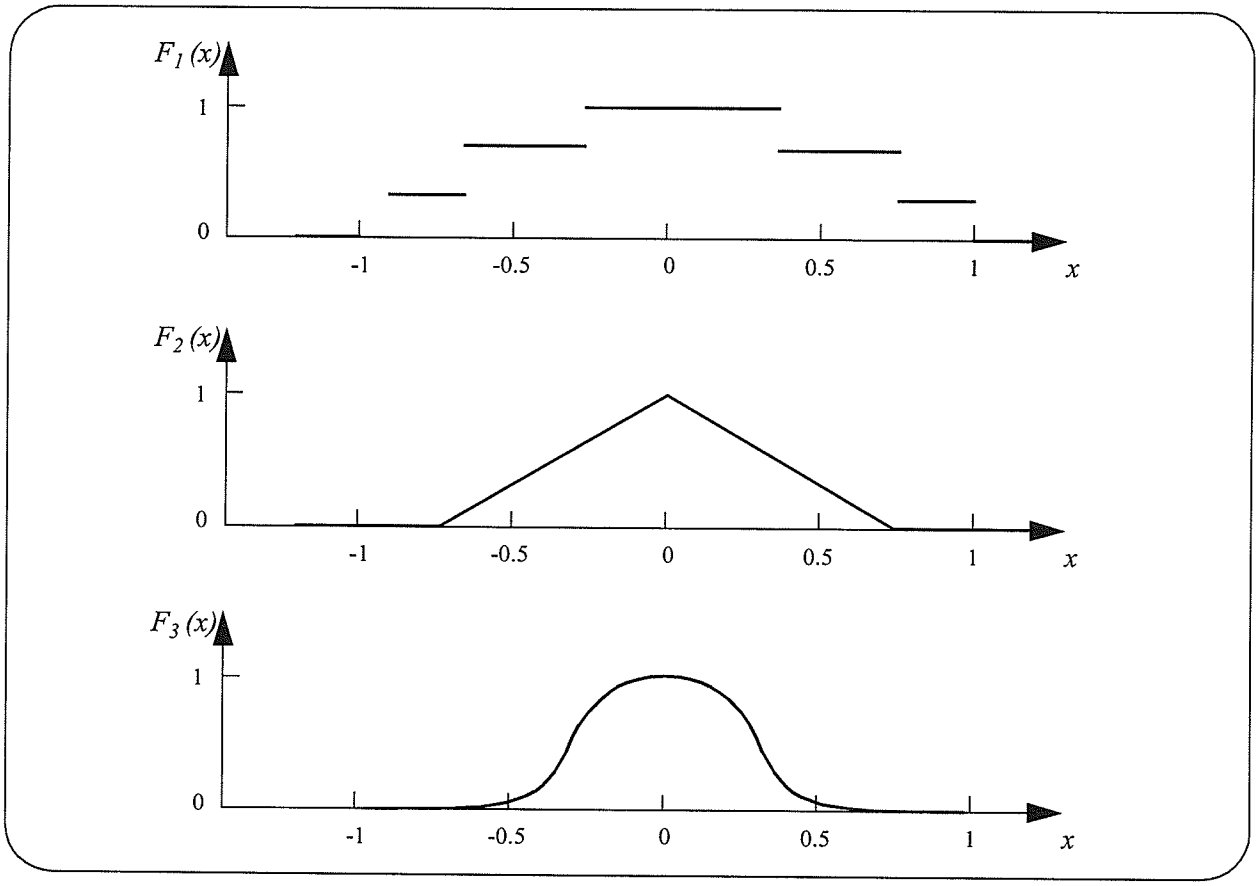

Fig. 5.3 Different possible membership functions for the fuzzy definition of "approximately zero".

5.4. FUZZY FORCE DISTRIBUTION

The main contribution of fuzzy logic is a methodology for computing with words [62]. No other methodology serves this purpose. A key aspect of computation with words is that it involves a fusion of natural languages and computation with fuzzy variables. For the upper limb force distribution problem at the elbow joint, three variables (speed of forearm segment, forearm rotation angle and the amount of load to be lifted) are considered as the input variables for the fuzzy model. The outputs of the fuzzy model are the weighting coefficients which determine the contribution of three muscles, biceps brachii, brachialis and brachioradialis, to the necessary force needed for the forearm movement. Fig. 5.4 shows the architecture of the fuzzy model for force distribution.

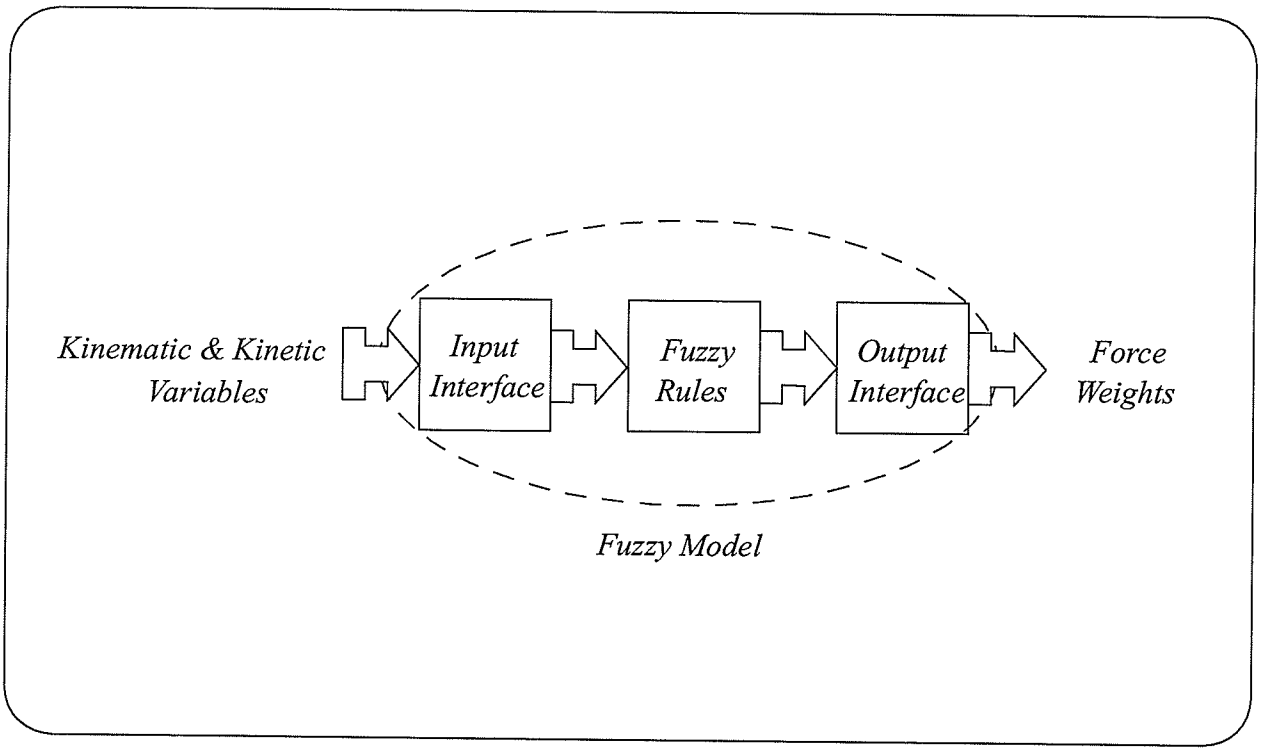

Fig. 5.4 Architecture of the fuzzy model for force distribution.

5.4.1. INPUT INTERFACE

For the considered problem, three parameters, rotation angle of the forearm segment, load and the speed of the forearm movement, are the inputs of the model. For the forearm angle three membership functions, shown in Fig. 5.5, are developed for the prone (PR), semiprone (SP) and supine (SU) positions of the forearm. When the angle is zero, the forearm is in a semiprone position and

$$\begin{cases} F_{SP}(Angle) = 1 \\ F_{PR}(Angle) = 0 \\ F_{SU}(Angle) = 0 \end{cases} \tag{5-5}$$

Similarly when the angle is -90 or +90 degrees the forearm is respectively in the prone or supine position, then the value for one membership function is one and zero for the other two. At an angle of 20 degrees

$$\begin{cases} F_{SP}(Angle) = 0.78 \\ F_{PR}(Angle) = 0 \\ F_{SU}(Angle) = 0.22 \end{cases} \tag{5-6}$$

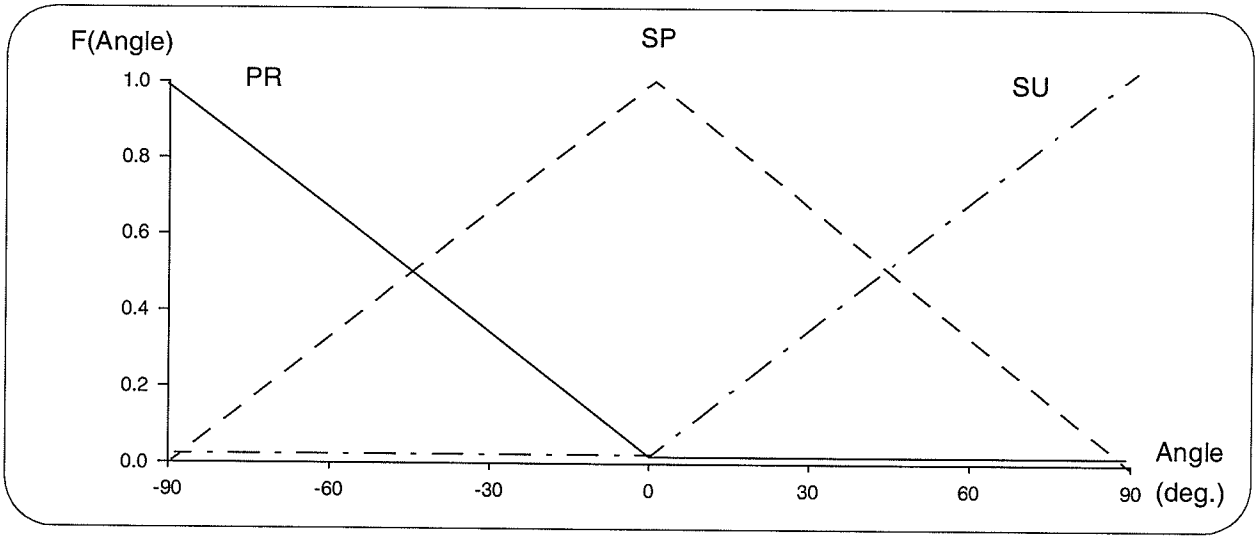

Fig. 5.5 Forearm rotation angle membership functions; PR: prone, SP: semiprone and SU: supine Positions.

which indicates that the forearm is considered to the supine and semiprone positions but not in the prone position and it is closer to the pure semiprone than supine position.

Two membership functions are chosen for the load. These, the low (LO) and high (HI) load membership functions, are shown in Fig. 5.6. The choice of 1 and 3 kg as the typical margins for membership functions is based on the experimental results from different papers as summarized by De Luca [58]. Of course, for a very muscular person or an abnormal subject different values should be considered.

Membership functions for the speed of the movement are shown in Fig. 5.7. The angular velocity is normalized to be between -1 and 1. Five membership functions are postulated for the speed; NH: negative high, NM: negative medium, ZE: zero, PM: positive medium, PH: positive high. Negative speed means extension of the forearm and positive speed means flexion. The ZE membership function is considered for an isometric contraction and slow motion when the absolute value of speed is less than 0.2. PM and NM membership functions are considered for the normal motion. When normalized speed is between 0.5 and 0.8, medium and high membership functions are active. However when the normalized speed exceeds 0.8 which is considered to be a quick motion only the high membership function is active.

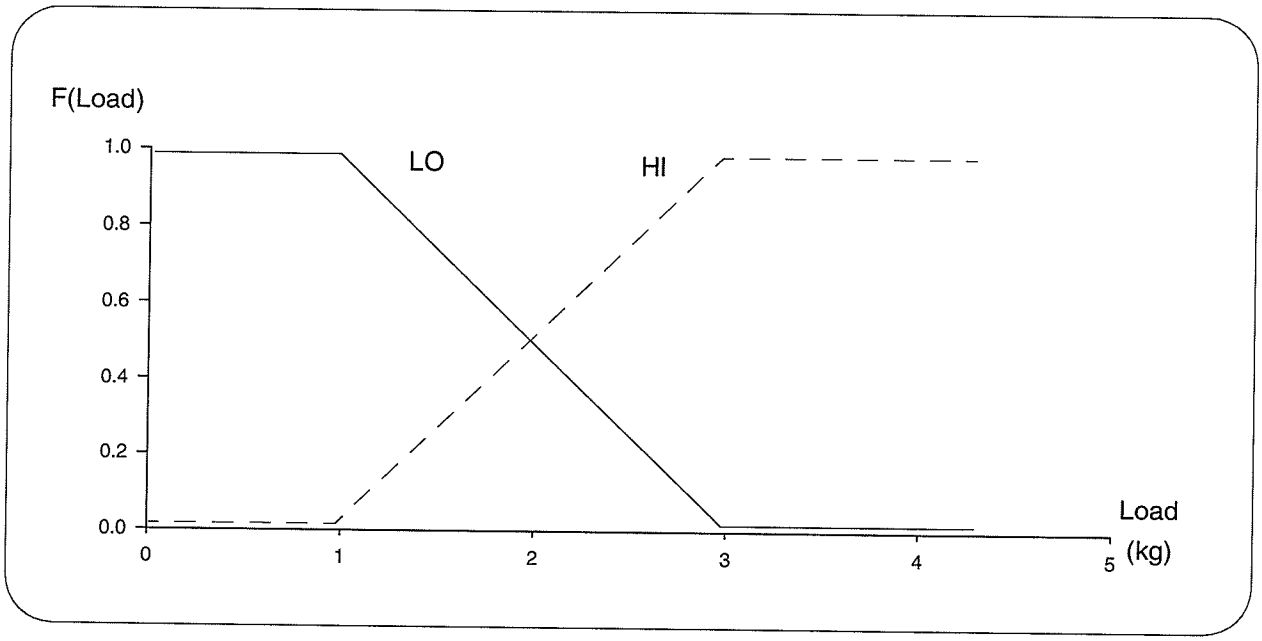

Fig. 5.6 Load membership functions, LO: low load, HI: high load.

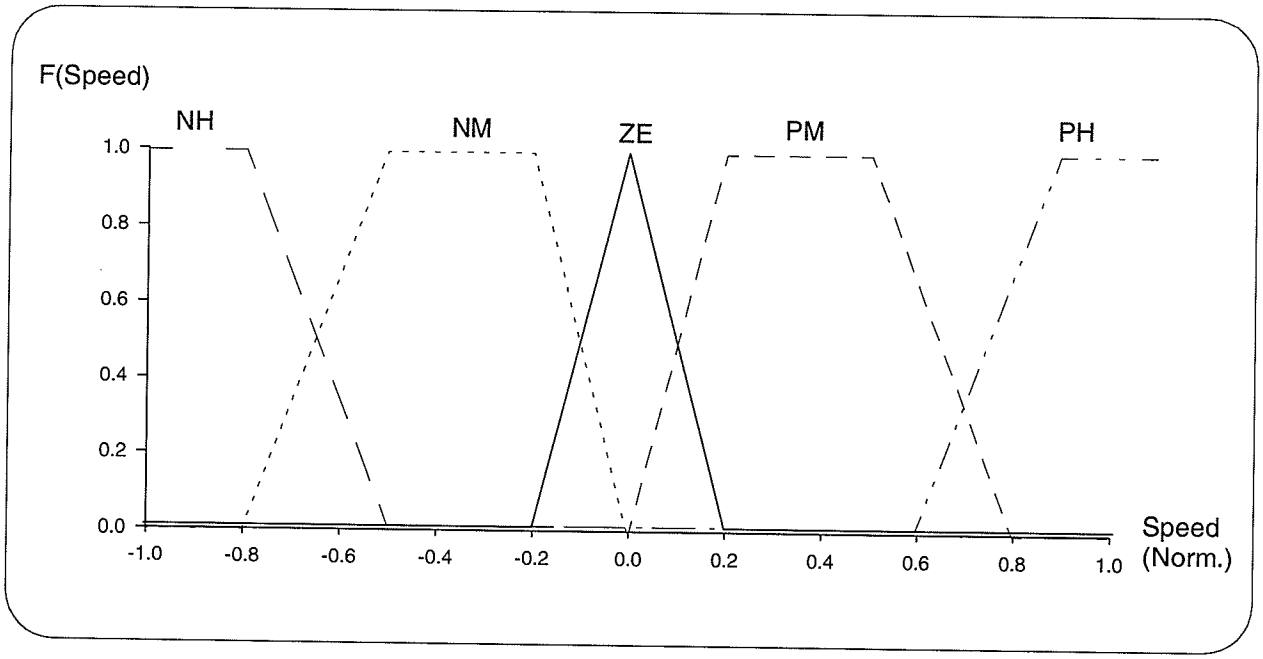

Fig. 5.7 Speed membership functions, NH: negative high, NM: negative medium, ZE: zero, PM: positive medium and PH: positive high.

5.4.2. OUTPUT INTERFACE

Four membership functions, as shown in Fig. 5.8, are considered for the muscles; NA: non active, LA: low active, AC: active, and HA: highly active. Although here the membership functions are identical for each of the three muscles, for more complicated cases they may be different. To calculate the output of the fuzzy model, the *s*-norm and *t*-norm, analogous to the intersection and union, should be considered. Here *min* and *max* were used as the *s*-norm and *t*-norm to calculate fuzzy outputs.

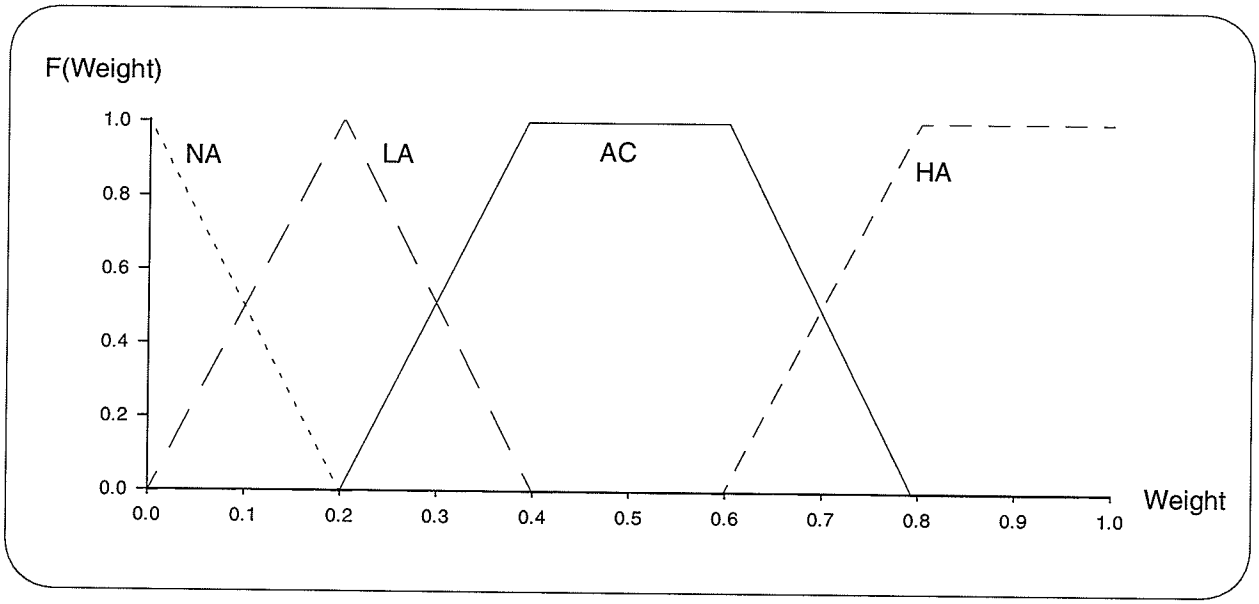

Fig. 5.8 Muscle weight membership functions, NA: nonactive, LA: low active, AC: active, and HA: highly active.

The three calculated forces should satisfy the following equation.

$$\sum_{m=1}^{N} b_m F_m = M_T - M_j \tag{5-7}$$

where b_m is moment arm of the muscle m. Since, the outputs of the fuzzy approach are three weighting coefficients, W_{Bic}, W_{Bra} and W_{Brd}, a postprocessing calculation is needed.

The left hand side of the Eq. (5-7) can be written as follows

$$\begin{aligned}\sum_{m=1}^{N} b_m F_m &= b_{Bic}F_{Bic} + b_{Bra}F_{Bra} + b_{Bic}F_{Brd} \\ &= \alpha\left(W_{Bic}b_{Bic}F_{Bic}(max) + W_{Bra}b_{Bra}F_{Bra}(max) + W_{Brd}b_{Brd}F_{Brd}(max)\right)\end{aligned} \tag{5-8}$$

In this equation $F_{Bic}(max)$, $F_{Bra}(max)$ and $F_{Brd}(max)$ are respectively, the maximum forces of the three muscles and can be calculated using the following equation.

$$F_{muscle}(max) = \sigma_{muscle} \cdot A_{muscle} \tag{5-9}$$

where σ_{muscle} and A_{muscle} are respectively maximum muscle stress and physiological cross sectional area of the muscle.

Using Eq. (5-7) and Eq. (5-8)

$$\alpha = \frac{W_{Bic}b_{Bic}F_{Bic}(max) + W_{Bra}b_{Bra}F_{Bra}(max) + W_{Brd}b_{Brd}F_{Brd}(max)}{M_T - M_j} \tag{5-10}$$

Therefore the three muscle forces can be calculated using the following equations

$$\begin{cases} F_{Bic} = \alpha W_{Bic}F_{Bic}(max) \\ F_{Bra} = \alpha W_{Bra}F_{Bra}(max) \\ F_{Bic} = \alpha W_{Brd}F_{Brd}(max) \end{cases} \tag{5-11}$$

With the muscle forces determined, the internal joint force can then be determined using dynamic equilibrium equation (Eq. (5-1)).

5.4.3. FUZZY RULES

Based on physiological and anatomical facts and experimental results from the different papers discussed in Section 5.2., 30 rules ($30 = 3 \times 2 \times 5$) were developed for each muscle. They are listed in Tables 5.1, 5.2 and 5.3.

Rule #	Rules for biceps muscle
1	If (Angle is PR) and (Load is LO) and (Speed is NH) then (BIC is NA)
2	If (Angle is PR) and (Load is HI) and (Speed is NH) then (BIC is AC)
3	If (Angle is PR) and (Load is LO) and (Speed is NM) then (BIC is NA)
4	If (Angle is PR) and (Load is HI) and (Speed is NM) then (BIC is NA)
5	If (Angle is PR) and (Load is LO) and (Speed is ZE) then (BIC is NA)
6	If (Angle is PR) and (Load is HI) and (Speed is ZE) then (BIC is LA)
7	If (Angle is PR) and (Load is LO) and (Speed is PM) then (BIC is NA)
8	If (Angle is PR) and (Load is HI) and (Speed is PM) then (BIC is AC)
9	If (Angle is PR) and (Load is LO) and (Speed is PH) then (BIC is NA)
10	If (Angle is PR) and (Load is HI) and (Speed is PH) then (BIC is AC)
11	If (Angle is SP) and (Load is LO) and (Speed is NH) then (BIC is NA)
12	If (Angle is SP) and (Load is HI) and (Speed is NH) then (BIC is AC)
13	If (Angle is SP) and (Load is LO) and (Speed is NM) then (BIC is NA)
14	If (Angle is SP) and (Load is HI) and (Speed is NM) then (BIC is NA)
15	If (Angle is SP) and (Load is LO) and (Speed is ZE) then (BIC is NA)
16	If (Angle is SP) and (Load is HI) and (Speed is ZE) then (BIC is AC)
17	If (Angle is SP) and (Load is LO) and (Speed is PM) then (BIC is NA)
18	If (Angle is SP) and (Load is HI) and (Speed is PM) then (BIC is HA)
19	If (Angle is SP) and (Load is LO) and (Speed is PH) then (BIC is NA)
20	If (Angle is SP) and (Load is HI) and (Speed is PH) then (BIC is HA)
21	If (Angle is SU) and (Load is LO) and (Speed is NH) then (BIC is NA)
22	If (Angle is SU) and (Load is HI) and (Speed is NH) then (BIC is AC)
23	If (Angle is SU) and (Load is LO) and (Speed is NM) then (BIC is NA)
24	If (Angle is SU) and (Load is HI) and (Speed is NM) then (BIC is NA)
25	If (Angle is SU) and (Load is LO) and (Speed is ZE) then (BIC is LA)
26	If (Angle is SU) and (Load is HI) and (Speed is ZE) then (BIC is AC)
27	If (Angle is SU) and (Load is LO) and (Speed is PM) then (BIC is LA)
28	If (Angle is SU) and (Load is HI) and (Speed is PM) then (BIC is HA)
29	If (Angle is SU) and (Load is LO) and (Speed is PH) then (BIC is LA)
30	If (Angle is SU) and (Load is HI) and (Speed is PH) then (BIC is HA)

Table 5.1 Fuzzy rules for the biceps muscle.

Rule #	Rules for brachialis muscle
31	If (Angle is PR) and (Load is LO) and (Speed is NH) then (BRA is NA)
32	If (Angle is PR) and (Load is HI) and (Speed is NH) then (BRA is NA)
33	If (Angle is PR) and (Load is LO) and (Speed is NM) then (BRA is NA)
34	If (Angle is PR) and (Load is HI) and (Speed is NM) then (BRA is NA)
35	If (Angle is PR) and (Load is LO) and (Speed is ZE) then (BRA is AC)
36	If (Angle is PR) and (Load is HI) and (Speed is ZE) then (BRA is HA)
37	If (Angle is PR) and (Load is LO) and (Speed is PM) then (BRA is AC)
38	If (Angle is PR) and (Load is HI) and (Speed is PM) then (BRA is HA)
39	If (Angle is PR) and (Load is LO) and (Speed is PH) then (BRA is HA)
40	If (Angle is PR) and (Load is HI) and (Speed is PH) then (BRA is HA)
41	If (Angle is SP) and (Load is LO) and (Speed is NH) then (BRA is NA)
42	If (Angle is SP) and (Load is HI) and (Speed is NH) then (BRA is NA)
43	If (Angle is SP) and (Load is LO) and (Speed is NM) then (BRA is NA)
44	If (Angle is SP) and (Load is HI) and (Speed is NM) then (BRA is NA)
45	If (Angle is SP) and (Load is LO) and (Speed is ZE) then (BRA is AC)
46	If (Angle is SP) and (Load is HI) and (Speed is ZE) then (BRA is HA)
47	If (Angle is SP) and (Load is LO) and (Speed is PM) then (BRA is AC)
48	If (Angle is SP) and (Load is HI) and (Speed is PM) then (BRA is HA)
49	If (Angle is SP) and (Load is LO) and (Speed is PH) then (BRA is HA)
50	If (Angle is SP) and (Load is HI) and (Speed is PH) then (BRA is HA)
51	If (Angle is SU) and (Load is LO) and (Speed is NH) then (BRA is NA)
52	If (Angle is SU) and (Load is HI) and (Speed is NH) then (BRA is NA)
53	If (Angle is SU) and (Load is LO) and (Speed is NM) then (BRA is NA)
54	If (Angle is SU) and (Load is HI) and (Speed is NM) then (BRA is NA)
55	If (Angle is SU) and (Load is LO) and (Speed is ZE) then (BRA is AC)
56	If (Angle is SU) and (Load is HI) and (Speed is ZE) then (BRA is HA)
57	If (Angle is SU) and (Load is LO) and (Speed is PM) then (BRA is AC)
58	If (Angle is SU) and (Load is HI) and (Speed is PM) then (BRA is HA)
59	If (Angle is SU) and (Load is LO) and (Speed is PH) then (BRA is HA)
60	If (Angle is SU) and (Load is HI) and (Speed is PH) then (BRA is HA)

Table 5.2 Fuzzy rules for the brachialis muscle.

Rule #	Rules for brachioradialis muscle
61	If (Angle is PR) and (Load is LO) and (Speed is NH) then (BRD is AC)
62	If (Angle is PR) and (Load is HI) and (Speed is NH) then (BRD is HA)
63	If (Angle is PR) and (Load is LO) and (Speed is NM) then (BRD is NA)
64	If (Angle is PR) and (Load is HI) and (Speed is NM) then (BRD is NA)
65	If (Angle is PR) and (Load is LO) and (Speed is ZE) then (BRD is LA)
66	If (Angle is PR) and (Load is HI) and (Speed is ZE) then (BRD is HA)
67	If (Angle is PR) and (Load is LO) and (Speed is PM) then (BRD is LA)
68	If (Angle is PR) and (Load is HI) and (Speed is PM) then (BRD is HA)
69	If (Angle is PR) and (Load is LO) and (Speed is PH) then (BRD is AC)
70	If (Angle is PR) and (Load is HI) and (Speed is PH) then (BRD is HA)
71	If (Angle is SP) and (Load is LO) and (Speed is NH) then (BRD is AC)
72	If (Angle is SP) and (Load is HI) and (Speed is NH) then (BRD is HA)
73	If (Angle is SP) and (Load is LO) and (Speed is NM) then (BRD is NA)
74	If (Angle is SP) and (Load is HI) and (Speed is NM) then (BRD is NA)
75	If (Angle is SP) and (Load is LO) and (Speed is ZE) then (BRD is LA)
76	If (Angle is SP) and (Load is HI) and (Speed is ZE) then (BRD is AC)
77	If (Angle is SP) and (Load is LO) and (Speed is PM) then (BRD is LA)
78	If (Angle is SP) and (Load is HI) and (Speed is PM) then (BRD is HA)
79	If (Angle is SP) and (Load is LO) and (Speed is PH) then (BRD is AC)
80	If (Angle is SP) and (Load is HI) and (Speed is PH) then (BRD is HA)
81	If (Angle is SU) and (Load is LO) and (Speed is NH) then (BRD is AC)
82	If (Angle is SU) and (Load is HI) and (Speed is NH) then (BRD is HA)
83	If (Angle is SU) and (Load is LO) and (Speed is NM) then (BRD is NA)
84	If (Angle is SU) and (Load is HI) and (Speed is NM) then (BRD is NA)
85	If (Angle is SU) and (Load is LO) and (Speed is ZE) then (BRD is NA)
86	If (Angle is SU) and (Load is HI) and (Speed is ZE) then (BRD is LA)
87	If (Angle is SU) and (Load is LO) and (Speed is PM) then (BRD is NA)
88	If (Angle is SU) and (Load is HI) and (Speed is PM) then (BRD is LA)
89	If (Angle is SU) and (Load is LO) and (Speed is PH) then (BRD is LA)
90	If (Angle is SU) and (Load is HI) and (Speed is PH) then (BRD is AC)

Table 5.3 Fuzzy rules for the brachioradialis muscle.

The fuzzy approach to distribute the force was studied both by simulation and also experimentally and compared with the optimization method. The simulation and experimental results are presented and discussed in the next two sections

5.5. SIMULATION RESULTS

Simulation results of force distribution between three elbow flexors muscles, biceps, brachialis and brachioradialis muscles are discussed in this section. In this simulation only the external load was increased linearly from zero to 4 kg and arm/forearm angles, α and β, shown in Fig. 5.1, were considered to be respectively 90° and 0° with the hand in a supine position as shown in Fig. 5.9.

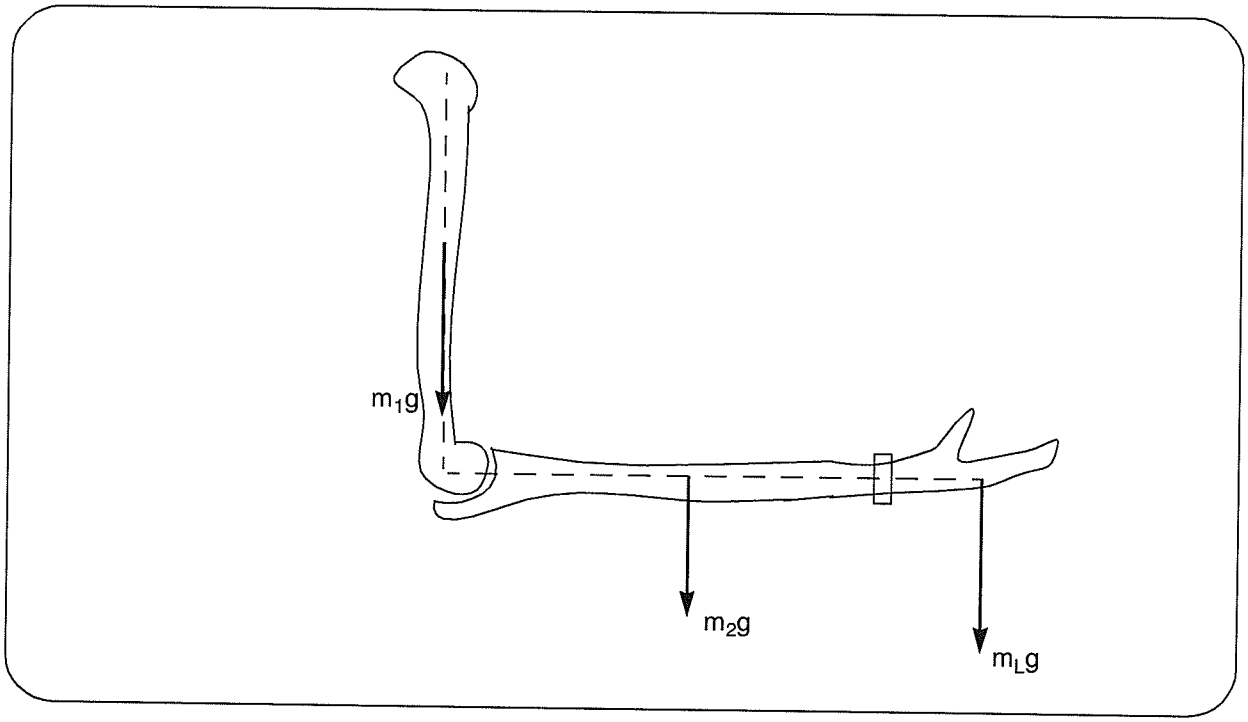

Fig. 5.9 Position of the arm and forearm for the experiment #1.

It should be noted that in this static situation, the left hand sides of the equilibrium equations, Eq. (5-1), are zero. In this section simulation results for the optimization method for two different objective functions discussed in Appendix E are presented first . Then simulation results of the fuzzy logic approach are presented.

The first cost function considered for the optimization problem was as follows.

$$Minimize \qquad F_{Bic}^{p} + F_{Bra}^{p} + F_{Brd}^{p} \tag{5-12}$$

Fig. 5.10 shows the results when $p = 1, 2$. The simplest case, $p = 1$, has a linear cost function. It turns out that only biceps muscle is selected to counterbalance the external force. This muscle has the largest moment arm with respect to the elbow coordinate system, and is the cheapest to use. Although when $p = 2$, all three muscles are involved, biceps has to generate more force because it has the largest moment arm. For this cost function and for the considered arm and forearm angles

$$F_{Bic} > F_{Brd} > F_{Bra} \tag{5-13}$$

always because

$$b_{Bic} > b_{Brd} > b_{Bra} \tag{5-14}$$

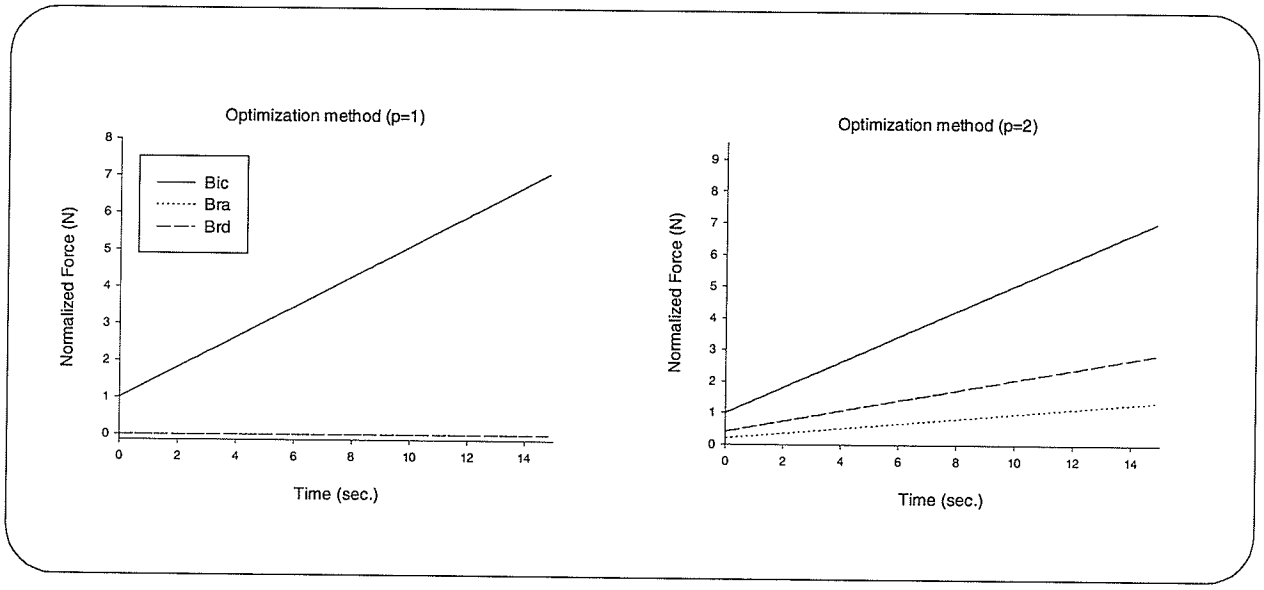

Fig. 5.10 Results of force distribution between three elbow flexors muscles using the optimization method when external load was increased with the cost function of $F_{Bic}^{p} + F_{Bra}^{p} + F_{Brd}^{p}$.

Fig. 5.11 shows the results of force distribution using the optimization approach when the second cost function is considered with $p = 2, 4$.

$$Minimize \qquad (F_{Bic}/A_{Bic})^{p} + (F_{Bra}/A_{Bra})^{p} + (F_{Brd}/A_{Brd})^{p} \tag{5-15}$$

For this cost function

$$F_{Bic} > F_{Bra} > F_{Brd} \tag{5-16}$$

because

$$b_{Bic} \cdot A_{Bic} > b_{Bra} \cdot A_{Bra} > b_{Brd} \cdot A_{Brd} \tag{5-17}$$

Comparing the two results in Fig. 5.11 shows that if p is increased, the forces are closer to each other.

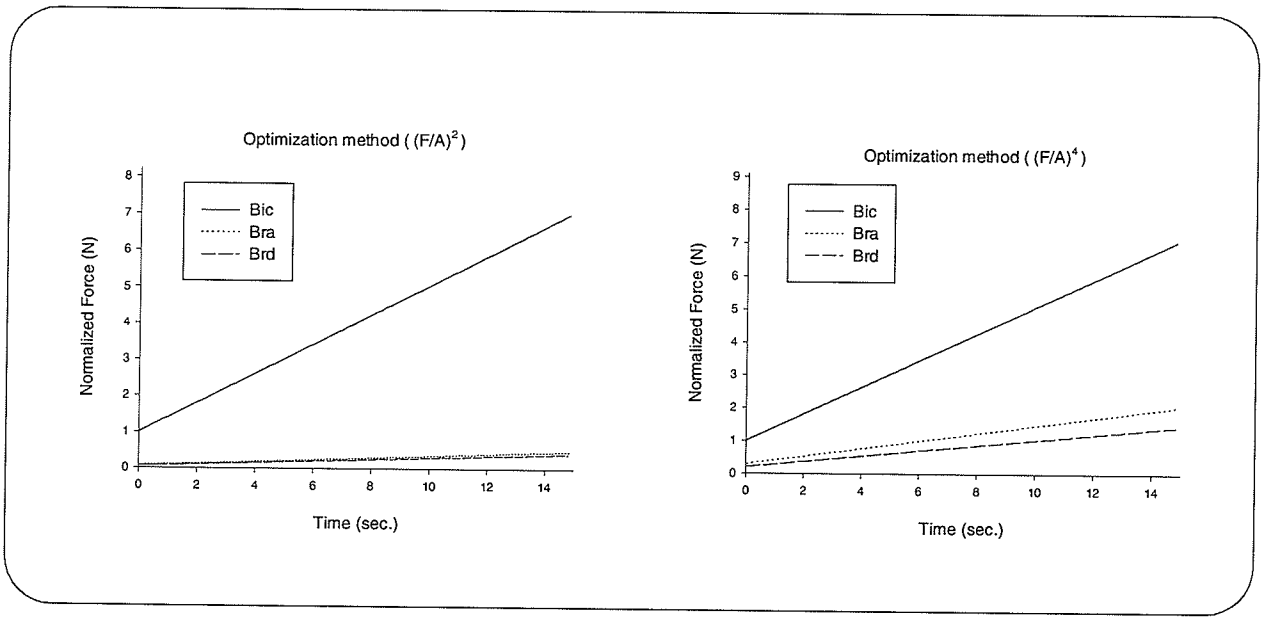

Fig. 5.11 Results of force distribution between three elbow flexor muscles using the optimization method when external load was increased with the cost function of $(F_{Bic}/A_{Bic})^p + (F_{Bra}/A_{Bra})^p + (F_{Brd}/A_{Brd})^p$.

In the results obtained using the optimization method (Appendix E), the moment arm and physiological cross-sectional area (muscle volume divided by its length), PCSA, of the muscle are important factors in the muscle force distribution. Previous formulations did not include other important factors for force distribution, e.g., forearm rotation angle. Using the fuzzy approach three important factors of the force distribution for the elbow flexor muscles, forearm rotation angle, external load and speed of the movement, are considered. Fig. 5.12 shows the weighting coefficient of biceps muscle vs. load and angle when the normalized speed is zero. This figure shows that by increasing the external load, biceps activity will increase. However the activity will be greater when the forearm is in supine position than in the prone position. The weighting coefficient of the biceps muscle vs. load and angle when normalized speed is 0.8 is shown in Fig. 5.13.

It shows that in flexion of the forearm, the biceps is more involved than during the maintenance of the forearm especially when the load is high. The weighting coefficient of the biceps muscle during the extension of the forearm with a normalized speed of -0.8 is shown in Fig. 5.14. It shows that biceps is active during forearm extension when the speed is high and it is more active when the load is high than when the load is low.

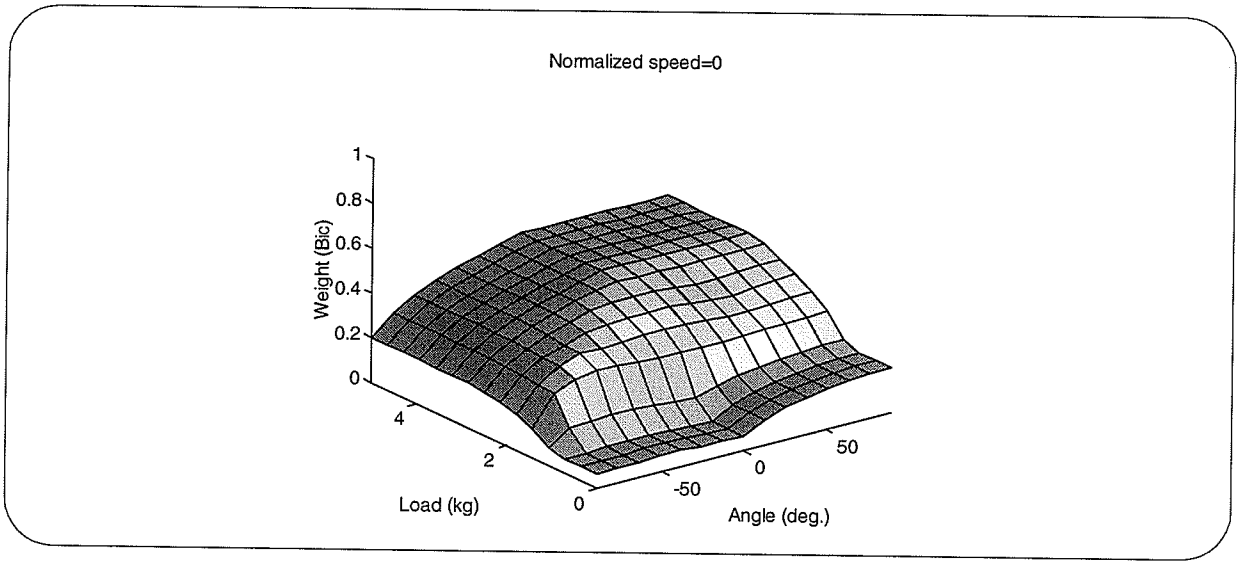

Fig. 5.12 Weighting coefficient calculated using the fuzzy approach for the biceps muscle vs. external load and forearm rotation angle when the normalized speed is zero.

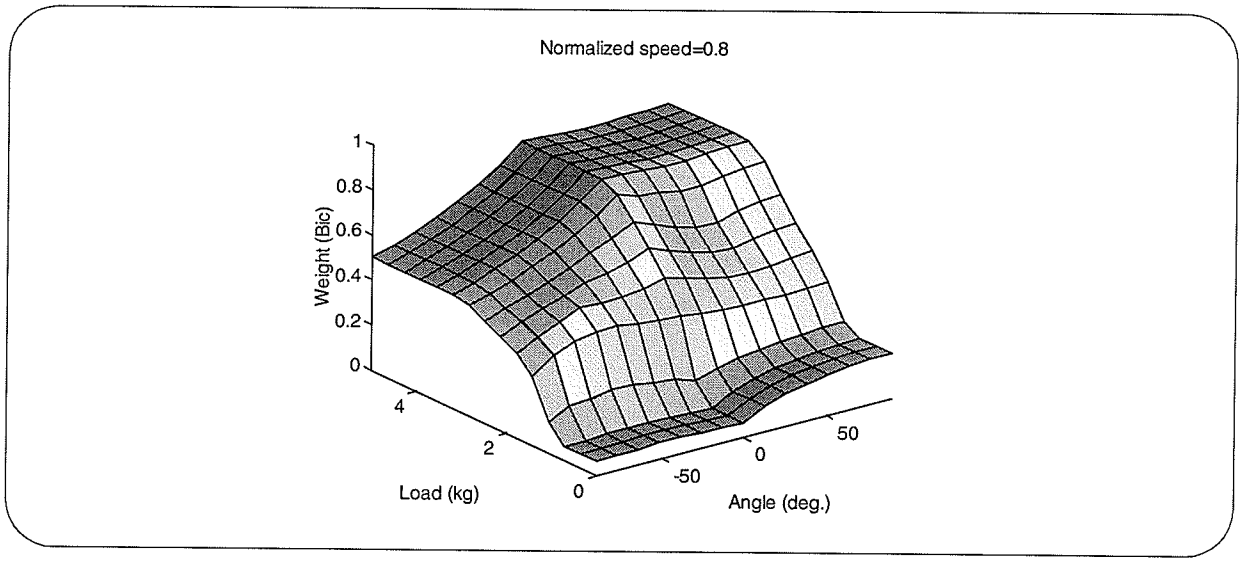

Fig. 5.13 Weighting coefficient calculated using the fuzzy approach for the biceps muscle vs. external load and forearm rotation angle when the normalized speed is 0.8.

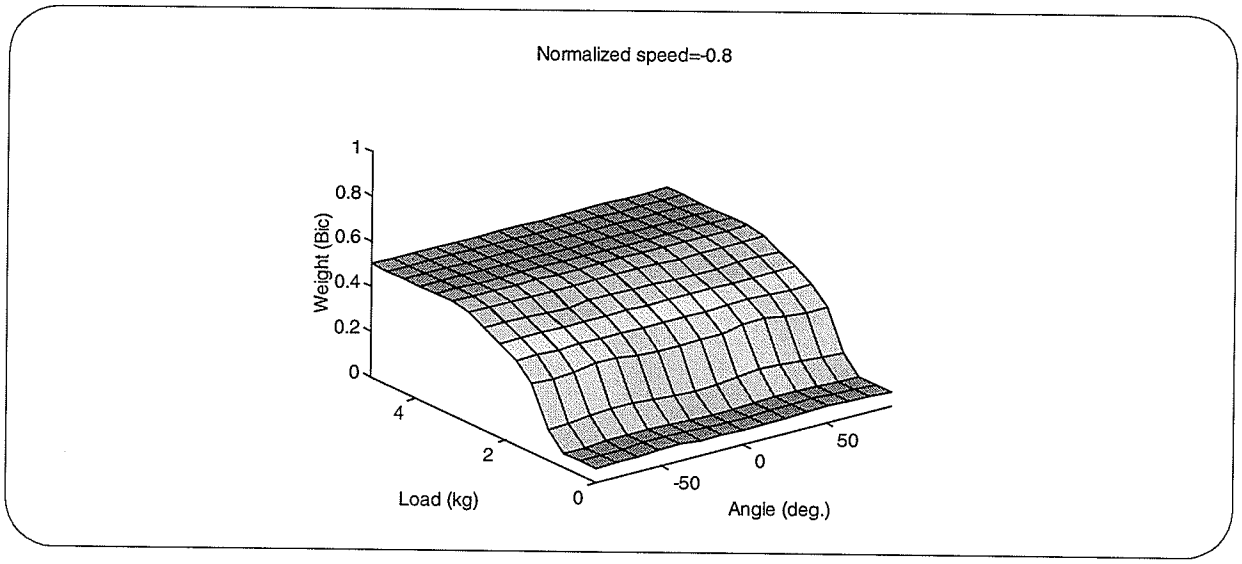

Fig. 5.14 Weighting coefficient calculated using the fuzzy approach for the biceps muscle vs. external load and forearm rotation angle when the normalized speed is -0.8.

The weighting coefficients calculated using the fuzzy approach for the brachialis muscle vs. external load and forearm rotation angle with the normalized speeds of 0, 0.8 and -0.8 are shown respectively in Fig. 5.15, Fig. 5.16 and Fig. 5.17. They show that the change in forearm rotation angle is not an important factor for this muscle. The reason for this is because the line of its pull does not change with pronation or supination. In zero speed, i.e., isometric contraction, its activity is increased with increasing load (Fig. 5.15). In high speed flexion shown in Fig. 5.16, the activity of the brachialis is maximum. Fig. 5.17 shows that brachialis is not active during the high speed extension of the forearm.

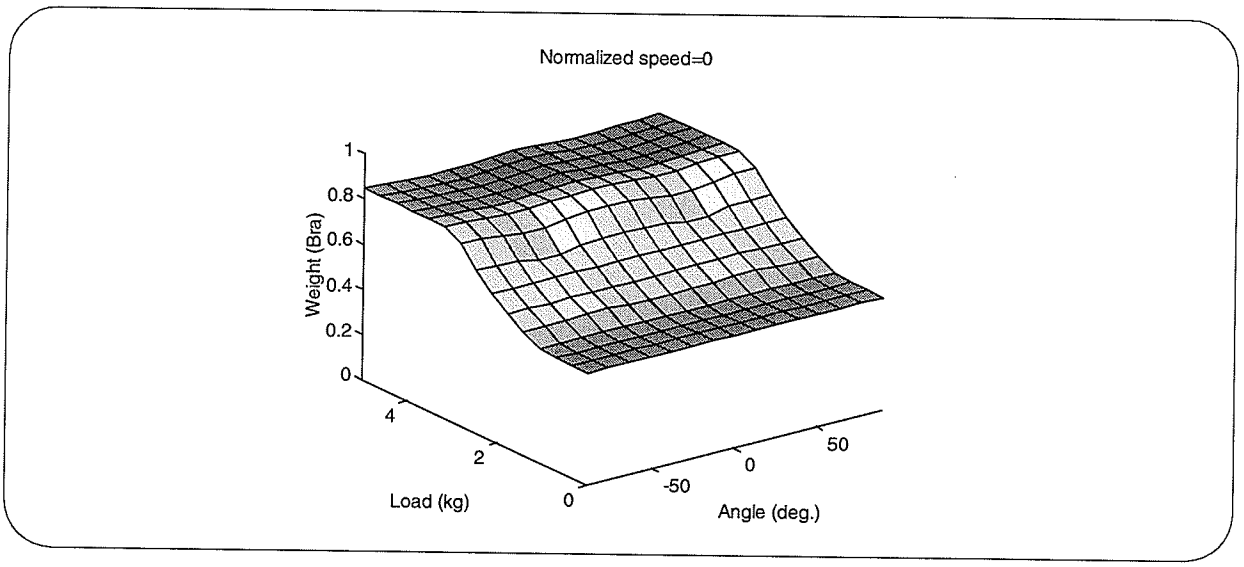

Fig. 5.15 Weighting coefficient calculated using the fuzzy approach for the brachialis muscle vs. external load and forearm rotation angle when the normalized speed is zero.

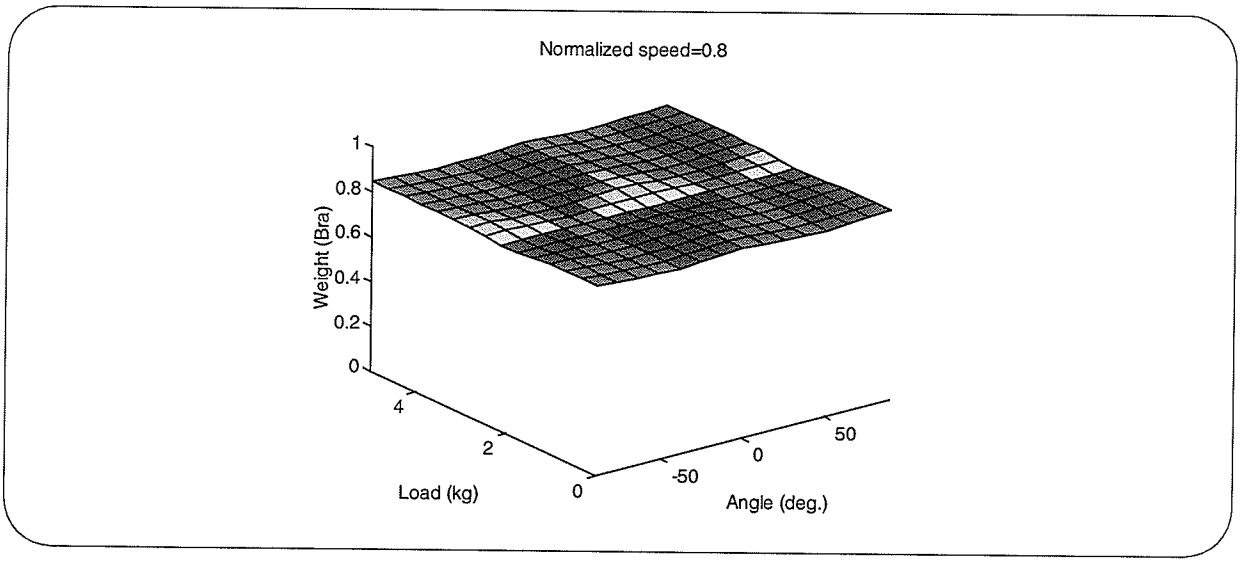

Fig. 5.16 Weighting coefficient calculated using the fuzzy approach for the brachialis muscle vs. external load and forearm rotation angle when the normalized speed is 0.8.

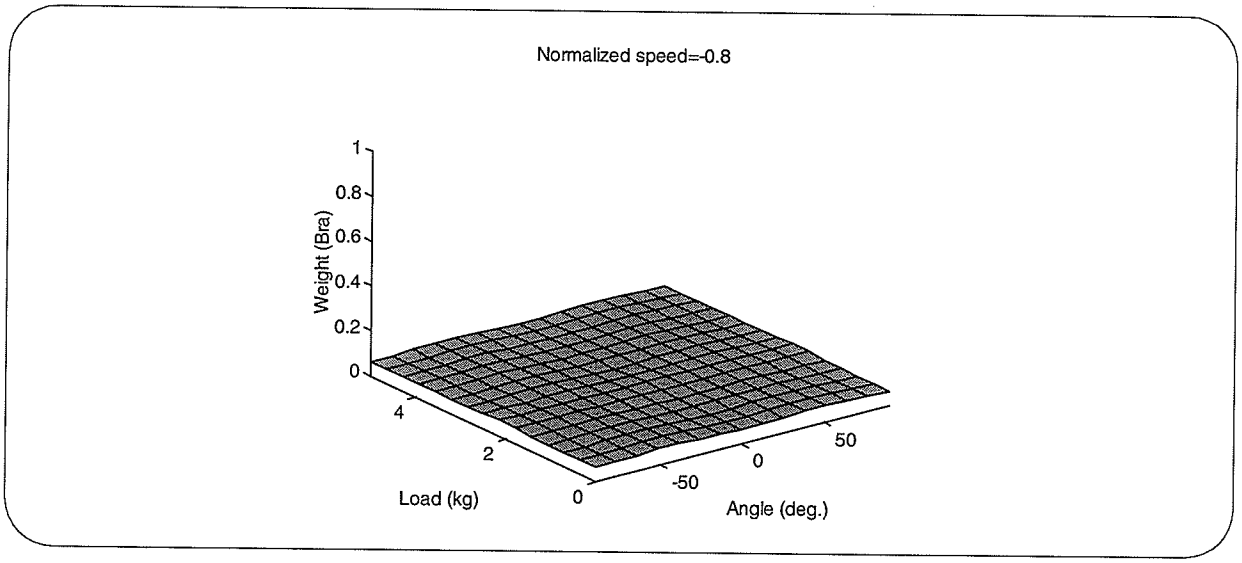

Fig. 5.17 Weighting coefficient calculated using the fuzzy approach for the brachialis muscle vs. external load and forearm rotation angle when the normalized speed is -0.8.

Activities of the brachioradialis muscle calculated using the fuzzy approach vs. external load and forearm rotation angle are shown in Fig. 5.18, Fig. 5.19 and Fig. 5.20 respectively with the normalized speeds of 0, 0.8 and -0.8. They show that this muscle is more active in semiprone and prone positions than in the supine position of the forearm. Also, it is quite active during quick flexion (Fig. 5.19) and extension (Fig. 5.20).

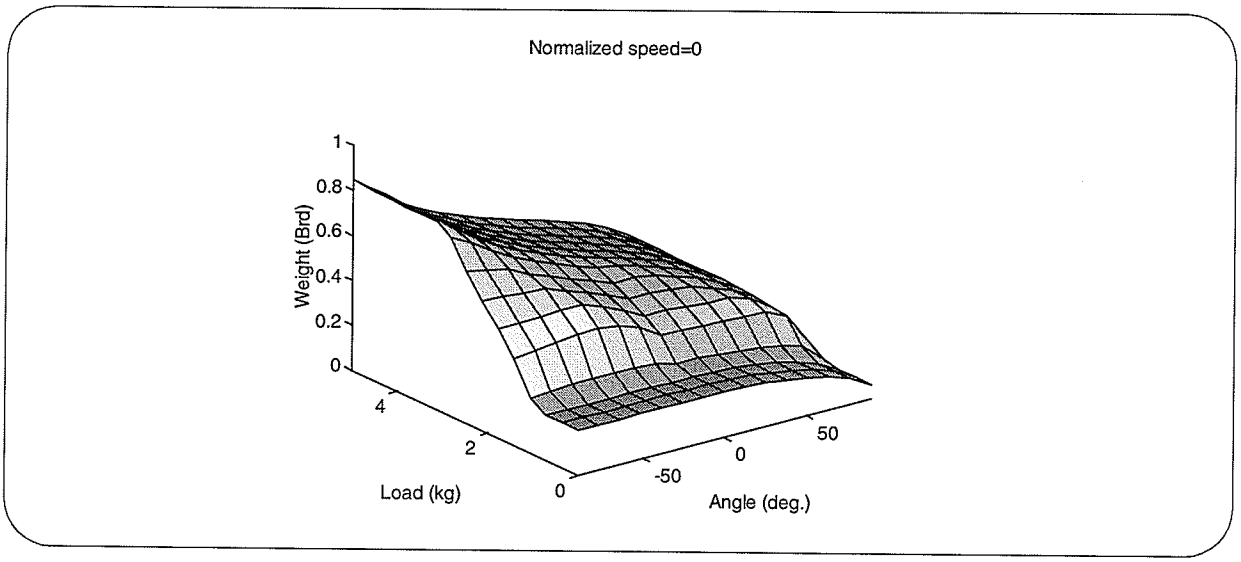

Fig. 5.18 Weighting coefficient calculated using the fuzzy approach for the brachioradialis muscle vs. external load and forearm rotation angle when the normalized speed is zero.

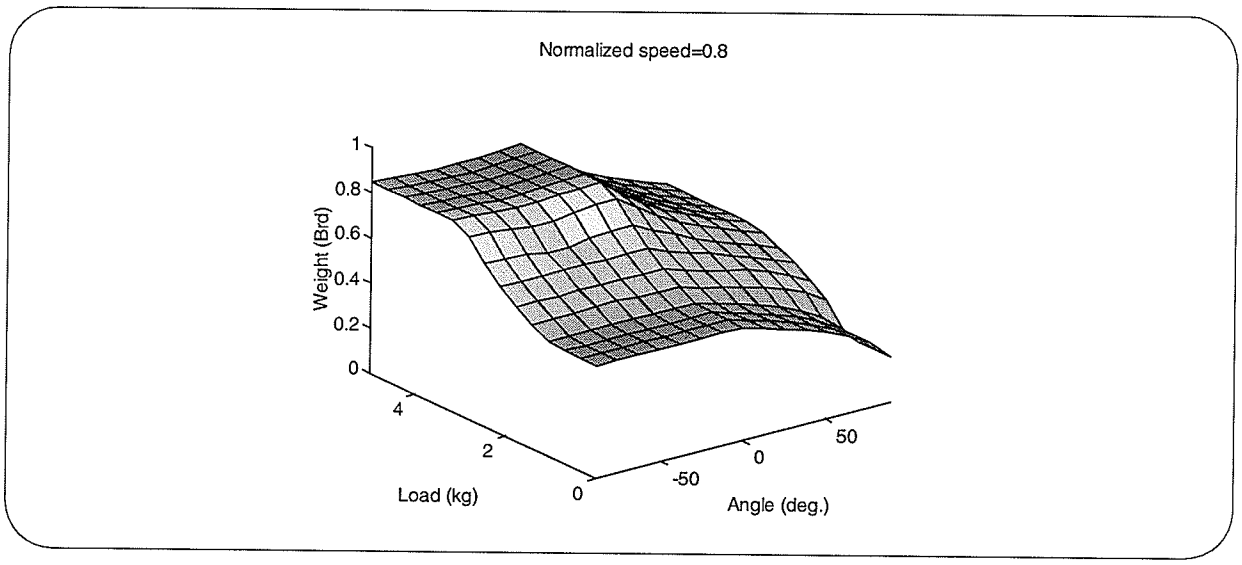

Fig. 5.19 Weighting coefficient calculated using the fuzzy approach for the brachioradialis muscle vs. external load and forearm rotation angle when the normalized speed is 0.8.

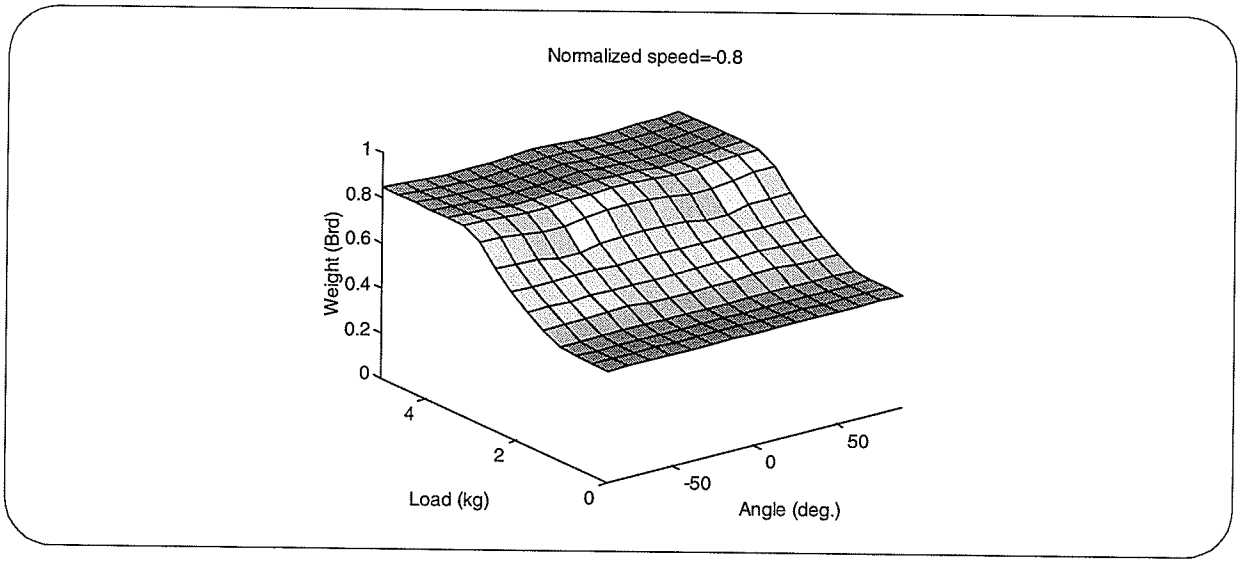

Fig. 5.20 Weighting coefficient calculated using the fuzzy approach for the brachioradialis muscle vs. external load and forearm rotation angle when the normalized speed is -0.8.

Fig. 5.21 shows simulation results of force distribution between three elbow flexor muscles using the fuzzy approach when external load is increased. At first the brachialis has more force than two other muscles. However when the load is increased the biceps is more active. Therefore the slope of the brachialis muscle force is decreased. At the end the brachialis muscle force reaches its maximum value and its force curve is flat.

Comparison of the results obtained using the fuzzy approach (Fig. 5.21) and the optimization method (Fig. 5.10 and Fig. 5.11) shows that, in this case, external load plays a major role in force distribution using the fuzzy approach. However in the optimization method, moment arm, cost function and p are important factors.

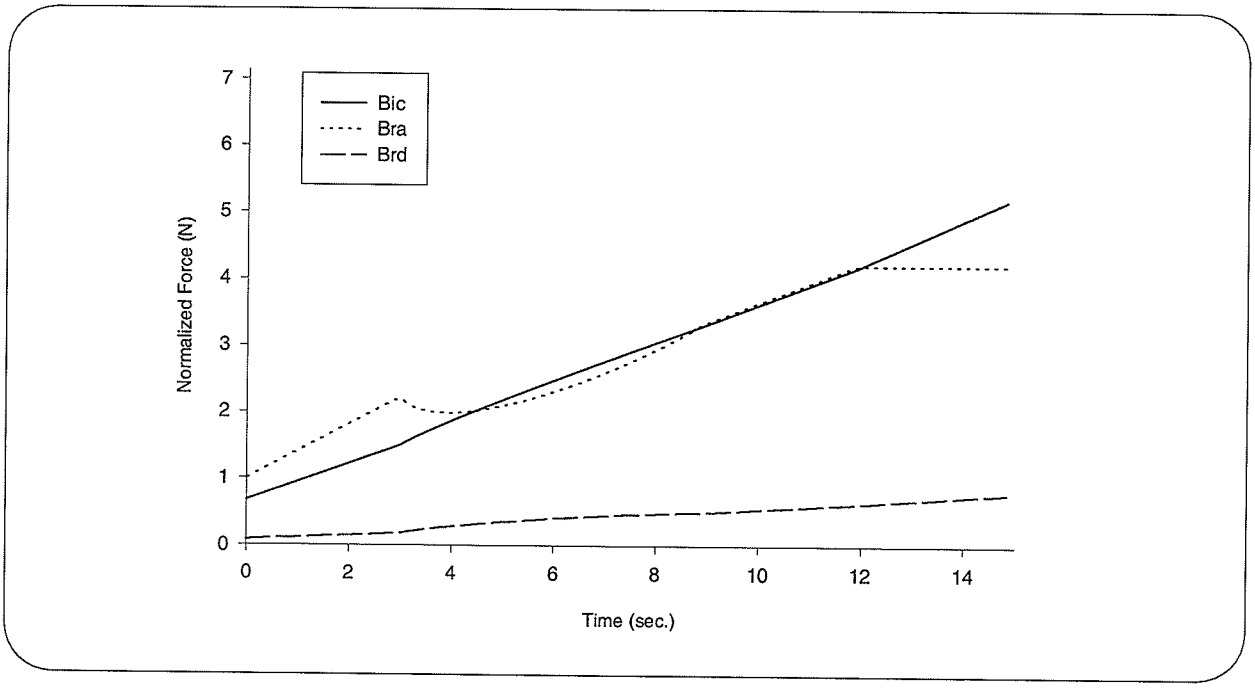

Fig. 5.21 Results of force distribution between three elbow flexor muscles using the fuzzy approach when external load was increased.

Results of force distribution for the biceps muscle using the fuzzy approach in supine, semi-prone and prone positions of the forearm when the external load was increased are shown in Fig. 5.22. It shows that in a prone position the biceps is always less active than in the two other positions. Also at first, when the load is low, the biceps has its greatest activity in the supine position. However by increasing load there is not much difference in biceps activity in supine and semi prone positions.

Comparing the results obtained using the fuzzy approach (Fig. 5.22) and the optimization method (Fig. 5.10 and Fig. 5.11) shows that the rotation angle of the forearm is an important factor in force distribution using the fuzzy approach. However in the optimization method, there will not be any change in biceps muscle force due to the change in the forearm rotation angles.

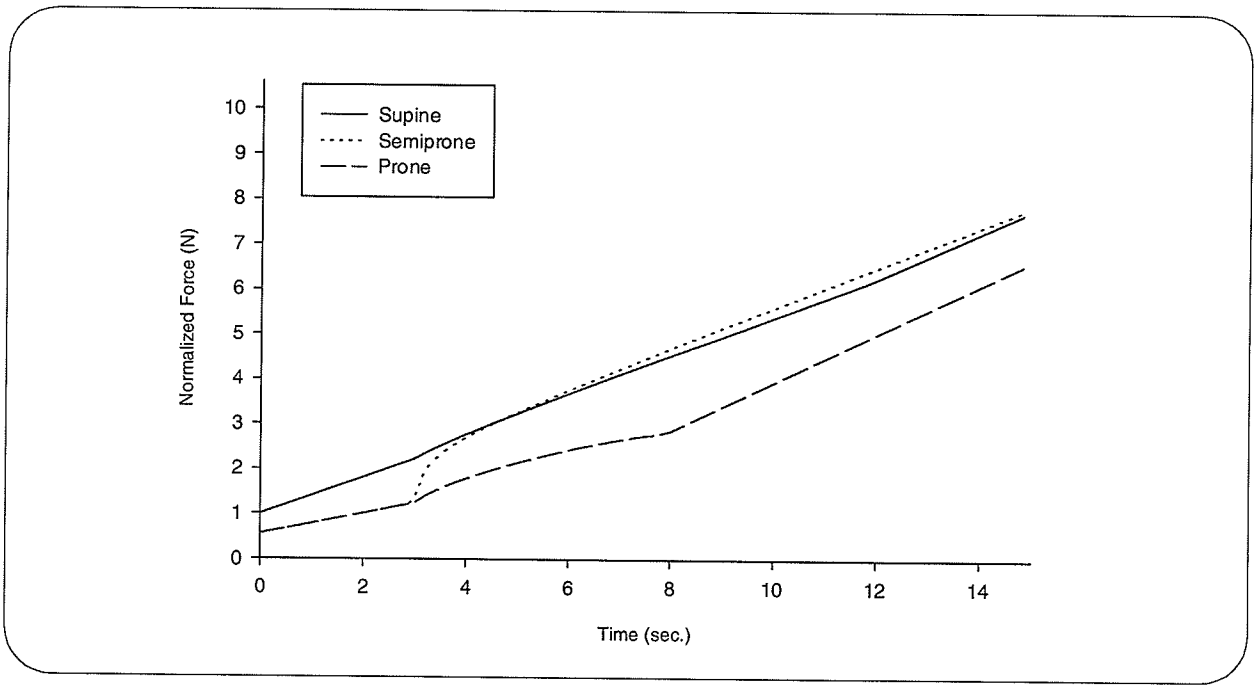

Fig. 5.22 Results of force distribution for the biceps muscle using the fuzzy approach in supine, semiprone and prone positions of the forearm when external load was increased.

5.6. EXPERIMENTAL RESULTS

Besides the simulation, an experiment was performed. Two types of experiments were done where the subjects were three healthy males. The purpose of the first experiment (Exp. #1) was to investigate the force produced by three muscles, Bic, Bra and Brd, in an isometric condition when a load is added to the hand. The purpose of the second experiment (Exp. #2) was to investigate the force produce by one of the muscles in three different orientations of the forearm, i.e. prone, semi-prone and supine.

5.6.1. EXPERIMENT #1

In this experiment, a subject was asked to hold a load in his hand with the upper limb in the position where the arm and forearm angles (α and β shown in Fig. 5.1) were respectively 90° and 0° and the hand in a supine position as shown in Fig. 5.9. Then load was added until the maximum value that the subject could hold was recorded. Electromyographic (EMG) signals were recorded from the three muscles, Bic, Bra and Brd, using surface electrodes. For each subject, there were four trials, each of 30 seconds duration with the sampling frequency of 1 KHz. Because the root mean square (RMS) value of the EMG signals in isometric condition is considered to be a good representation for muscle force [58], the RMS was calculated over every 250 msec of the EMG signals. Then the average of RMS values was calculated over six windows each of 5 seconds in length.

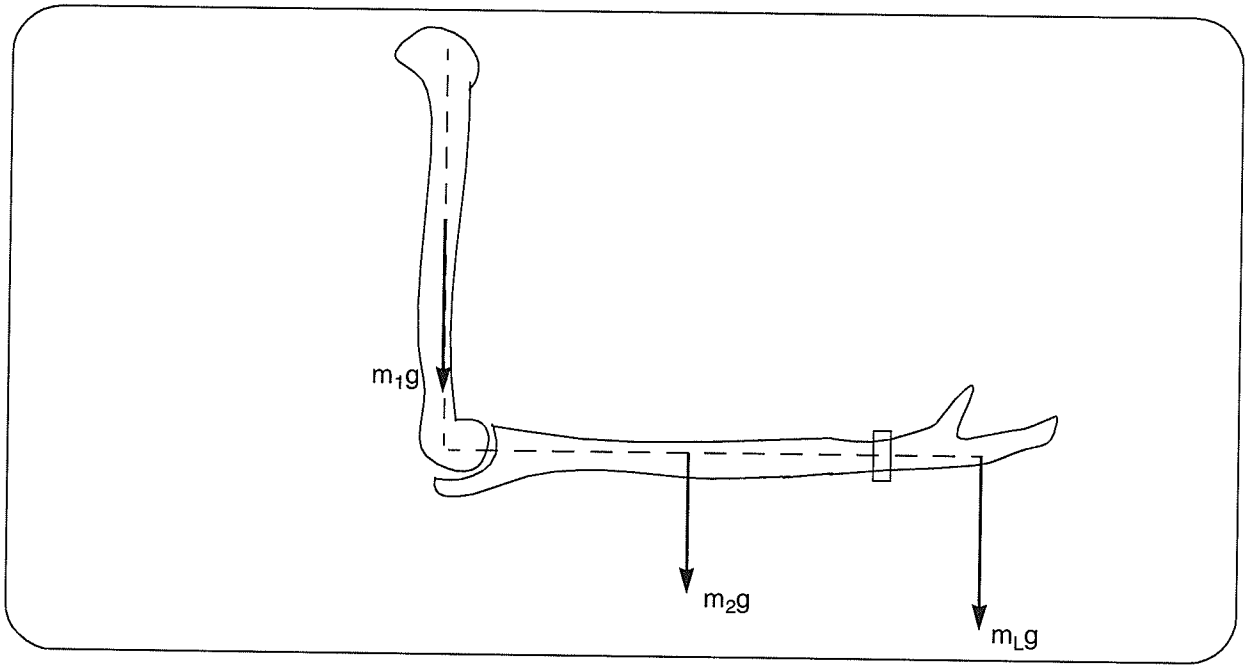

Fig. 5.23 Position of the arm and forearm for the experiment #1.

Fig. 5.24 shows the RMS values of EMG signals from the first subject for four trials of the first experiment. The RMS of each muscle was normalized so that the maximum value is one. It should be noted that RMS values of the EMG signals from different muscles are not comparable with each other. The results of the first experiment for subjects 2 and 3 are shown respectively in Fig. 5.25 and Fig. 5.26. The results showed that in most cases the slope of the RMS of the brachialis muscle decreased at the end of the experiment which means that the brachialis muscle was the first muscle whose force reached its maximum value and was saturated. This supports the results of the force distribution using the fuzzy approach shown in Fig. 5.21. A decrease in slope of the RMS value of the EMG from brachialis muscle and an increase in the RMS value of EMG from biceps muscle at the middle of the experiment were seen in some cases of the experimental results. This supports the idea that biceps is less active when the load is low and it becomes more active as the load increased.

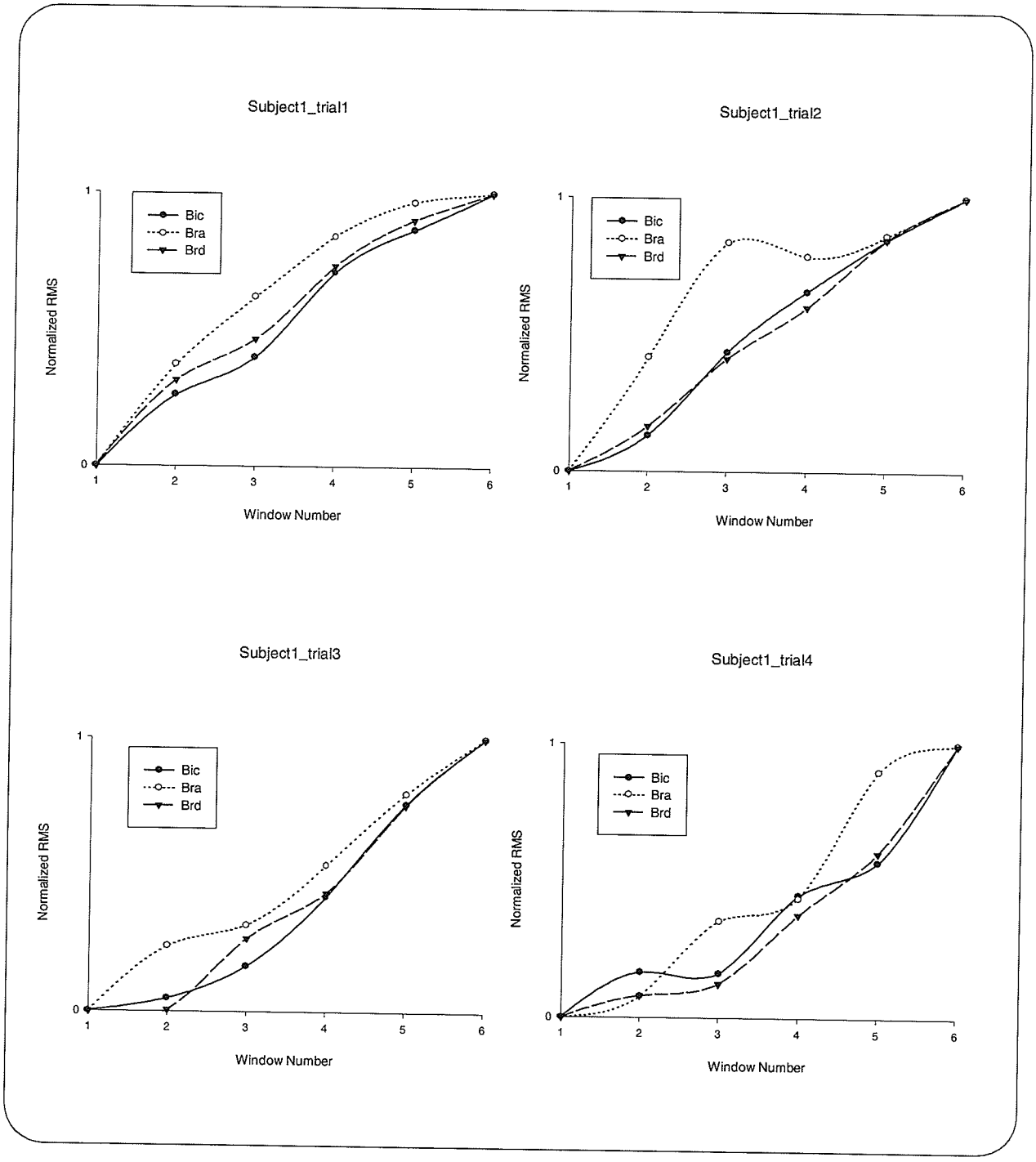

Fig. 5.24 Normalized RMS of EMG signals when external load was increased for subject 1.

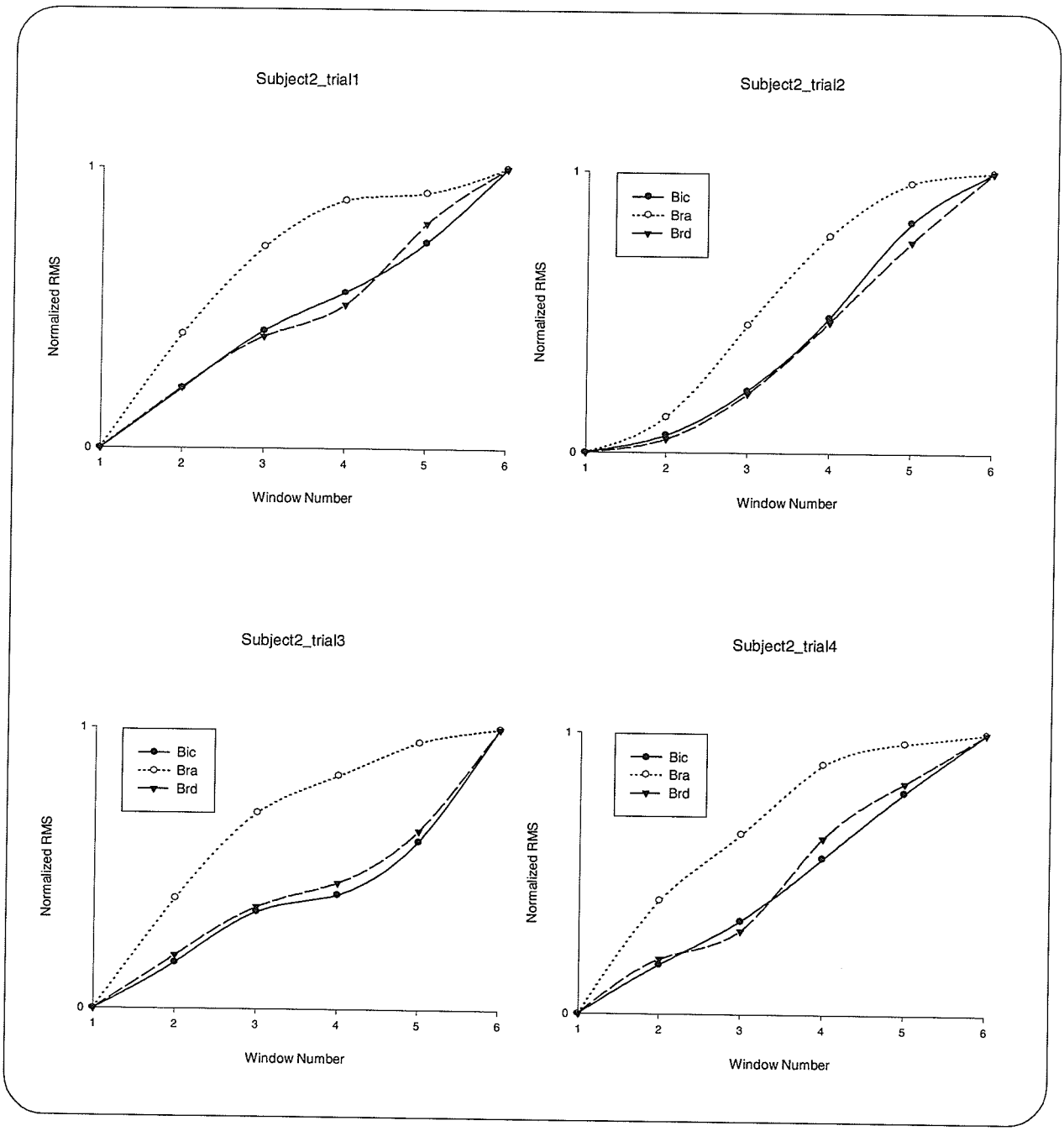

Fig. 5.25 Normalized RMS of EMG signals when external load was increased for subject 2.

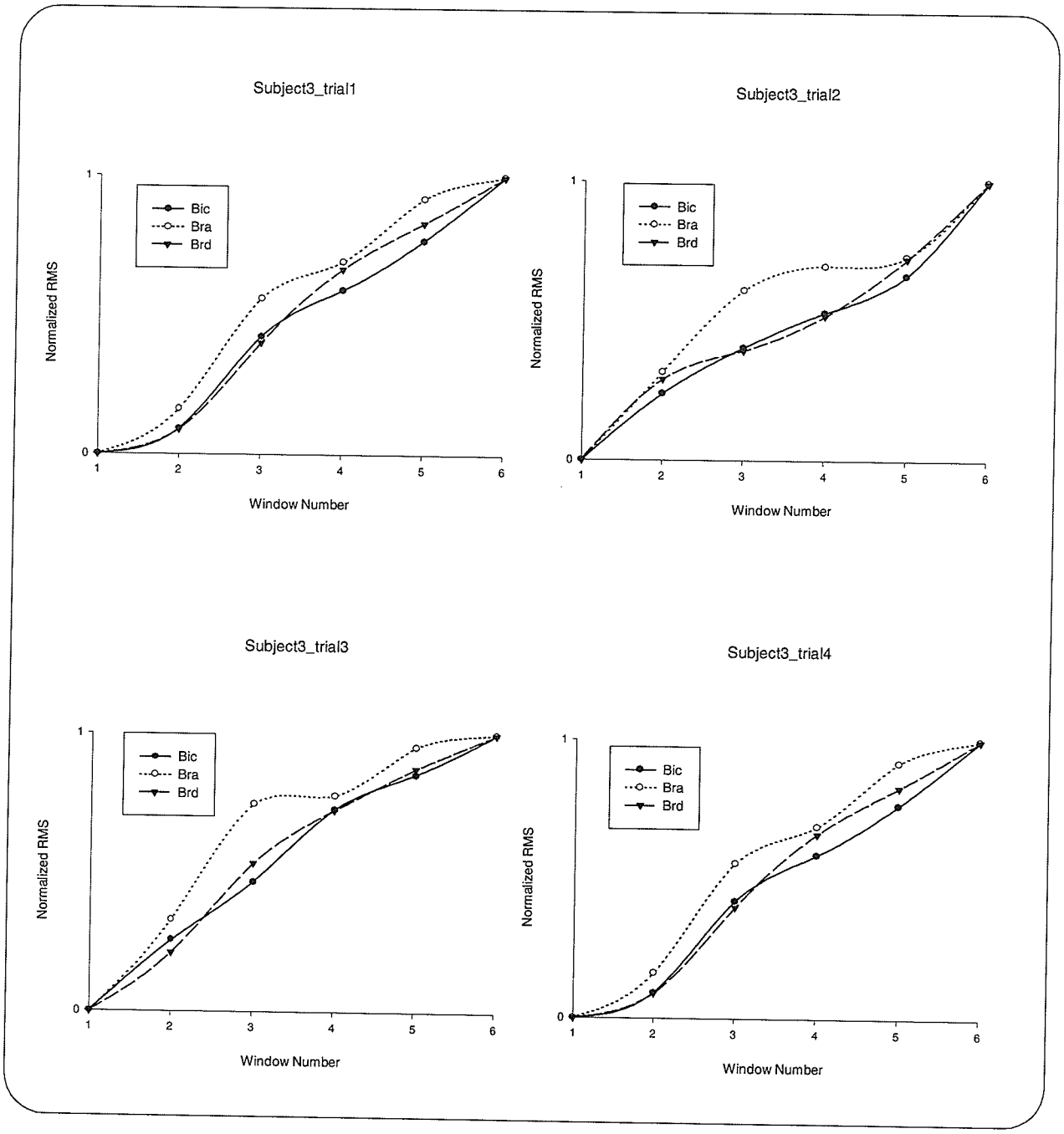

Fig. 5.26 Normalized RMS of EMG signals when external load was increased for subject 3.

5.6.2. EXPERIMENT #2

The second experiment was performed with the same arm and forearm angles shown in Fig. 5.9, but for three different orientations of the forearm and hand- supine, semiprone and prone. Load was increased during the course of experiment, but not to its maximum value as in Exp #1. The three orientations of the forearm were randomly assigned. Because the purpose of this experiment was to compare the force generated by one muscle in different orientations of the forearm, the EMG signals recorded by surface electrodes from the muscle should be comparable directly. Among the three muscles, Bic is the only one that is superficial and offers a large area of recording. Therefore its EMG signals can be compared in different orientations of the forearm. The relative position of the surface electrodes with respect to the Bra and Brd muscles will be changed in different orientations of the forearm; therefore, in this experiment only signals from the Biceps muscle were recorded and it was assumed that these EMG signals are comparable in different orientations of the forearm.

Fig. 5.27/5.28 and Fig. 5.29/5.30 show respectively, the RMS value of EMG signals from subject 1 and subject 2 for two trials. RMS values in the prone orientation of the forearm were always less than those in the two other orientations, i.e., the biceps muscle was least active in the prone orientation. This supports the results of force distribution using the fuzzy approach (Fig. 5.22). Also, at no load (the first point in the curves), the biceps always had the highest activity with the forearm in the supine position. This also supports the prediction of the forces using the fuzzy approach. It should be noted that when the optimization method is used to distribute the force, the position of the forearm is not an important factor and the muscle force is the same for all different positions of the forearm.

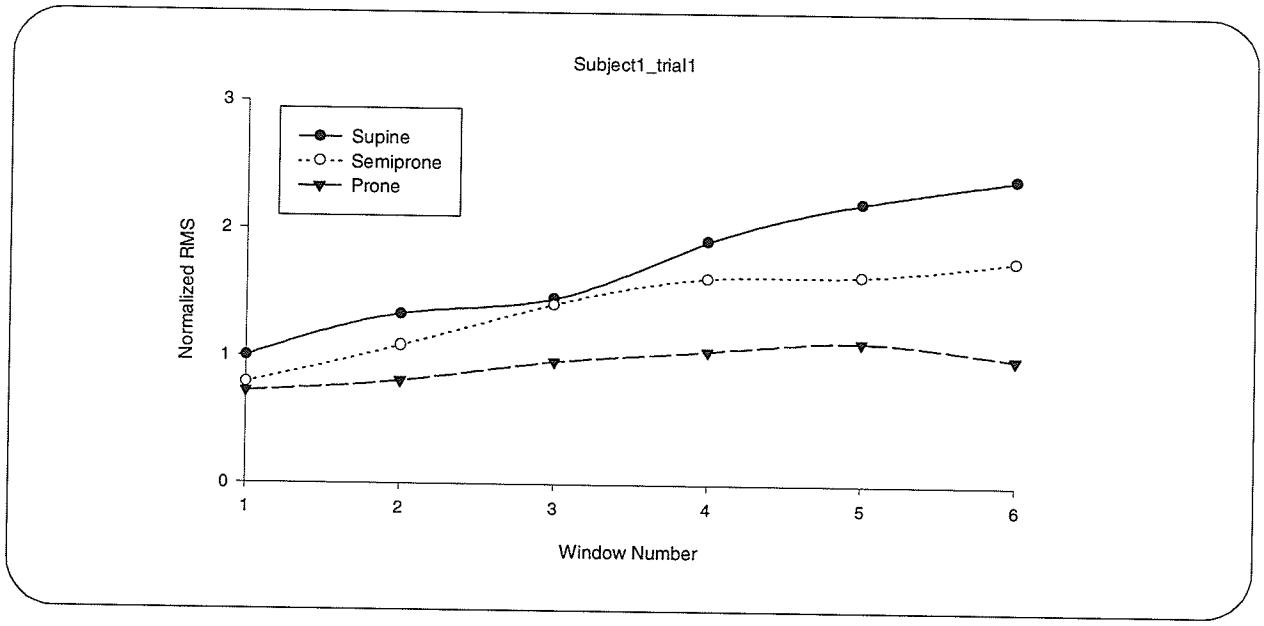

Fig. 5.27 Normalized RMS of the biceps EMG signal when external load was increased in supine, semiprone and prone positions of the forearm for the subject1_trial1.

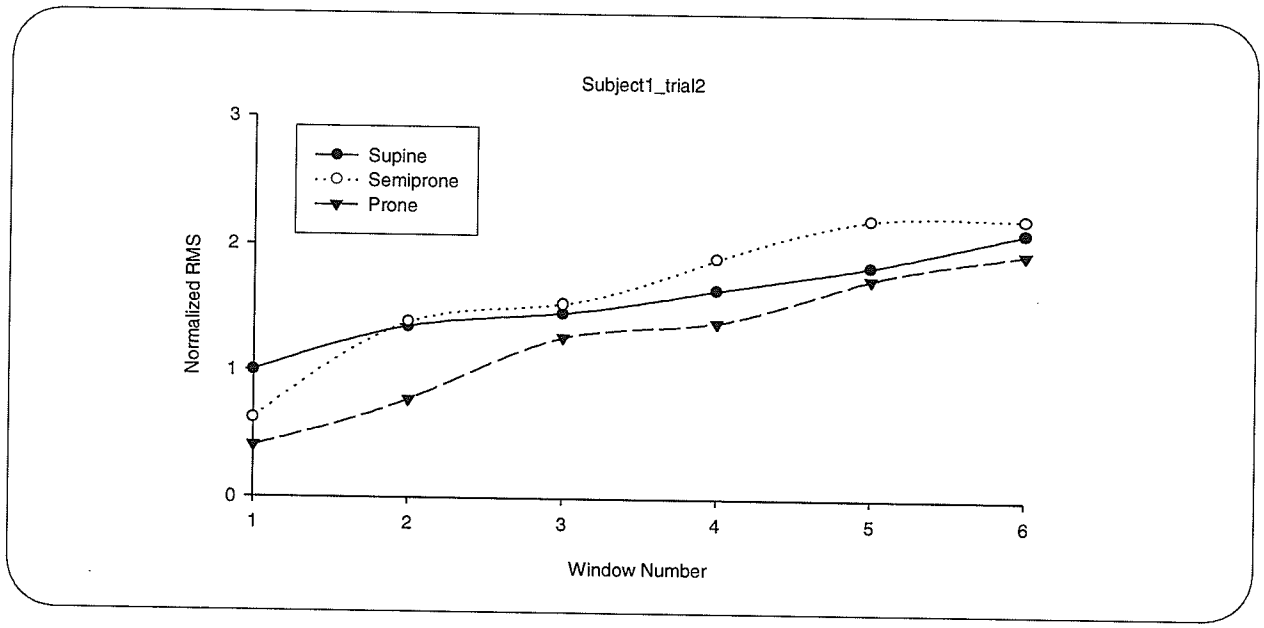

Fig. 5.28 Normalized RMS of the biceps EMG signal when external load was increased in supine, semiprone and prone positions of the forearm for the subject1_trial2.

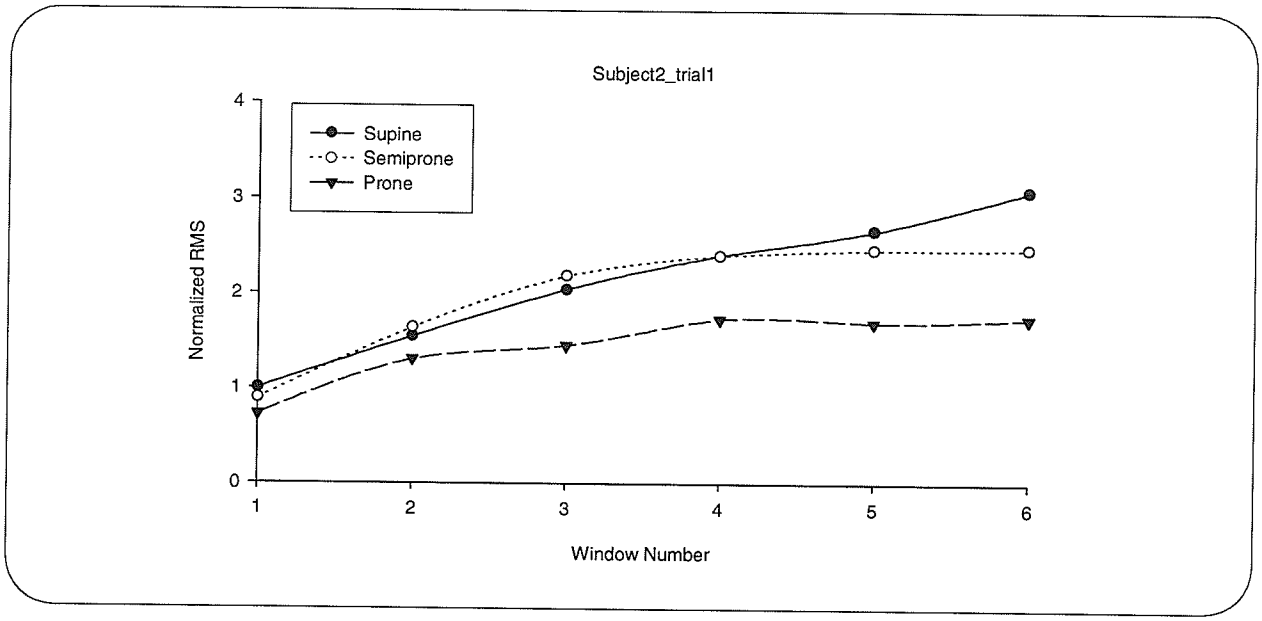

Fig. 5.29 Normalized RMS of the biceps EMG signal when external load was increased in supine, semiprone and prone positions of the forearm for the subject2_trial1.

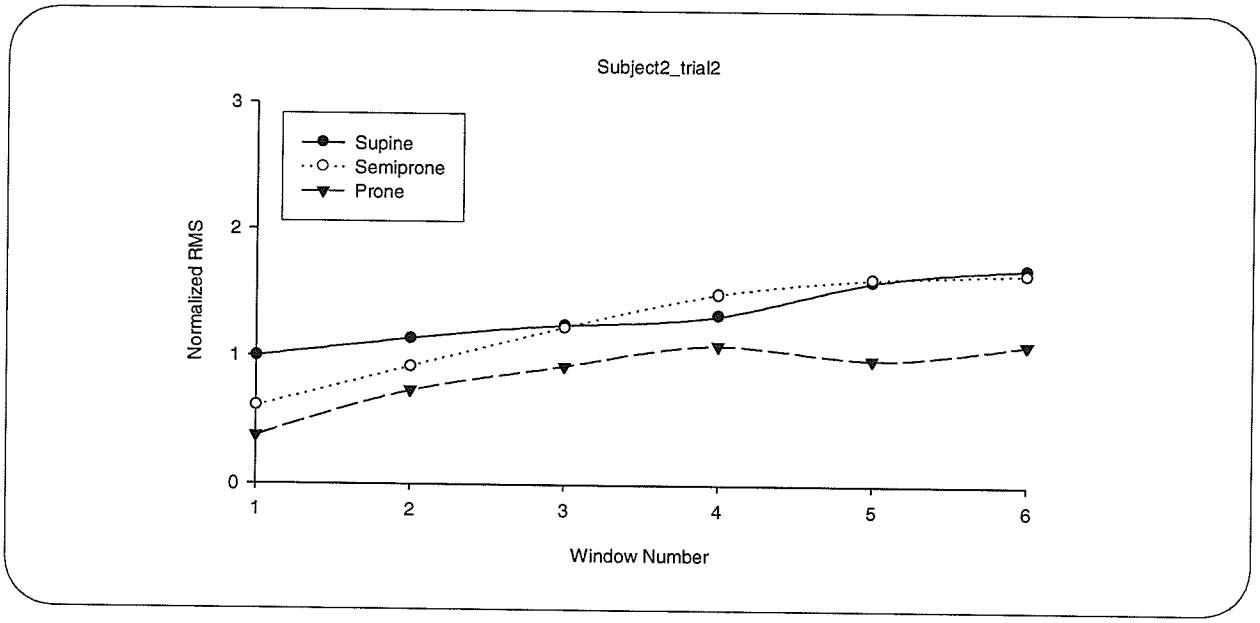

Fig. 5.30 Normalized RMS of the biceps EMG signal when external load was increased in supine, semiprone and prone positions of the forearm for the subject2_trial2.

5.7. SUMMARY

In many applications, such as orthopedics and rehabilitation, it is desired to know the forces in individual skeletal muscles. A new approach for the partitioning of the intersegmental forces, i.e., the force distribution problem, using fuzzy logic is discussed in this chapter. The approach is illustrated by partitioning the muscle forces acting on the elbow joint. The rotation angle of the forearm, the speed of the movement and the external load are three inputs of the fuzzy model. Ninety rules are developed for the relation between input interface and output interface of the fuzzy model.

The results of optimization method for the specific tasks are presented and compared with the fuzzy logic method. Although there is a great need to perform more experiments to validate the predictions, experimental results showed that the fuzzy logic approach distributes force between muscles better than a commonly used optimization method. The new method therefore should be a promising paradigm for the force distribution problem.

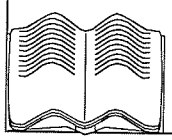

CHAPTER 6. CONCLUSION AND RECOMMENDATIONS

6.1. CONCLUSION

This thesis addressed the problem of determining joint forces and moments, power and energy flows, individual muscle forces and internal joint forces for the upper limb. To find these kinetic variables, kinetic equations were established. A 3D link-segment model, along with the kinematic variables based on motion data, was used to develop the kinetic equations which govern the dynamic behaviour of a limb.

The model has ten degrees of freedom (DOF), three translational and three rotational DOF for the shoulder joint, two rotational DOF for the elbow joint and two rotational DOF for the hand joint. The seven rotational DOF were represented by nine Euler angles with three translational DOF obtained by an approach developed in this research. It was shown that there is a significant difference in the calculated power if the three translational DOF are ignored.

Four methods of smoothing the kinematic data (Butterworth filter, polynomial curve fitting, median filter and splines method) were reviewed and compared at three levels, raw data, first derivative and second derivative. The results showed that in most cases at the first level of comparison, i.e., raw data, all methods except the median filter have similar results. However at the first and second levels, the splines method had significantly less error.

The kinematic data was the input to the kinetic equations developed using both Lagrangian and Newtonian methods. The analytical relationship between the two methods was shown in the thesis. Besides developing the kinetic equations, two methods for determining power flows were explained. It was shown that the two methods produce the same result. The major significance of

this is that correlation between them can not be used as a measure to validate the model as suggested in some literature.

Finally the force distribution problem was discussed. A new approach to the problem using fuzzy logic was introduced. The method was developed for the flexion/extension of the elbow joint. The intersegmental force was distributed between the three flexor muscles- biceps, brachialis and brachioradialis- using both the optimization method and the fuzzy approach. Both simulation and experimental results were used to compare the two methods. Although there is a great need to perform more experiments to validate the predictions, experimental results show that the fuzzy approach includes the parameters that distribute force between muscles better than the optimization method.

6.2. CONTRIBUTIONS OF THIS RESEARCH

The major contributions of this research are listed as follows.

- A link-segment model was developed for the upper limb using 6 markers. Using this model seven rotational and three translational DOF variables of the upper limb can be calculated.
- An analytical proof was provided that shows the equivalence between two methods to calculate power. This negates the hypothesis that correlation between the calculated powers can be used as a measure to verify the kinematic model.
- A new approach was presented to calculate three translational DOF variables of the upper limb. These are very important for kinetic analysis.
- A new technique was established for force distribution using fuzzy logic. This method distributes force between muscles better than the commonly used optimization method.

6.3. RECOMMENDATIONS FOR FUTURE RESEARCH

In this research different areas of upper limb motion analysis and dynamic analysis were covered. However several areas of future investigation are suggested.

Rotational degrees of freedom of the model presented in this research are obtained using Euler angles. However, the mapping between Euler angles and anatomical angles was not determined. Finding this mapping and/or a way to describe the motion mathematically based on the anatomical angles is an interesting area for a future research.

The force distribution problem presented in this research using fuzzy logic has great flexibility. Although some experiments were performed, there is a need to perform more experiments to refine the fuzzy rules and verify them. To extend the fuzzy logic approach the following steps should be considered:

- Study the functional behaviour of the muscle of interest, i.e., determine the parameters that affect the force generated by that muscle.
- Consider those parameters as the inputs to the model.
- Assign membership functions to the model inputs.
- Set fuzzy rules based on functional behaviour of the muscle and model inputs.
- Perform experiments to compare and verify the fuzzy logic method results.

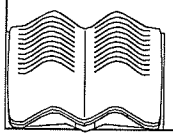

REFERENCES

[1] P. Allard, I. A. F. Stokes, J. P. Blanchi, *Three-dimensional analysis of human movement.* Champaign: Human Kinetics, 1995.

[2] A. I. King, "A review of biomechanical models," *Journal of Biomechanical Engineering,* vol. 106, pp. 97-106, 1984.

[3] G. L. Kinzel and L. J. Gutkowski, "Joint models, degrees of freedom, and anatomical motion measurement," *Journal of Biomechanical Engineering,* vol. 105, pp. 55-62, 1983.

[4] E. Y. Chao and B. F. Morrey, "Three-Dimensional rotation of the elbow," *Journal of Biomechanics*, vol. 11, pp. 57-73, 1978.

[5] K. M. Jackson, J. Joseoh and S. J. Wyard, "A mathematical model of arm swing during human locomotion," *Journal of Biomechanics*, vol. 11, pp. 277-289, 1978.

[6] Y. Youm, R. F. Dryer, K. Thambyrajah, A. E. Flatt and B. L. Sprague, "Biomechanical analysis of forearm pronation-supination and elbow flexion-extension," *Journal of Biomechanics,* vol. 12, pp. 245-255, 1979.

[7] N. A. Langrana, "Spatial kinematic analysis of the upper extremity using a bipolar videotaping method," *Journal of Biomechanical Engineering*, vol. 103, pp. 11-17, 1981.

[8] K. Schneider, R. F. Zernicke, R. A. Schmidt and T. Hart, "Changes in limb dynamics during the practice of rapid arm movements," *Journal of Biomechanics*, vol. 22, pp. 805-817, 1989.

[9] R. Safaee-Rad, E. Shwedyk and A. O. Quanbury, "Three-dimensional measurement system for functional arm motion study," *Medical & Biological Engineering & Computing*, vol. 28, pp. 569-573, 1990.

[10] C. F. Small, J. T. Bryant and D. R. Pichora, "Rationalization of kinematic descriptors for three-dimensional hand and finger motion," *Journal of Biomedical Engineering*, vol. 14, pp. 133-141, 1992.

[11] D. P. Romilly, C. Anglin, R. G. Gosine, C. Hershler and S. U. Raschke, "A functional task analysis and motion simulation for the development of a powered upper-limb orthosis," *IEEE Transactions on Rehabilitation Engineering*, vol. 2, pp. 119-129, 1994.

[12] E. Sprigings, R. Marshall, B. Elliott and L. Jennings, "A three-dimensional kinematic method for the determining the effectiveness of arm segment rotations in the producing racquet-head speed," *Journal of Biomechanics*, vol. 27, pp. 245-254, 1994.

[13] J. P. Schade, *Introduction to functional human anatomy*, Philadelphia, Saunders, 1974.

[14] G. L. Kinzel, A. S. Hall and B. M. Hillbery, "Measurement of the total motion between two body segments -I. Analytical development," *Journal of Biomechanics*, vol. 5, pp. 93-105, 1972

[15] M. D. Zimmerman, "Designing thee ultimate man/machine interface technology for the handicapped," *Machine Design*, vol. 8, pp. 38,43, 1982.

[16] S. C. Jacobsen, D. F. Knutti, R. T. Johnson and H. H. Sears, " Development of the Utah artificial arm," *IEEE Transactions on Biomedical Engineering*, BME-29, No. 4, pp. 249-269, 1982.

[17] R. Fazel-Rezai, E. Shwedyk and S. Onyshko, "Three dimensional kinematic model of the upper limb with ten degrees of freedom," *Proceedings of IEEE EMBS Conference,* p. 137, 1997.

[18] V. H. Frankel and M. Nordin, *Basic biomechanics of the skeletal system*, Lea & Febiger, Philadelphia, 1980.

[19] J. J. Crisco, X. Chen, M. M. Panjabi and S. W. Wolfe, "Optimal marker placement for the calculating the instantaneous center of rotation," *Journal of Biomechanics*, vol. 27, pp. 1183-1187, 1994.

[20] K. N. An, E. Y. Chao, "Kinematic analysis of human movement," *Annals of Biomedical Engineering*, vol. 12, pp. 585-597, 1984.

[21] M. M. Panjabi, V. K. Goel, S. D. Walter and S. Schick, "Errors in the center and angle of rotation of a joint: An experimental study," *Transactions of the ASME*, vol. 104, pp. 232-237, 1982.

[22] S. Holzereiter, "Calculation of the instantaneous center of rotation for a rigid body," *Journal of Biomechanics*, vol. 24, PP. 643-647, 1991.

[23] J. J. Spiegelman and S. L. Y. Woo, "A rigid-body method for determining centers of rotation and angular displacements of planar joint motion," *Journal of Biomechanics*, vol. 20, pp. 715-721, 1987.

[24] R. O. Duda and P. E. Hart, *Pattern classification and scene analysis.* New York: Wiley, 1973.

[25] R. Safaee-Rad, "Functional human arm motion study with a new 3-D measurement system," *M. Sc. dissertation,* Electrical & Computer Engineering Department, University of Manitoba, Winnipeg, Manitoba, 1987.

[26] D. A. Winter, *Biomechanics and motor control of human movement.* New York: Wiley, 1990.

[27] H. J. Woltring, "On optimal smoothing and derivative estimation from displacement data in biomechanics," *Human Movement Science,* vol. 4, pp. 229-245, 1985.

[28] R. L. Eubank, *Spline smoothing and nonparametric regression.* New York: Marcel Dekker, 1988.

[29] J. A. Fessler, "Nonparametric fixed-interval smoothing with vector splines," *IEEE Transactions on Signal Processing,* vol. 39, pp. 852-859, 1991.

[30] G. R. Arce and N. C. Gallagher, "State description for the root-signal set of median filters," IEEE *Transactions on Acoustics, Speech and Signal Processing*, vol. ASSP-30, pp. 894-902, 1982.

[31] N. C. Gallagher and G. J. Wise, "A theoretical analysis of the properties of median filters," *IEEE Transactions on Acoustics, Speech and Signal Processing*, vol. ASSP-29, pp. 1136-1141, 1981.

[32] R. Fazel-Rezai, E. Shwedyk and S. Onyshko, "Comparison of different biomechanical data smoothing methods," *Proceedings of Canadian Medical and Biological Engineering Society Conference*, pp. 32-33, 1997.

[33] R. Fazel-Rezai and E. Shwedyk, "Biomechanic signal filtering for dynamic analysis purpose: A quantitative comparison between different methods," *Journal of Biomechanics*, vol. 31, p. 85, 1998.

[34] L. G. Portney, M. P. Watkins, *Foundation of clinical research, application to practice*, Appleton & Lange, Norwalk, Connecticut, 1993.

[35] A. D. Aczel, *Statistics, concepts and applications*, Richard D. Irwin, INC., 1995.

[36] C. L. Vaughan and J. G. Hay, "Closed loop problems in biomechanics Part I- A classification System," *Journal of Biomechanics*, vol. 15, pp. 197-200, 1982.

[37] Gordon, E. Robertson and D. A. Winter, "Mechanical energy generation, absorption and transfer amongst segments during walking," *Journal of Biomechanics*, vol. 13, pp. 845-854, 1980.

[38] A. O. Quanbury, D. A. Winter, "Instantaneous power & power flow in body segments during walking," *Journal of Human Movement Studies*, vol 1, pp. 59-67, 1975.

[39] H. Elftman, "Forces and energy changes in the leg during walking," *Journal of physiology*, vol. 125, pp. 339-356, 1938.

[40] H. Elftman, "The function of muscles in locomotion," *Journal of physiology*, vol. 125, pp. 357-366, 1938.

[41] H. Elftman, "The work done by muscles in running," *Journal of physiology*, vol. 127, pp. 672-684, 1940.

[42] D. A. Winter, "Moments of force and mechanical power in jogging," *Journal of Biomechanics*, vol. 16, pp. 91-97, 1983.

[43] F. Prince, D. A. Winter, G. Sjonnesen and Robyn Wheeldon, "A new technique for the calculation of the energy stored, dissipated, and recovered in different ankle-foot prostheses," *IEEE Transactions on Rehabilitation Engineering*, vol. 2, pp. 247-255, 1994.

[44] M. P. Looze, J. B. J. Bussmann, I. Kingma and H. M. Toussaint, "Different methods to estimate total power and its components during lifting," *Journal of Biomechanics*, vol. 25, pp. 1089-1095, 1992.

[45] J. Ripat, The relationship between functional upper limb kinematics, pain and perceived disability in individuals with rheumatoid arthritis, *M. Sc. dissertation,* School of Medical Rehabilitation, University of Manitoba, Winnipeg, Manitoba, 1997.

[46] R. Fazel-Rezai, E. Shwedyk, J. E. Cooper, J. Ripat and S. Onyshko, "Changes in upper limb dynamics in patients with rheumatoid arthritis," *Journal of Biomechanics*, vol. 31, p. 15, 1998.

[47] R. Fazel-Rezai, J. E. Cooper, S. Onyshko and E. Shwedyk, "Generated moments at the upper limb during movement," *Proceedings of IXth Biennial Conference of Canadian Society for Biomechanics,* 1996.

[48] K. R. Kaufman, K. N. An, W. J. Litchy and E. Y. S. Chao, "Physiological prediction of muscle forces-I. Theoretical formulation," *Journal of Biomechanics,* vol. 40, pp. 781-792, 1991.

[49] K. R. Kaufman, K. N. An, W. J. Litchy and E. Y. S. Chao, "Physiological prediction of muscle forces-II. Application to isometric exercise," *Journal of Biomechanics,* vol. 40, pp. 793-804, 1991.

[50] K. N. An, K. R. Kaufman and E. Y. S. Chao, "Physiological considerations of muscle force through the elbow joint," *Journal of Biomechanics,* vol. 22, pp. 1249-1256, 1989.

[51] K. N. An, B. M. Kwak, E. Y. Chao and B. F. Morrey, "Determination of muscle and joint forces: A new technique to solve the indeterminate problem," *Transactions of the ASME,* vol. 106, pp. 364-367, 1984.

[52] S. A. Kautz and M. L. Hull, "Dynamic optimization analysis for equipment setup problems in endurance cycling," *Journal of Biomechanics*, vol. 28, pp. 1391-1401, 1995.

[53] J. Cholewicki, S. M. McGill and R. W. Norman, "Comparison of muscle forces and joint load from an optimization and EMG assisted lumbar spine model: Towards development of a hybrid approach," *Journal of Biomechanics*, vol. 28, pp. 321-331, 1995.

[54] E. Y. S. Chao and K. Rim, "Application of optimization principles in determining the applied moments in human leg during gait," *Journal of Biomechanics,* vol. 6, pp. 497-510, 1973.

[55] A. Pedotti, V. V. Krishnan and L. Stark, "Optimization of muscle-force sequencing in human locomotion," *Mathematical Biosciences*, vol. 38, pp. 57-76, 1978.

[56] J. Cholewicki and S. M. McGill, "EMG assisted optimization: A hybrid approach for estimating muscle forces in an indeterminate biomedical model," *Journal of Biomechanics*, vol. 27, pp. 1287-1289, 1994.

[57] J. Dul, G. E. Johnson, R. Shiavi and M. A. Townsend, "Muscular synergism-II. A minimum-fatigue criterion for load sharing between synergistic muscles," *Journal of Biomechanics*, vol. 17, pp. 675-684, 1984.

[58] J. V. Basmajian, C. J. De Luca, *Muscle alive, their functions revealed by electromyography,* Williams & Wilkins, 1985.

[59] L. A. Zadeh, "Fuzzy sets," *Information and Control*, vol. 8, pp. 338-53, 1965.

[60] C. V. Negotia, *Fuzzy systems*, Tubridge Wells: Abacus Press, 1981.

[61] L. A. Zadeh, "A computational approach to analysis of complex systems and decision process," *IEEE Transactions on System Man and cybernetics.*, vol. 9, pp. 149-84, 1983.

[62] L. A. Zadeh, "Fuzzy logic = Computing with words," *IEEE Trans Fuzzy Systems.*, vol. 4, pp. 103-11, 1996.

[63] R. Shapiro, "Direct linear transformation for the three-dimension cinematography," *The Research Quarterly,* vol. 49, pp. 197-205, 1978.

[64] N. R. Miller, R. Shapiro and T. M. McLaughlin, "A technique for obtaining spatial kinematic parameters of segments of biomechanical system from cinematographic data," *Journal of Biomechanics,* vol. 13, pp. 535-547, 1980.

[65] H. Hatze, "High-precision three-dimensional photogrammetric calibration and object space reconstruction using a modified DLT approach," *Journal of Biomechanics,* vol. 21, pp. 533-538, 1988.

[66] J. H. Challis and D. G. Kerwin, "Accuracy assessment and control point configuration when using the DLT for photogrammetry," *Journal of Biomechanics,* vol. 25, pp. 1053-1058, 1992.

[67] B. Yu, T. J. Koh and J. G. Hay, "A panning DLT procedure for three-dimensional videography," *Journal of Biomechanics,* vol. 26, pp. 741-751, 1993.

[68] L. Chen, C. W. Armestrang and D. D. Raftopoulos, "An investigation on the accuracy of three dimensional space reconstruction using the direct linear transformation technique," *Journal of Biomechanics*, vol. 27, pp. 493-500, 1994.

[69] G. A. Wood and R. N. Marshall, "The accuracy of DLT extrapolation in three-dimensional film analysis," *Journal of Biomechanics*, vol. 19, pp. 781-785, 1986.

[70] R. Fazel-Rezai, E. Shwedyk, S. Onyshko and J. E. Cooper, "Power analysis of upper limb movement," *Proceedings of IEEE Engineering in Medicine and Biology Conference*, Paper no. 210, 1996.

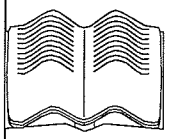

APPENDIX A. UNIVERSITY OF MANITOBA MOTION ANALYSIS SYSTEM (UM^{2}AS)

A.1. THE UM^{2}AS SETUP

The system used to record motion data was the University of Manitoba Motion Analysis System (UM^{2}AS) [9][25]. This system records motion on video tapes that can be used for analysis later. In this system, three orthogonally placed charge coupled device (CCD) video cameras record upper limb motion (Fig. A.1).

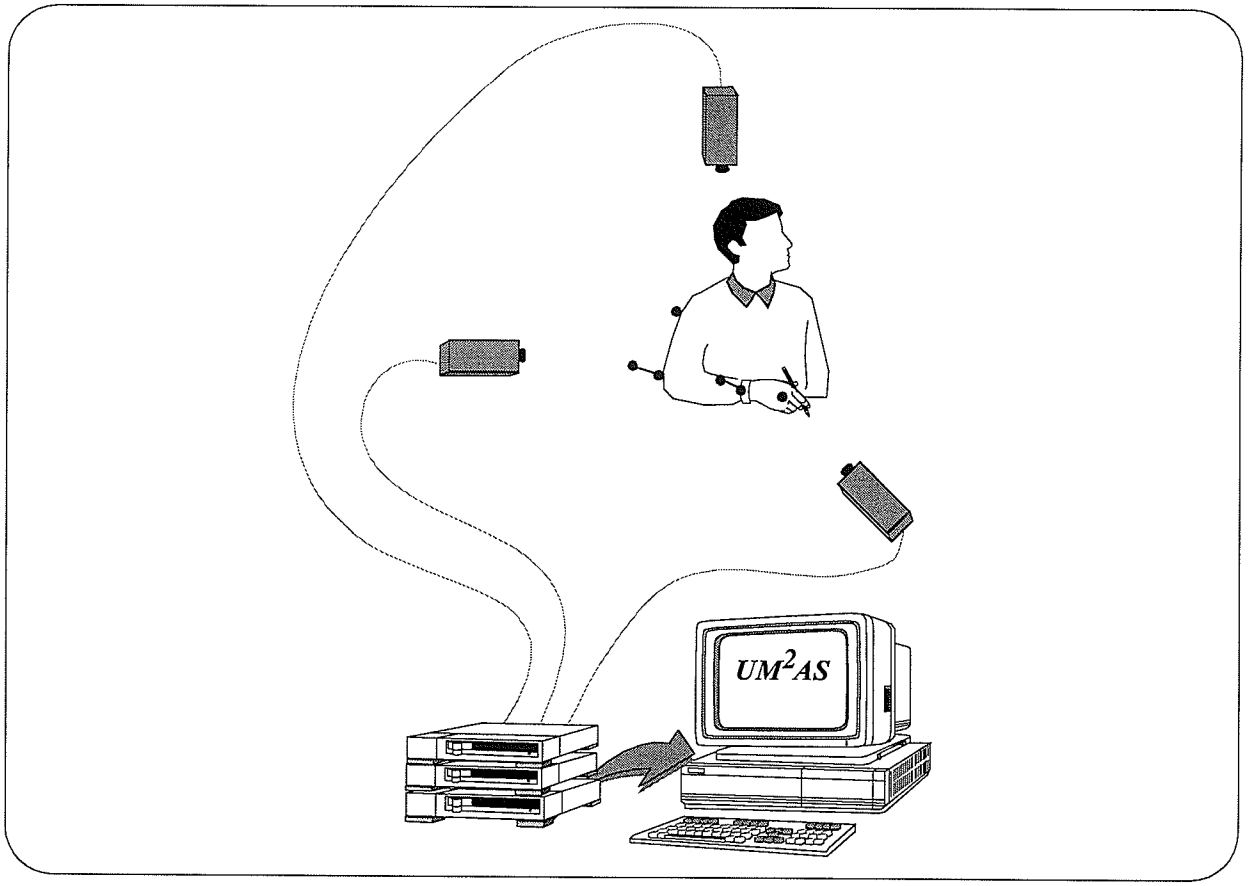

Fig. A.1 UM^{2}AS laboratory set up.

Reflective markers are placed on the upper limb landmarks in such a way that cause no disruption to the normal pattern of movement. Markers are one-inch Styrofoam balls. These are securely attached to the skin of the subject's upper limb with double sided adhesive tape. The imaging space is approximately one cubic meter in volume, illuminated by three pot lights and the walls are draped in non-reflective material. Although two cameras are enough to calculate three components of the markers in three-dimensional space, using three cameras prevents the problem of disappearing markers and overlapping. A camera flash is used to synchronize the video-tapes; this was done at the beginning of each trial recording. The motion was recorded at the rate of 30 frames/second (30 Hz) by three Beta recorders. However during the digitizing of the video-taped sequences, every fifth frame was digitized. Therefore the sampling rate was 6 HZ. The video-taped sequences were played back manually. The image was displayed on a black and white monitor. The frame after the synchronization flash was considered as the first frame for all three cameras. Then UM^{2}AS software was used to digitize the tapes. The process of digitizing three video-taped motion produces three two-dimensional images. The direct linear transformation algorithm was used to reconstruct three-dimensional trajectories of the markers as explained in the next section.

A.2. THREE DIMENSIONAL RECONSTRUCTION METHOD

Among three dimensional reconstruction methods, the most widely applied and discussed is the direct linear transformation (DLT) algorithm. The DLT equations [63] are

$$\begin{cases} x_i = \dfrac{L_1 X_i + L_2 Y_i + L_3 Z_i + L_4}{L_9 X_i + L_{10} Y_i + L_{11} Z_i + 1} \\ y_i = \dfrac{L_5 X_i + L_6 Y_i + L_7 Z_i + L_8}{L_9 X_i + L_{10} Y_i + L_{11} Z_i + 1} \end{cases} \tag{A-1}$$

where x_i, y_i are the coordinates of the *ith* point, X_i, Y_i, Z_i are the object space coordinates of the *ith* point, and $L_1, \ldots, L_{11}$ are DLT parameters. Eleven parameters of DLT are used to characterize the calibration, position and orientation of a single camera [64]. DLT parameters permit the computation of the unknown spatial coordinates of a point whose image coordinates have been recorded by at least two cameras. Because there are three unknowns and two equations, at least two cameras are necessary to find the three components of a point in 3D space.

Determination of the DLT parameters of each camera requires a calibration procedure [65], where at least six control points with known spatial coordinates are chosen and recorded by each of the cameras to be calibrated [66][67][68][69]. The control points are normally mounted on a calibration structure which is placed in the space of interest, filmed and removed. By rearranging Eq. (A-1), a matrix equation results in which DLT parameters appear as the vector of unknowns. Linear least-squares techniques may then be employed to compute this vector from the overdetermined system [65]. It is imperative that the position, orientation and focal length of each camera be unchanged during the experiment.

To find the best angle between two cameras to minimize error, consider Fig. A.2. Let the optical axis of the two cameras be AC_1 and BC_1. Point C_1 represents the position of a point to be digitized by the cameras.

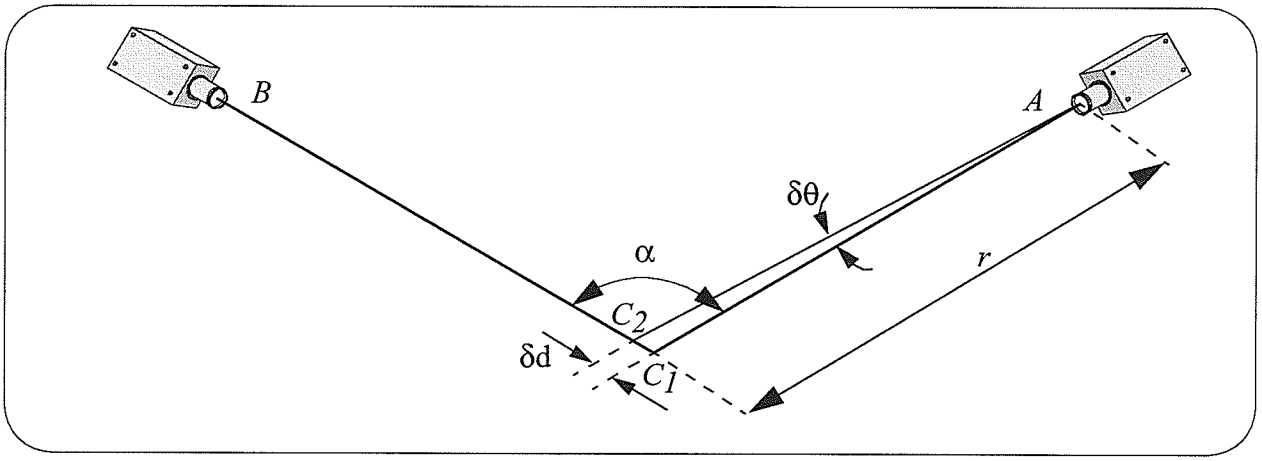

Fig. A.2 Error generated due to error in the optical axis.

If one considers errors due to the digitizing, calibration procedure, change in the camera orientation and/or DLT technique, the optical axis of camera A can be modelled as AC_2. In terms of the angle between cameras (α), distance between the camera and the object point (r), and optical axis error ($\delta\theta$), the error (δd) can be written as

$$\delta d \approx \frac{r\delta\theta}{Sin\,(\alpha)} \qquad \text{(A-2)}$$

Obviously, the error will be minimum if α equals to 90 degrees and r is chosen to be as small as possible.

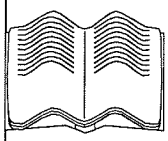

APPENDIX B. SMOOTHING RESULTS

This appendix shows individual graphs of the output of the four smoothing techniques with the input experimental data of Fig. 3.1. Also the first and second derivatives of the resultant output are shown. Finally, error results shown graphicly in Fig. 3.6 and Fig. 3.7 are tabulated in Tables B.1-B.6.

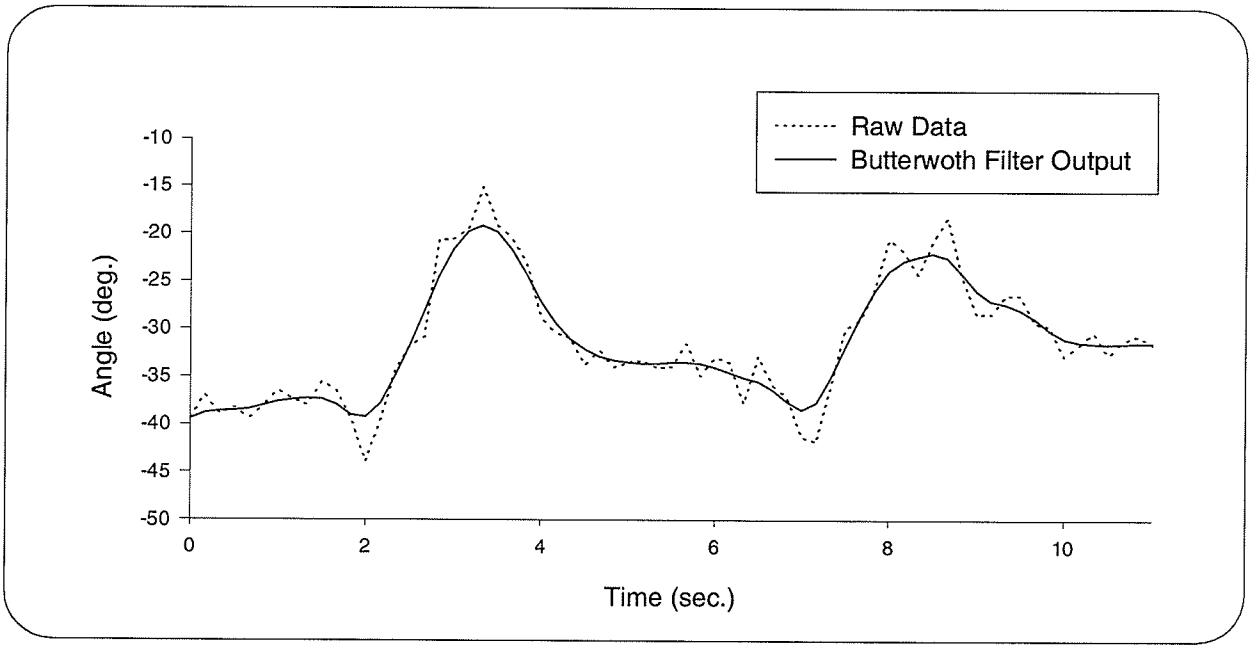

Fig. B.1 Raw data and the output of the Butterworth filter.

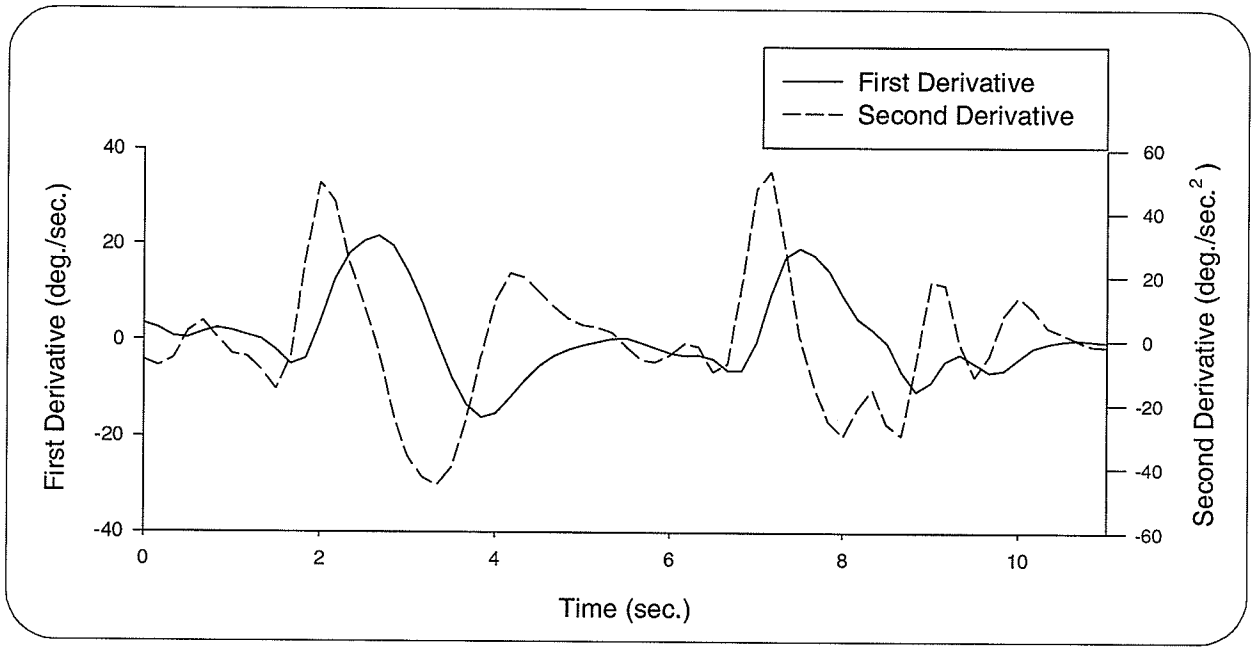

Fig. B.2 First and second derivatives of the filtered data by Butterworth filter.

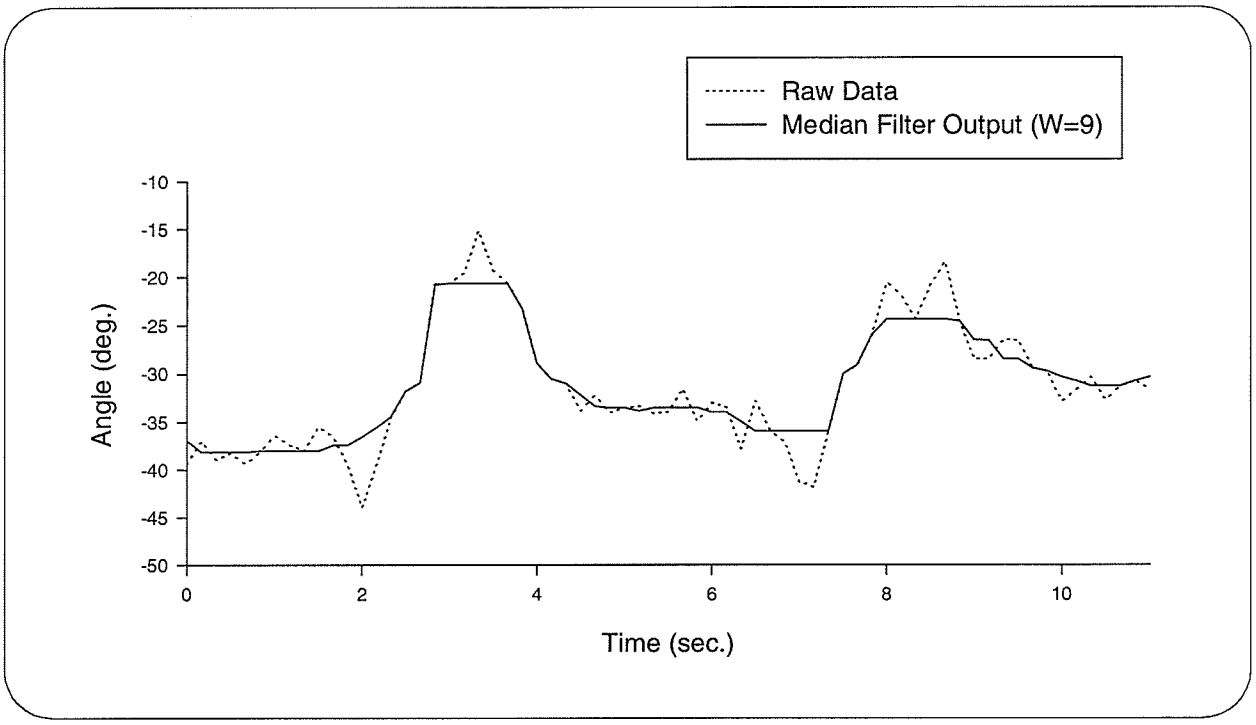

Fig. B.3 Median filtering when window size is equal to nine.

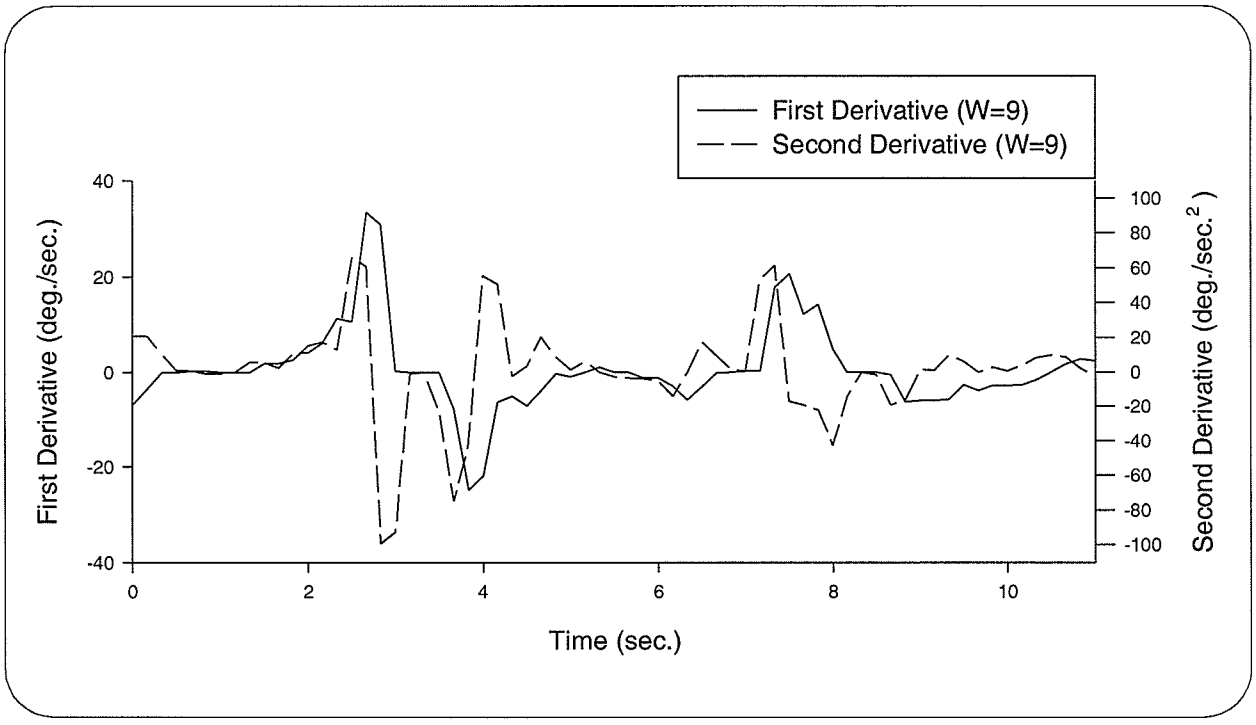

Fig. B.4 First and second derivative of the filtered data by median filter.

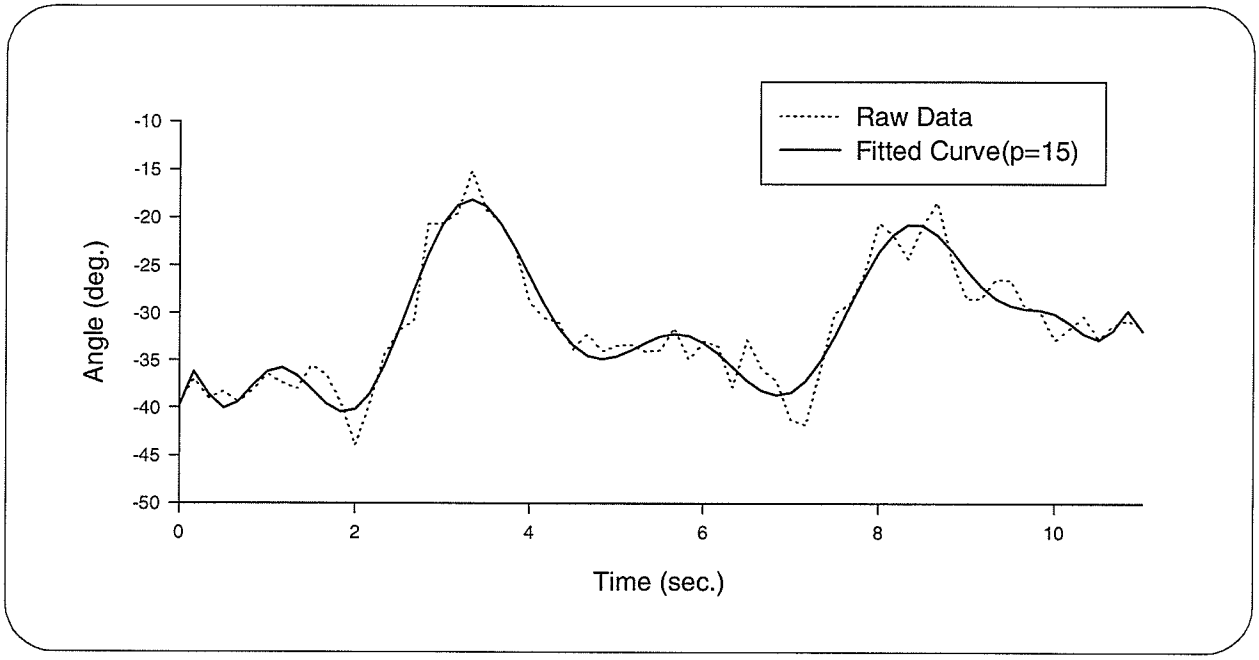

Fig. B.5 Curve fitting when the polynomial degree is equal to fifteen.

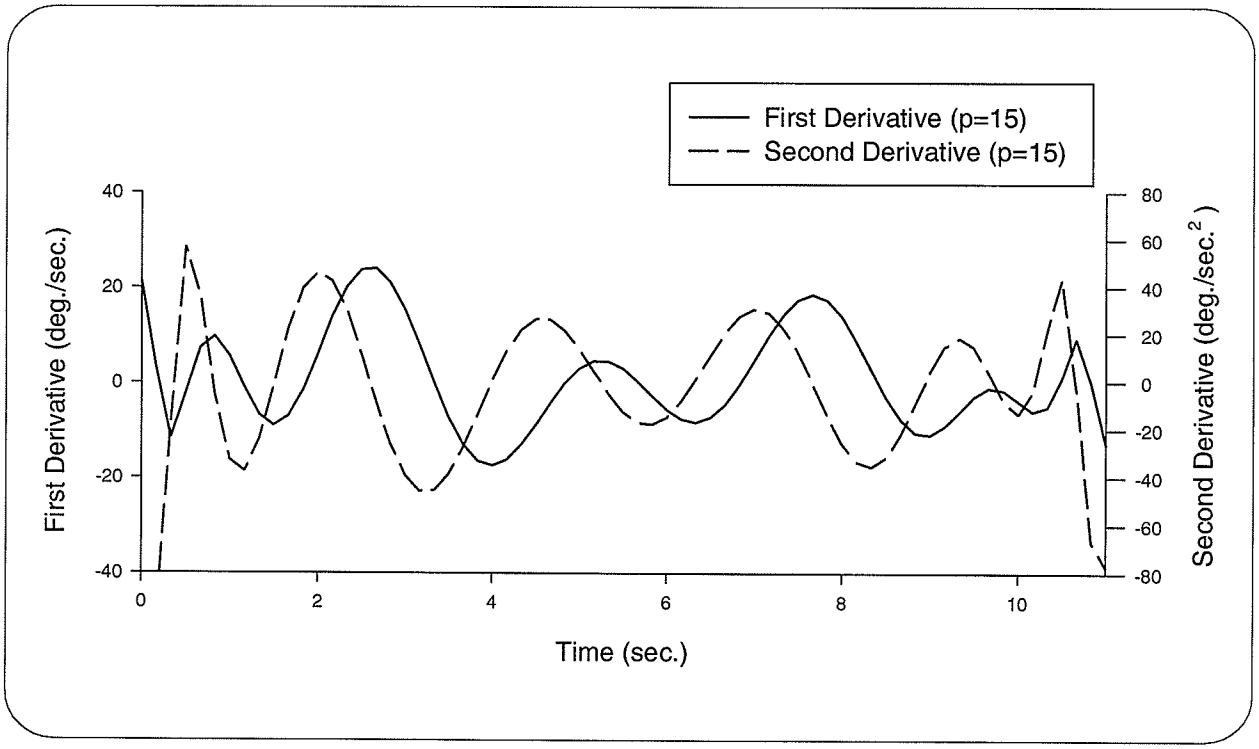

Fig. B.6 First and second derivative of the fitted curve.

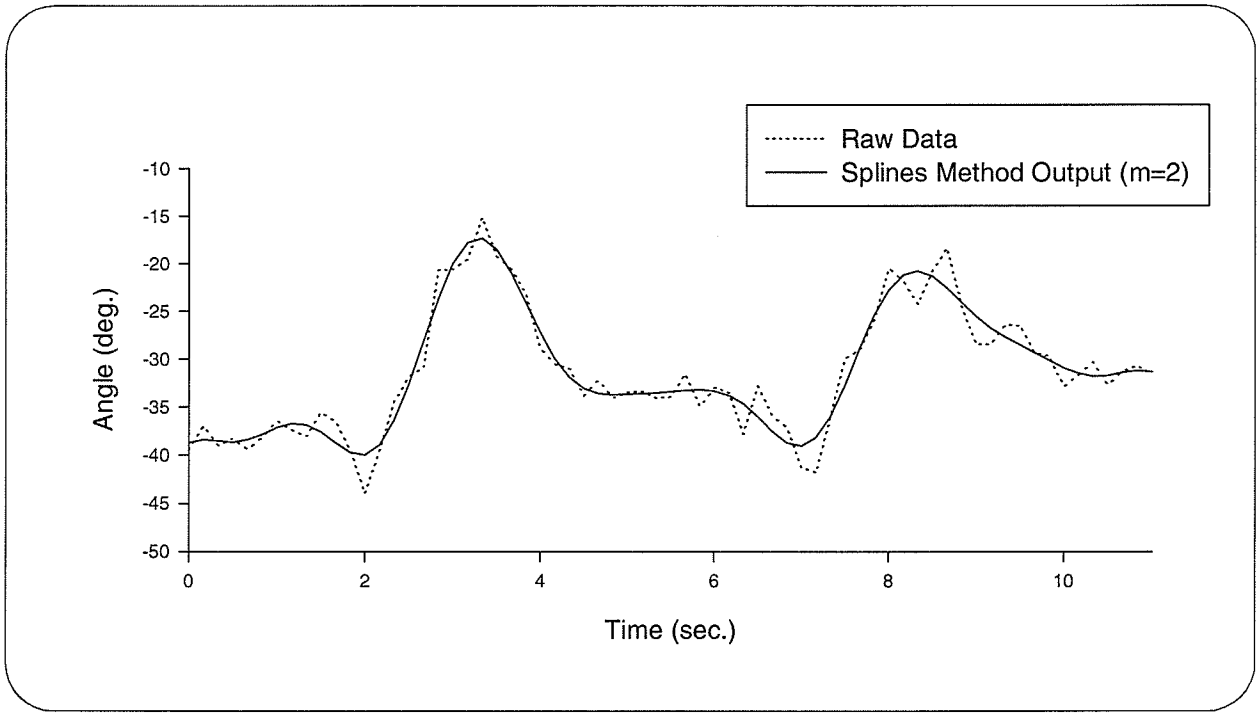

Fig. B.7 Raw and smoothed data using the cubic splines method.

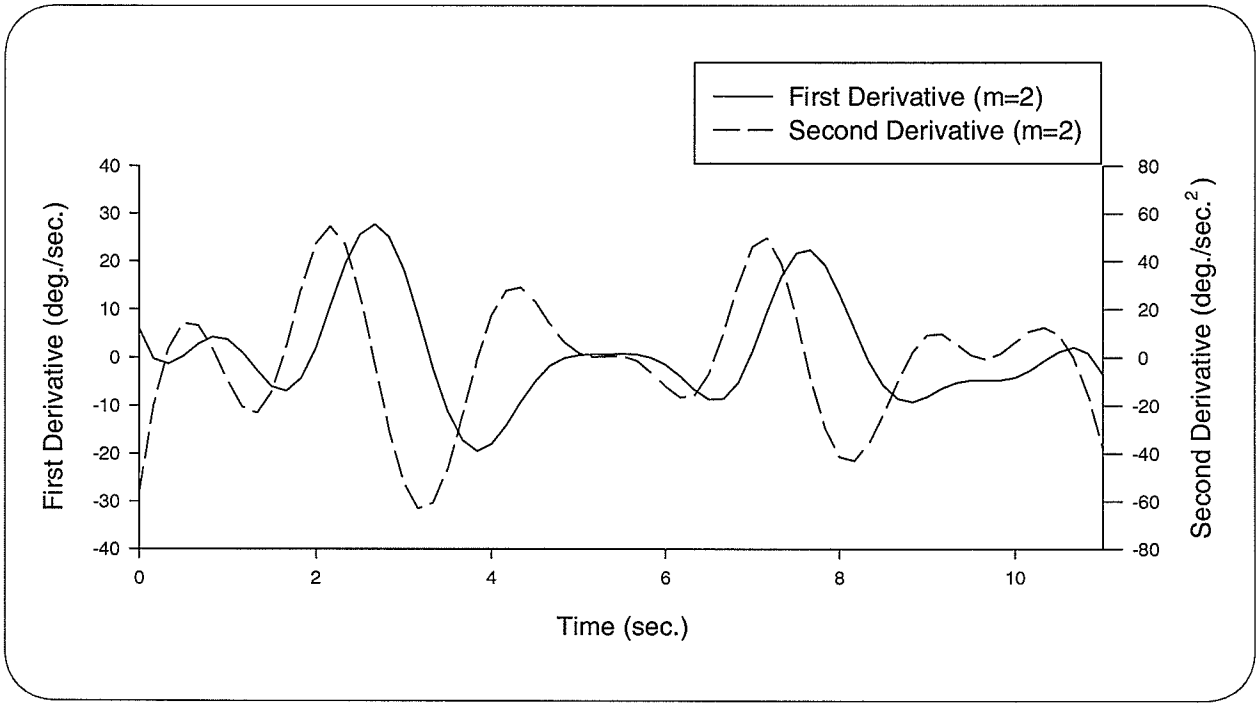

Fig. B.8 First and second derivatives of the smoothed data using the cubic splines method.

Noise Distribution	Uniform			Gaussian		
Signal to Noise Ratio	13db	10db	7db	13db	10db	7db
Butterworth Filter	3.43 %	4.98 %	8.67 %	4.38 %	6.78 %	11.91 %
Median Filter	7.07 %	9.55 %	13.64 %	7.09 %	10.15 %	15.64 %
Curve Fitting	2.82 %	3.93 %	6.16 %	3.49 %	5.19 %	8.62 %
Splines Method	2.21 %	3.10 %	4.90 %	3.27 %	4.55 %	7.87 %

Table B.1 Mean value of the error at the first level over ten test signals.

Noise Distribution	Uniform			Gaussian		
Signal to Noise Ratio	13db	10db	7db	13db	10db	7db
Butterworth Filter	4.73 %	7.52 %	13.22 %	4.01 %	5.96 %	9.71 %
Median Filter	15.58 %	18.66 %	24.07 %	14.70 %	17.25 %	24.63 %
Curve Fitting	5.29 %	6.70 %	9.58 %	4.22 %	4.51 %	5.12 %
Splines Method	2.63 %	3.46 %	5.21 %	1.71 %	1.80 %	1.99 %

Table B.2 Mean value of the error at the second level over ten test signals.

Noise Distribution	Uniform			Gaussian		
Signal to Noise Ratio	13db	10db	7db	13db	10db	7db
Butterworth Filter	11.71 %	21.5 %	41.45 %	11.11 %	19.68 %	36.81 %
Median Filter	60.65 %	64.20 %	76.49 %	55.06 %	66.90 %	87.20 %
Curve Fitting	13.83 %	17.53 %	25.21 %	11.60 %	12.34 %	13.83 %
Splines Method	4.79 %	6.03 %	8.96 %	3.32 %	3.50 %	3.81 %

Table B.3 Mean value of the error at the third level over ten test signals.

Noise Distribution	Uniform			Gaussian		
Signal to Noise Ratio	13db	10db	7db	13db	10db	7db
Butterworth Filter	0.51 %	0.69 %	2.31 %	1.65 %	2.75 %	4.57 %
Median Filter	1.43 %	1.71 %	2.56 %	1.42 %	2.05 %	3.08 %
Curve Fitting	1.57 %	1.62 %	1.86 %	1.69 %	1.91 %	2.59 %
Splines Method	0.64 %	0.69 %	0.79 %	1.14 %	1.21 %	1.98 %

Table B.4 Standard deviation of the error at the first level over ten test signals.

Noise Distribution	Uniform			Gaussian		
Signal to Noise Ratio	13db	10db	7db	13db	10db	7db
Butterworth Filter	0.63 %	1.15 %	2.30 %	0.81 %	0.81 %	1.44 %
Median Filter	1.65 %	1.27 %	3.74 %	2.88 %	4.80 %	4.02 %
Curve Fitting	3.16 %	3.12 %	3.11 %	3.31 %	3.34 %	3.38 %
Splines Method	0.96 %	0.96 %	0.67 %	0.70 %	0.73 %	0.77 %

Table B.5 Standard deviation of the error at the second level over ten test signals.

Noise Distribution	Uniform			Gaussian		
Signal to Noise Ratio	13db	10db	7db	13db	10db	7db
Butterworth Filter	2.59 %	5.33 %	10.88 %	2.10 %	4.43 %	9.04 %
Median Filter	8.46 %	19.75 %	23.63 %	21.58 %	24.42 %	32.37 %
Curve Fitting	6.78 %	6.32 %	6.33 %	9.03 %	9.27 %	9.69 %
Splines Method	1.69 %	1.86 %	1.53 %	1.69 %	1.82 %	2.04 %

Table B.6 Standard deviation of the error at the third level over ten test signals.

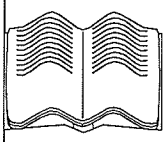

APPENDIX C. EXPERIMENTAL RESULTS OF POWER ANALYSIS

To verify experimentally the equivalence between power flows shown analytically in Chapter 4, an experiment was done. Kinematic data were collected from two subjects: age 50 and 65 years, weight 84 and 88 kg, and height 155 and 181 cm. Each subject performed two tasks: lifting a bottle (task #1) and a can (task #2). After obtaining the Euler angles of the segments and solving the kinetic equations, the power of each segment was calculated in the two different ways as described [70]. As expected cross correlations between P_{es}, the rate of change of energy, and P_{ps}, the sum of generated or absorbed power by muscles and transmitted power through joints, were close to one in all cases (Table C.1). As a representative curve, the power patterns of three segments of subject #1 during the performance of task #1 are shown in Fig. C.1.

		Arm segment	Forearm segment	Hand segment
Subject #1	Task #1	0.9988	0.9992	0.9938
	Task #2	0.9997	0.9998	0.9998
Subject #2	Task #1	0.9988	0.9922	0.9798
	Task #2	0.9983	0.9954	0.9855

Table C.1 Cross correlations between total power and rate of energy change.

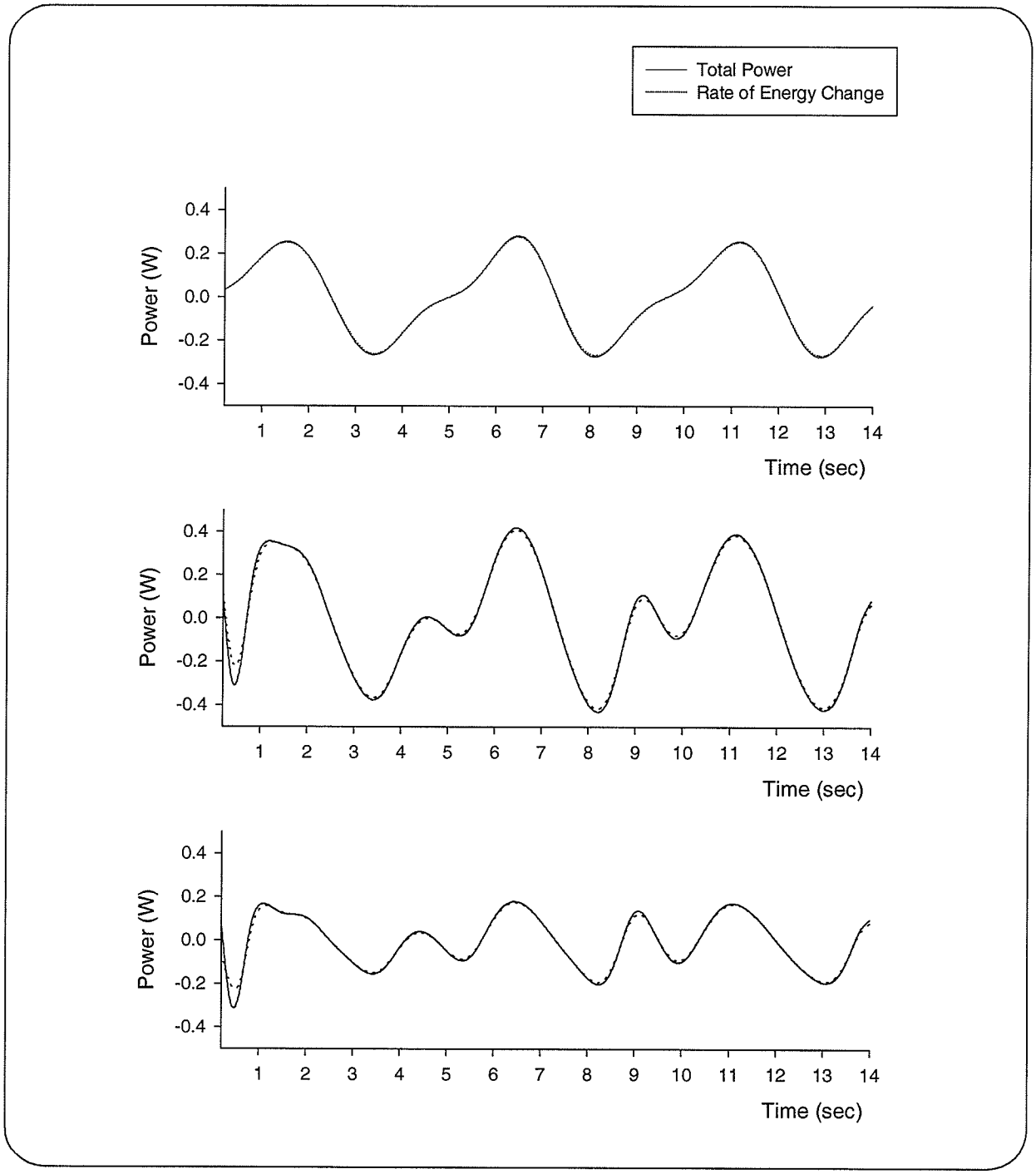

Fig. C.1 Total power and rate of energy change for the subject #1 and task #1.

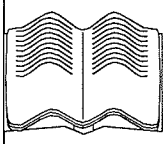

APPENDIX D. DEMOGRAPHICS OF SUBJECTS IN RHEUMATOID ARTHRITIS STUDY

In this appendix normal and RA subject demographics are presented [45]. Subjects were ten normal (NR) and ten subjects with rheumatoid arthritis (RA) who had shoulder joint involvement. The average and standard deviation of age weight and height for the normal and RA subjects are shown in Table D.1 The average (±standard deviation) duration of RA subjects was 16 years, 2 months (±7 years). More information about subjects can be found in [45].

	Age (years, months)	Weight (kg)	Height (cm)
NR subjects	43,8 (±14,2)	73.5 (±10.4)	172.0 (±10.1)
RA subjects	52,2 (± 8,5)	68.0 (±16.5)	167.9 (±11.2)

Table D.1 The average (± standard deviation) of age, weight and height for normal and RA subjects.

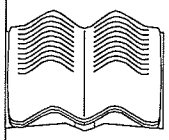

APPENDIX E. OPTIMIZATION METHOD

E.1. INTRODUCTION

To arrive at a specific solution for the indeterminate equations, one method is to specify a criterion or objective function and to find the solution that minimizes or maximizes this criterion [49][50][51][52][53]. A common criterion is based on the hypothesis that efficiency principles are inherent to neuromuscular control and this is used as the rationale for optimization. With this approach the indeterminate problem can be solved uniquely. The objective function to be optimized represents the physiological cost to be minimized. Different objective functions have been used for the force distribution problem [54][55][56]. The two most commonly used objective functions are

$$Obj = \sum_{m=1}^{N} F_m^p \tag{E-1}$$

$$Obj = \sum_{m=1}^{N} (F_m / A_m)^p \tag{E-2}$$

where F_m is the muscle force, A_m is its physiological cross-sectional area (muscle volume divided by its length), PCSA. Different values of p have been chosen by different authors.

E.2. LAGRANGE MULTIPLIER FOR NONLINEAR OPTIMIZATION METHOD

The general form of the optimization for the objective function shown in Eq. (E-1) is

$$\text{Minimize: } \sum_{m=1}^{N} F_m^p \tag{E-3}$$

subject to the constraint

$$\sum_{m=1}^{N} b_m F_m = M_T - M_j \tag{E-4}$$

where b_m is moment arm of the muscle m.

To solve this optimization problem, the Lagrangian function is defined as follows

$$L = \sum_{m=1}^{N} F_m^p + \lambda (b_m F_m - M_T + M_j) \tag{E-5}$$

Extreme values for L are

$$\begin{cases} \dfrac{\partial L}{\partial F_m} = 0 & (m = 1, 2, \ldots, m) \\ \dfrac{\partial L}{\partial \lambda} = 0 \end{cases} \tag{E-6}$$

Solving Eqs. (E-5) and (E-6) gives the muscle force

$$F_m = \frac{M_T - M_j}{b_m \sum_{k=1}^{N} (b_k / b_m)^{p/(p-1)}} \tag{E-7}$$

In the same way, the solution when optimization for the objective function in Eq. (E-2) is used can be written as

$$F_m = A_m \frac{M_T - M_j}{b_m A_m \sum_{k=1}^{N} (b_k A_k / b_m A_m)^{p/(p-1)}} \tag{E-8}$$